

Alma Mater Studiorum - Università di Bologna

DOTTORATO DI RICERCA IN
INGEGNERIA CIVILE, CHIMICA, AMBIENTALE E DEI MATERIALI

Ciclo 35

Settore Concorsuale: 08/A4 - GEOMATICA

Settore Scientifico Disciplinare: ICAR/06 - TOPOGRAFIA E CARTOGRAFIA

IMPACT OF GEOMATIC TECHNIQUES ON TOPO-BATHYMETRIC SURVEYS
FOR COASTAL ANALYSIS

Presentata da: Enrica Vecchi

Coordinatore Dottorato

Alessandro Tugnoli

Supervisore

Stefano Gandolfi

Co-supervisore

Nunzio De Nigris

Esame finale anno 2023

A mio nonno, che mi ha insegnato l'amore per la vita

Acknowledgments

I would like to thank my supervisor, Stefano Gandolfi, for his constructive support throughout this project, involving me in many stimulating activities. Thanks to him for always being enthusiastic about my research and for transmitting to me his passion for our scientific topics.

I'm also grateful to my Co-Supervisor Nunzio De Nigris, who enthusiastically supported the whole project and research. A sincere thanks to Prof. Alessandro Antonini, for giving me the opportunity to share our research at TUDelft University, during a period that will always remain a good memory for me, hoping to collaborate again in the future.

A special heartfelt thanks also should be given to my colleagues, that will remain one of the best sides of this period, the best team I could have asked for.

Last, but not least, special thanks to my family and my old friends to be always a certainty.

Abstract

Among the environmental heritages, sandy coasts represent vital areas whose preservation and maintenance also involve economic and tourist interests. Besides, sandy coastal areas are dynamic environments undergoing the erosion process at different levels depending on their specific characteristics. For this reason, defence interventions are commonly realized by combining engineering solutions and management policies to evaluate their effects over time. In this context, monitoring activities represent the fundamental instrument to obtain a deep knowledge of the investigated phenomenon, i.e. the coasts' current state and morphological variations. Thanks to technological development, several possibilities both in terms of geomatic surveying techniques and processing tools are available, allowing to reach high performances and accuracy. Nevertheless, when the littoral definition includes both emerged and submerged beaches, several issues have to be considered to identify a suitable approach. Therefore, the geomatic surveys and all the following steps need to be calibrated according to the individual application, with the reference system, accuracy and spatial resolution as primary aspects. This study provides the evaluation of the available geomatic techniques, processing approaches, and derived products, aiming at optimising the entire workflow of coastal monitoring by adopting an accuracy-efficiency trade-off. The presented analyses highlight the balance point when the increase in performance becomes an additional value for the obtained products ensuring proper data management. This perspective can represent a helpful instrument to properly plan the monitoring activities and investment decisions according to the specific purposes of the analysis. Finally, the primary uses of the acquired and processed data in monitoring contexts are presented, also considering possible applications for numerical modelling as supporting tools. Moreover, the theme of coastal monitoring has been addressed throughout this thesis by considering a practical point of view, linking to the activities performed by Arpae (Regional agency for prevention, environment and energy of Emilia-Romagna). Indeed, the Adriatic coast of Emilia-Romagna, where sandy beaches particularly exposed to erosion are present, has been chosen as a case study for all the analyses and considerations.

Keywords

- Monitoring
- Coast
- Emilia-Romagna
- Geodetic reference system
- GNSS
- Echo sounder
- UAV
- Bathymetry
- Shoreline
- Accuracy

Acronyms List

- 3D: three-dimensional
- ALS: Airborne Laser Scanner
- Arpae: Regional agency for prevention, environment and energy of Emilia-Romagna
- CORS: Continuously Operating Reference Stations
- CPU: Central Processing Unit
- DEM: Digital Elevation Model
- DSAS: Digital Shoreline Analysis Systems
- DSM: Digital Surface Model
- DTM: Digital Terrain Model
- EE: Earth Engine
- EGM: Earth Geopotential Model
- ENAC: Ente Nazionale per l'Aviazione Civile
- EPR: End Point Rate
- ESA: European Space Agency
- FKP: Flächen-Korrektur-Parameter
- GCP: Ground Control Point
- GIS: Geographic Information System
- GLONASS: Global'naya Navigastionaya Sputnikovaya Systema
- GNSS: Global Navigation Satellite System
- GPS: Global Positioning System
- GSD: Ground Sampling Distance
- IGM: Istituto Geografico Militare
- IGM: Istituto Geografico Militare
- IHO: International Hydrographic Organization
- IMU: Inertial Measurement Unit
- IPCC: Intergovernmental Panel on Climate Change
- LASER: Light Amplification by Stimulated Emission of Radiation
- LAT: Low Astronomical Tide
- LHS: Latin Hypercube Sampling
- LIDAR: Light Detection and Ranging
- MAC: Master Auxiliary Concept
- MBES: Multibeam Echo Sounder
- MDT: Mean Dynamic Topography
- MSL: Mean Sea Level
- MSS: Mean Sea Surface
- NASA: National Aeronautics and Space Administration
- NDVI: Normalized Difference Vegetation Index

- NIR: Near Infrared
- NSE: Nash and Sutcliff coefficient
- OGC: Open Geospatial Consortium
- OTF: On The Fly
- OWS: Open Geospatial Web Services
- PPK: Post Processing Kinematic
- PSMSL: Permanent Service for Mean Sea Level
- QCP: Quality Control Point
- QGIS: Quantum GIS
- RADAR: Radio Detection And Ranging
- RER: Emilia-Romagna Region
- RF: Reference Frame
- RMSE: Root Mean Square Error
- RON: Rete Ondametrica Nazionale
- RS: Reference System
- RTK: Real Time Kinematic
- SAR: Synthetic Aperture Radar
- SBAS: Satellite-Based Augmentation Systems
- SBES: Singlebeam Echo Sounder
- SD: Standard Deviation
- SDB: Satellite Derived Bathymetry
- SDS: Satellite Derived Shoreline
- SfM: Structure from Motion
- SGS: Sequential Gaussian Simulation
- SONAR: Sound Navigation And Ranging
- SVP: Sound Velocity Probe
- SVS: Sound Velocity Sensor
- TLS: Terrestrial Laser Scanner
- TRF: Trust Region Reflective
- TS: Total Station
- TVU: Total Vertical Uncertainty
- UAV: Unmanned Aerial Vehicles
- VRS: Virtual Reference Station
- WGS84: World Geodetic System 1984
- WMS: Web Map Service

Contents

| | |
|---|-------------|
| Acknowledgments | iii |
| Abstract | iv |
| Keywords | v |
| Acronyms List | vi |
| Contents | viii |
| Introduction | 1 |
| Chapter 1 | 5 |
| 1 Coastal monitoring | 5 |
| Chapter 2 | 17 |
| 2 Geodetic Reference Systems | 17 |
| 2.1 Altimetric reference systems | 20 |
| 2.2 Geoid undulation | 26 |
| 2.3 Sea level reference..... | 37 |
| Chapter 3 | 43 |
| 3 Geomatic Techniques for coastal monitoring | 43 |
| 3.1 Global Navigation Satellite Systems (GNSS) | 47 |
| 3.1.1 Real-time Kinematic | 52 |
| 3.1.2 Network Real-time Kinematic..... | 55 |
| 3.2 Singlebeam and multibeam echo sounders | 59 |
| 3.3 Unmanned Aerial Vehicles (UAV) photogrammetry..... | 68 |
| 3.4 Light Detection And Ranging (LiDAR) | 78 |
| 3.4.1 Terrestrial Laser Scanner..... | 81 |
| 3.4.2 Airborne Laser Scanner..... | 82 |
| Chapter 4 | 87 |
| 4 Case Study: Emilia-Romagna littoral | 87 |

| | | |
|-------------------------|---|------------|
| 4.1 | Coastal Geodetic Network (RGC) | 92 |
| 4.2 | Nourishment interventions | 96 |
| 4.3 | Marine dynamics | 101 |
| Chapter 5..... | | 107 |
| 5 | Processing and Products | 107 |
| 5.1 | Topo-bathymetric maps | 110 |
| 5.2 | Profile sections..... | 117 |
| 5.3 | Maps of height variation..... | 123 |
| 5.4 | Shoreline | 127 |
| 5.5 | GNSS and photogrammetric UAV-derived products | 134 |
| Chapter 6..... | | 143 |
| 6 | Statistical analysis of geomatic data accuracy | 143 |
| 6.1 | Elevation differences | 146 |
| 6.2 | Variogram analysis | 149 |
| 6.3 | Kriging..... | 157 |
| 6.4 | Monte-Carlo simulation..... | 163 |
| 6.5 | Considerations | 169 |
| Conclusions..... | | 173 |
| References | | 177 |
| | Articles..... | 177 |
| | Websites..... | 188 |

Introduction

Coastal areas are vital environments involving the coexistence of environmental, tourist and economic interests. Therefore, their preservation and maintenance are essential for any policy about natural and economic heritages. In this regard, environmental problems are generally experiencing an increase in public perception. This leads to a desired better and more sustainable management of the environment, which implies a more deep knowledge of its current state and variations over time. In practice, monitoring activities represent the instrument to acquire this information in several contexts. In such complex and dynamic areas, such as sandy coasts, these activities present several significant issues and are primarily related to correctly understanding erosion processes.

The theme throughout this thesis is coastal monitoring, which has been addressed by adopting a proper trade-off between scientific and practical points of view. In this regard, this study provides the evaluation of available techniques, processing methods and approaches, required products and primary issues, aiming at optimising the entire workflow of coastal analysis. Moreover, some related activities, not entirely centred on coastal monitoring but linked to the overall study, have been carried out during the PhD period. Indeed, these mentioned analyses focused on applications along the Emilia-Romagna littoral and are given in summary inside the thesis.

Furthermore, all the reported discussions and results are placed in the context of Arpae's activities (the Regional agency for prevention, environment and energy of Emilia-Romagna), i.e. the authority involved in the coastal monitoring in the Emilia-Romagna region.

The outline of the thesis is organised as follows. The first chapter introduces general monitoring aspects, meaning observing objects' variations over time. Then, the object of our observations is defined, i.e. the coast, together with some considerations addressing coastal environments and, particularly, sandy beaches. A more detailed description of the erosion problem is provided, explaining the primary impacting factors and their effects in detail. After, the main quantities involved in the coastal analysis are introduced, with particular emphasis on the separation between heights and depths. Finally, the primary goals and practical approaches of coastal monitoring are described, linking to the Regional agency for prevention, environment and energy of Emilia-Romagna (Arpae).

The second chapter goes into a detailed description of Geodetic Reference Systems concerning the distinction between system and frame and modern or classic systems. This chapter's primary purpose is to identify the altimetric aspect, considering heights and depths and the procedure to transform or link different references. To this objective, geoid and ellipsoid surfaces are introduced, together with their associated orthometric and ellipsoidal heights. Moreover, throughout this discussion, the reference system is considered a fundamental support for coastal monitoring activities. A detailed description is provided regarding the geoid undulation since it has been addressed by a paper published during the PhD period in the context of the Emilia-Romagna littoral, *Definition of the Local Geoid Undulation Using Non-contemporary GNSS-Levelling Data on Subsidence Area: Application on the Adriatic Coastline*. The last part of the second chapter refers to sea level references, which help to understand the following specifications of different techniques and products.

The suitable geomatic techniques for coastal monitoring, both in emerged and submerged areas, are described in the third chapter, after a first general introduction about some aspects impacting the chosen method. A deeper discussion addresses four techniques: Global Navigation Satellite Systems (GNSS), echo sounders, photogrammetry from Unmanned Aerial Vehicles (UAV), and LiDAR, which are the most well-established for the monitoring activities performed in the Emilia-Romagna region. The sub-chapters structure is organised in the same way, describing the general characteristics of the technique and focusing on the approaches and reachable accuracy, specifically in the coastal environment. At last, the main benefits and disadvantages are highlighted from a practical point of view.

The fourth chapter examines the Adriatic coast of Emilia-Romagna, chosen for several reasons as a case study for all the analysis and considerations within the present thesis. The Emilia-Romagna littoral is a particular area because it is mainly characterised by sandy coasts and, thus especially exposed to coastal erosion. Moreover, at the same time, it is affected by natural and anthropic subsidence, like most of the Pianura Padana region. For these reasons, a more detailed characterisation of this territory is provided regarding both subsidence and erosion rates. A sub-chapter describes the Coastal Geodetic Network (RGC), a fundamental supporting infrastructure for all the surveys performed along the regional coast, and others describe the realised defence intervention and the typical wave climate.

In the introduction of the fifth chapter, a general background about available software and approaches is provided. Afterwards, the primary products employed for coastal studies are analysed in detail: topo-bathymetric maps (i.e. Digital Elevation Models), profile sections, maps of height variation, and shoreline. For each of these products, the basic principle and the possible processing approaches are described together with examples and in-situ tests in the Emilia-Romagna littoral. Moreover, the last part summarises the primary results acquired in the context of a paper published during

the PhD period: *GNSS and Photogrammetric UAV Derived Data for Coastal Monitoring: A Case of Study in Emilia-Romagna, Italy.*

The study developed during the abroad period is the object of the last chapter. The investigation aims to provide a framework to statistically model elevation errors of public sources with respect to measured datasets. Therefore, an extensive description of the adopted approach and the main achieved results are provided. The workflow has been completed, even if this should be considered a preliminary analysis. Moreover, some considerations concerning possible applications are reported, meaning the evaluation of the impact of the bed level data's accuracy on coastal hydro-morphodynamic models' results or the proper planning and investment decisions related to particular coastal studies.

Chapter 1

1 Coastal monitoring

Generally, monitoring objects or phenomena consists of observing their variations over time. Therefore, this activity becomes fundamental whenever dealing with dynamic phenomena characterized by a specific evolution, being the way to provide qualitative and quantitative information about their modifications. In order to be able to observe the movements or changes of a particular feature, a stable point of view is reasonably required. This is true for several applications since the observer's movement directly impacts the measured quantities. Consider, for example, the simple case of evaluating the velocity of a ship: by changing the observation point, the computed values of the velocity will accordingly change (Figure 1.). In particular, if the "absolute" velocity is needed, it should be computed from a position independent of the ship's movement.

Going back to a more specific context, in Geomatics, the observation point is realised through the definition of a fixed reference system. Moreover, since, in practice, monitoring activities consist of repeated observations of the same object, this requirement becomes even more fundamental to enable the observed quantities to be appropriately compared. The observation is carried out through the survey operation,

i.e. the measurement of a specific quantity employing a particular instrument. Therefore, monitoring activities can be seen as performing periodical measurements on the observed object and comparing the obtained results to deduce the variations over time. In other words, the chosen phenomenon is observed through measures repeated at subsequent epochs.

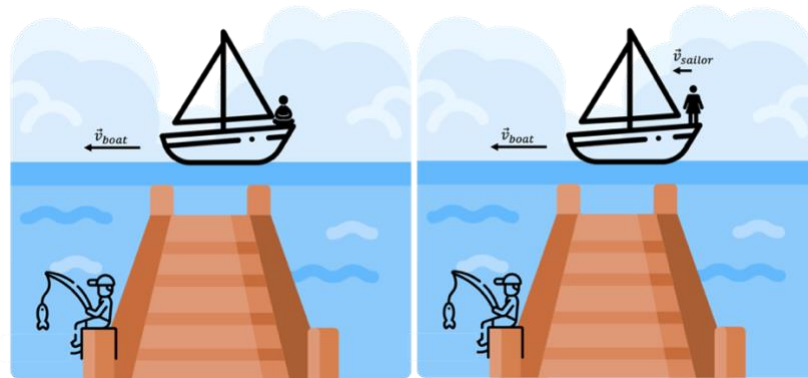


Figure 1.1 – Simple example showing the importance of ensuring the stability of the observation point. While the sailor remains seated, her velocity relative to the pier is the same as the ship, whereas when she moves, her velocity increases.

After these considerations, two general aspects of monitoring should be underlined: 1) the measurements must be realized following well-proven procedures to allow correct evaluations and comparisons after a certain time, 2) they must be referred to a shared reference system, which is stable over time, or at least less variable compared to the observed phenomenon.

In dealing with natural objects in three-dimensional space, there is a need to distinguish between the planimetric and altimetric aspects. Even if Chapter 2.1 deeply addresses this concept, it should be introduced here to contextualise some specific aspects in the coastal context.

Commonly, we define the coast as the strip of land that extends between the coastline and the first significant changes in the terrain's morphology, where the coastline is the boundary between the land and sea itself [94]. Nevertheless, the definition of the coast can also include part of the so-called *submerged beach*, i.e. the part which lies under the sea level.

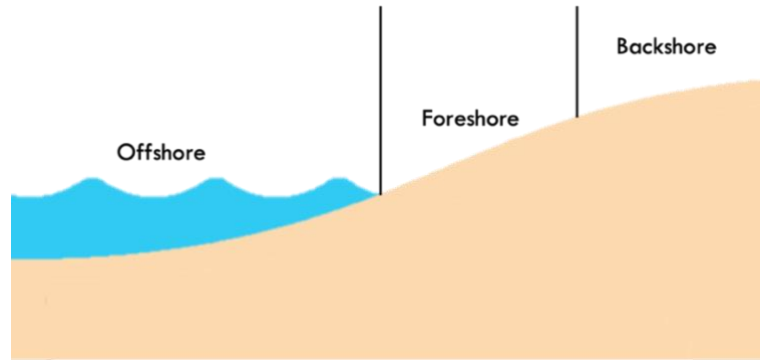


Figure 1.2 – Common shape of sandy coasts.

Many processes affecting the natural conditions of the coast come from offshore processes. Depending on the specific application, the coast's limit in the offshore direction can vary, leading to different extensions. Commonly, a valid parameter to identify this limit, or at least to select the area that should be certainly included in all the coastal analysis, is the closure depth (d_c). This parameter is used to identify the boundary between the beach groundward's active zone and the seaward's less active area, valid for a selected time span [135] [104]. Active zones are those affected by sediment transport, thus including both the submerged and emerged beach. The evaluation of the closure depth is a statistical analysis that needs to be referred to a specific period since it relies on observing wave climate-related events that can impact sediment transport at different depths. The approach proposed by Pranzini and Wetzel, 2008 relies on two different values of the d_c , typical and extreme [120]. The typical closure depth refers to the short-term analysis, thus daily, seasonal and annual events, while the extreme closure depth results from long-term events (from decades to centuries).

Then, a possible approach to measure this quantity relies on the formula by Hallermeier [65][66][138] (Eq 1.1):

$$d_c = 2.28H_{12} - 68.5 \frac{H_{12}^2}{gT_p^2} \quad \text{Eq 1.1}$$

Where H_{12} is the significant wave height that exceeds 12 hours per year; T_p is the associated peak period; g is the gravity acceleration.

Note that all the following analyses will refer to the bathymetry (depth) of about 8-10 meters as the offshore boundary, corresponding to the area involved in the monitoring activities considered throughout the present study.

The emerged beach is commonly identified as the *backshore*, the area between the shoreline and the first significant change in the morphology. Typically, this can be easily detected through the presence of natural dunes, cliffs, or artificial structures, especially if considering touristic beaches. The backshore zone can also be identified as the area usually affected by the waves' action only during storms or with high tide conditions (Figure 1.). The coastal environment is a complex landform characterized by a highly dynamic balance in time and space. Several coastline types can be distinguished globally, and their classification primarily depends on the sediment texture and composition of the in-situ material.

This study will focus on sandy coasts, which constitute a significant part of the world's coastlines, approximately 31% of the world's ice-free coasts and about 22% of the European shorelines [89] (Figure).

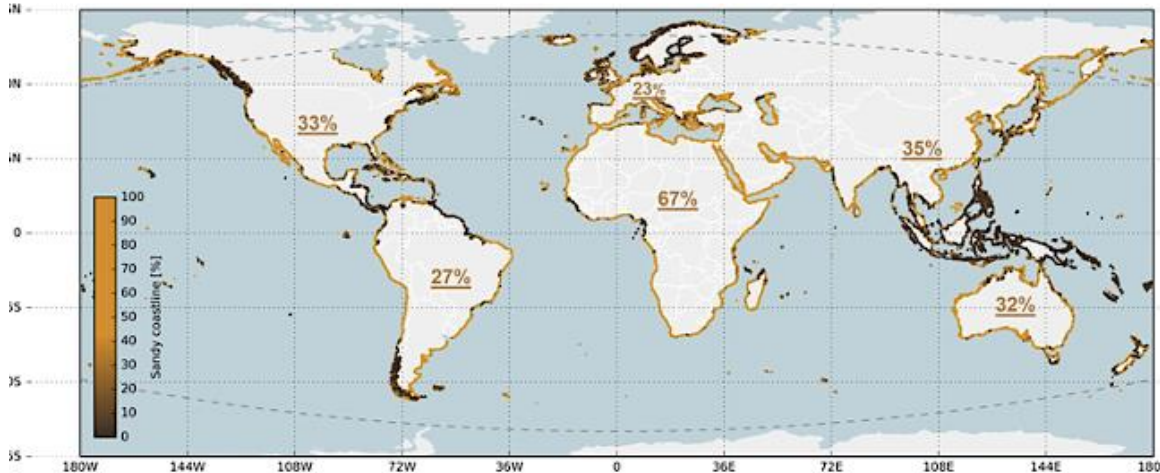


Figure 1.3 - Global distribution of sandy shorelines; the coloured dots along the world's shorelines represent the local percentage of sandy shorelines (yellow is sand, dark brown is non-sand). Source: [89] (modified).

Referring specifically to sandy beaches, phases of erosion and accretion can naturally occur (and are visible) within cycles operating over different ranges of time. Some of these cycles operate on short time scales, with frequent individual events primarily

related to the seasonal weather. This is the case, for example, of storm seasons leading to very variable erosion rates, which tend to stabilize after those periods. These processes can also be seen as short-term or episodic erosion (storm-driven), commonly followed by short-term accretion phases, therefore not significantly impacting over a more extended time scale for overall analysis [140][89]. The accretion process is generally slower than the erosion, and it naturally occurs during the quiescent seasons [198].

The coastal studies we are dealing with in the present work use to detect beach erosion when the amount of sand leaving a specific site is greater than the amount arriving (or remaining), and this situation persists with an established trend for long periods, thus resulting as a chronic problem [29][82][89]. This scenario is where monitoring plans over medium/long time scales are commonly realized, as it will be deeply explained in the following paragraphs.

In general, the erosion process is the result of the interaction between several processes, such as [48][49] (Figure):

- waves;
- sediment transport;
- subsidence of the coastal area;
- climate changes;
- human activities.

Wind-generated waves are significant as energy-transfer agents, and it is essential to evaluate their effects in the coastal zone, where they can create a variety of nearshore currents and sand transport patterns [82]. Littoral sediments play an essential role in maintaining beaches' balance because they can be naturally transported by the sea currents, leading to the rearrangement of the shoreline [82]. Rivers represent the primary source of sediments in coastal areas, subjected to directional movements from the river mouths. However, rivers' sediments have suffered from anthropic activities over time, such as the extraction of inert materials from river beds and rivers' regulation through damming, leading to a substantial decrease in supplied sediment

rates [34]. Subsidence is the phenomenon of lowering the Earth's surface caused by natural and anthropic processes. It only involves vertical movements, thus impacting the boundary between land and sea. Its anthropic contribution is primarily related to extractive activities, which significantly spread as standard practice during the last century. More recently, the awareness of their impact on the subsidence's velocity rates led to more limiting policies in this context. However, in some areas, even the subsidence's natural contribution can significantly impact the erosion process. Climate change is known to represent an issue regarding all environmental contexts. In particular, in coastal areas, the relative sea level rise and the increase in the frequency of storms should be considered on long-term scales, leading to possible accelerations of the erosion processes [198][129]. Finally, human activities in coastal areas primarily regard intense urbanization through the construction of touristic establishments involving both permanent and temporary structures on the beach. This creates higher pressure on coastal areas since, on the one hand, the amount of beaches designated for public use is reduced, and on the other hand, some of the natural processes may be altered or obstructed. This fact is particularly evident where the variations in beach morphology are linked to the longer cyclical changes in climate [198]. Sometimes, even the introduction of hard defence structures could have increased erosion due to the induced changes in the shoreline's configuration and the natural sediment transport patterns related to mismanagement practices. Moreover, the tourist use of coastal areas can lead to removing the protective vegetation induced by recreational activities and traffic [198]. All the listed aspects become even more critical if considering low sandy beaches, such as the ones addressed by the present study, where the land behind the coast is firmly flat and sometimes located under the sea level. In fact, as boundary areas, coasts also represent a natural defence which can protect the backside areas from potential water ingress.

It should be highlighted that since all the factors affecting the coastal dynamic interact, the morphology of sandy beaches continuously varies in time and space, and both in

the alongshore and cross-shore directions [35]. In this context, the discrimination between significant variations and other changes within the expected short-scale variability represents another potential issue.

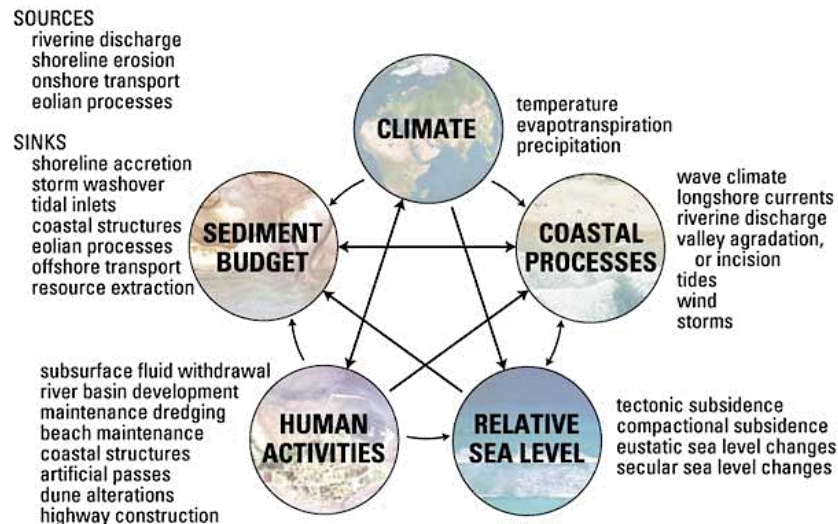


Figure 1.4 - Interactions of factors that influence land loss. Source: [200].

When referring to coastal areas, not only their environmental nature should be considered. In fact, several studies showed that the population densities in coastal regions are about three times higher than the global average [136][152], with a total of more than 200 million people living in areas lying less than five meters above the sea level [9]. This fact is historically due to the prosperity of such environments, with the coexistence of several ecosystems and important aesthetic qualities particularly suitable for many human activities. Therefore, the attraction of coastal areas resulted in their continuous development with the growth of economic and touristic activities over time and consequent intense urbanization. The study by [89] presented an up-to-date assessment of the erosion rates affecting sandy shorelines worldwide by applying a fully automated analysis of 33 years (1984–2016) of satellite images. Their founding showed, at a global scale, a 24% rate of sandy beaches experiencing erosion exceeding 0.5 m/y and about 16% exceeding 1.0 m/y. Moreover, other more severe erosion rates (up to 10 m/y) have been found with lower distributions.

In the Mediterranean area, more than 30% of the population lives close to the coasts [213], which also experiences very high tourist rates yearly [129]. The approximate rate of erosion occurrence in this area is about one-fourth of the coastline, depending on the specific country [153]. With its 7.500 km of natural coast, Italy is one of the European countries with the higher extension of coastline exposed to erosion processes: about 1250 km are underlying erosion processes [100] (Figure).

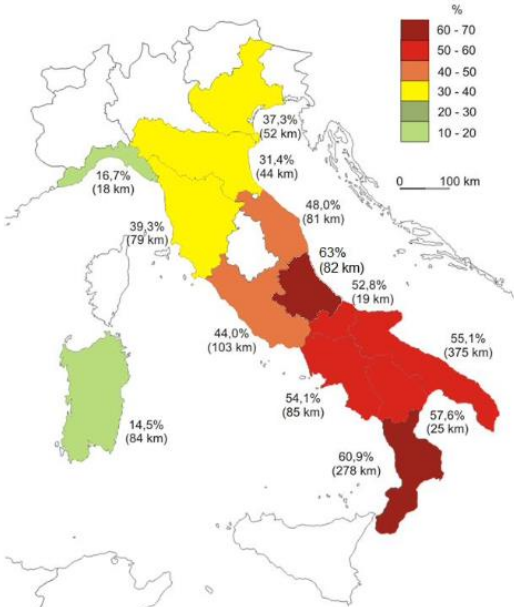


Figure 1.5 – Percentage of eroding coasts in the Italian regions. Source: [100].

Most of the analysis addressed by the present study concerns the Adriatic coast of the Emilia-Romagna region in Italy. This specific coastline has morphological characteristics that make it one of the most vulnerable areas, especially considering the touristic rates it yearly experiences, leading to even higher impacts during the summer period [152]. All the mentioned considerations reasonably make coastal monitoring a fundamental activity, that is, the way to recognize, assess and counteract the erosion phenomenon. Indeed, the monitoring represents the instrument for understanding the variability of the observed areas.

In the coastal environment, monitoring surveys deal in particular with two main quantities, heights and depths. The first refers to positive values, i.e. points above the considered sea level, while depths denote points under the sea level. Therefore, the

first issue to be addressed in this separation is related to the sign, also considering that sometimes, mainly for hydraulic applications, depths could be defined using positive values. This fact must be adequately considered when managing data, and the chosen reference system must properly contemplate this separation. For these reasons, the altimetric reference is the most significant aspect in coastal surveys, needing to ensure seamless measurements in the emerged and submerged beach. Hence, the broader concept of topo-bathymetry arises, i.e. the union between topography on land, and bathymetry on the sea.

The certainty of ensuring a stable perspective for observing any coastal change, i.e. the proper definition of the reference system to be used, is another essential issue. This is true for environmental monitoring in general, even though coastal areas require some additional clarifications. The chosen reference should be suitable for surveys on land and sea, with different specific characteristics and requirements. This fact also addresses the proper materialisations of the points to support the surveying activities. Moreover, since these areas represent a natural resource, many data sources could be available, needing a shared reference to be easily managed.

Coasts are areas of public interest in several fields, such as tourism, navigation, fishing, and maritime transport. For this reason, coastal monitoring activities are strictly connected with environmental policies and management, possibly aiming at maintaining stable situations on different time scales. Indeed, the erosion phenomenon is commonly handled by realizing defence interventions with different requirements according to the specific area [42]. As these activities are commonly carried out at a public level, there is usually the need to manage data from different sources, leading to even significant relevance of the supporting reference system. This is also true, considering that certain studies could need to deal with older data to perform long-term analysis on long observation windows [35].

In general, the main goals of coastal monitoring can be summarized as follows [25]:

- Coastal evolution analysis on a middle/long-term time scale in order to correctly set up management and intervention plans;
- analysis of the sedimentary rate to define the relation between river contribution and along/cross-shore dissipation of the material;
- short-term analysis of the coastal evolution to evaluate the impact of possible or already existing defence interventions;
- short-term analysis of the coastal evolution to evaluate the efficiency of newly completed defence interventions;
- investigation on the beachfront extension and quality, aiming at optimizing the anthropic use of the area.

About this last point and considering the tourist interest in coastal areas, usually monitoring plans include the definition of a beach width to be maintained as a target. All the mentioned activities addressed by coastal monitoring share the typical requirement of having a reliable overview of the territory of interest and of its critical issues. The study of any coastal evolution, and thus any environmental policy regarding the coast, is based on several parameters able to characterize the area, such as morphological aspects, shoreline, wave-climate, and sediment rates.

In particular, considering the dynamic nature of sandy coasts, affected by the interrelationship between agents, it is necessary to circumscribe the analysis to find possible solutions. Some key considerations are usually needed first to identify the specific object to focus on within a study, or in other words, which class of processes will be addressed. In these terms, a notable distinction could be between long-term processes rather than rapidly evolving ones (e.g. in the context of early warning). In fact, this first characterization can impact the exploitable methodology to carry out specific assessments. Other considerations should be addressed to define the suitable intervention approach for implementing adaptation plans or sustainable strategies [129]. This is also related to the time scale of the monitoring itself since each kind of intervention has different associated adaptation responses. Apart from early warning systems, which usually deal with storms' time scales, realized defence interventions

generally involve engineered hard structures or material filling, such as nourishments [140]. Lastly, the scale factor must be adequately defined, according to the expected size of the experienced processes, ensuring the ability to analyse the coastal evolution precisely.

In any case, monitoring projects for specific areas should include all this information, together with the plan for the topo-bathymetric surveys to be carried out. The common practice involves the definition of several cross-shore and along-shore transects where repeated data are required. Indeed, different geomatic techniques can be employed, whereas the approach always concerns repeated survey campaigns. Afterwards, advanced tools are required to process and manage coastal data properly. It should be underlined that coastal analysis relies mainly on 3D maps, named topo-bathymetric maps, representing heights and depths in the area. Moreover, the post-processing computations should be coupled with an analysis of the impact of different drivers on the empirical analysis. Anyway, a robust understanding of the critical physical processes driving the shoreline dynamics is always challenging [140]. Numerical modelling could represent additional helpful support to understanding how different factors can impact the observed phenomenon. In fact, to date, numerical modelling analysis represents a topic of great interest for sandy systems. Usually, these studies are based on long-term and large-scale continuous datasets to model the future evolution of the coast, together with theoretical assumptions, such as increased number and strength of storms, sea level rise, changes in rainfall or human pressure on the coast [140]. About this, reasonably, a certain level of uncertainty should always be considered since the rates of sea level rise are unknown, the available projections depend on global climate models, and the decadal oscillations in climate variability cannot be easily predicted. Moreover, numerical models usually rely on high-quality bathymetry data that is expensive to acquire [140]. This is another linking factor between all the suitable analyses and studies within the commonly applied framework in the context of coastal monitoring.

The following considerations aim to identify the correct and more suitable procedures to detect the evolution of erosion processes, starting from the need for a proper supporting reference system and studying possible employable survey techniques and processing approaches (Figure).

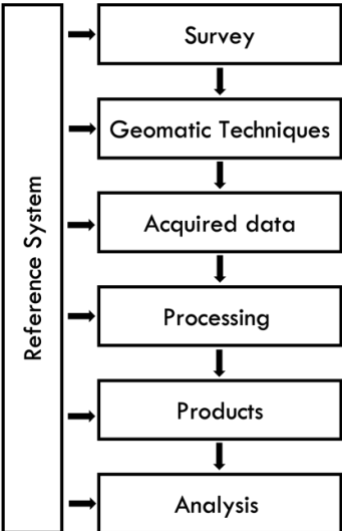


Figure 1.6 – Workflow of monitoring activities.

The close link between coastal monitoring and public authorities brings us to mention the Regional agency for prevention, environment and energy of Emilia-Romagna (Arpae), which manages several monitoring activities along the regional coast, together with the associated analysis and environmental policies. All the following considerations will address the Emilia-Romagna littoral, focusing on the procedures Arpae commonly carries out in the context of coastal erosion. The specific characteristics of this coastline will be deeply described in Chapter 4, bearing in mind that this region is exposed to erosion processes. Therefore, it should be noted that this study’s monitoring activities aim to identify any erosion/accretion patterns along the coast. Thus, the subject of all the observations is the erosion process itself. Moreover, all the activities are framed in the context of periodic nourishment interventions, representing the primary adopted strategy to counteract coastal erosion in the Emilia-Romagna region. For this reason, considerable attention will be given to the parameters required for this kind of activity, particularly sand volumes, i.e. the amount of sand exposed to changes due to the morphological variations of the beach.

Chapter 2

2 Geodetic Reference Systems

Everybody uses coordinates to share their position in several contexts of everyday life. However, by definition, the use of whatever coordinates is linked to a specific reference system, and different possibilities can be employed relating to the particular application. However, the systems' inherent characteristics and definitions must be known to share different sources of information.

When performing a survey, the first discerning parameter could be to observe an object independently or with respect to a particular geodetic reference system. In the first case, one can describe the object's shape and geometry using whatever local system tied to it. This means that any object's deformation can be detected, while its movements cannot. Indeed, the object's position is unknown since the local reference is not bound to any particular location. Nevertheless, evaluating any objects' movements over time (i.e. the monitoring) definitely requires knowledge of its location. In fact, a movement occurs when a change in position is observed. Therefore, a global reference system is required in this case, or the parameters describing the relation between the employed system and a global one. The use of a fixed reference system, indeed, provides the precise location of the observed object. For this purpose,

the reference must be bound in a certain way, impacting the detected movements. In particular, the observation's point should be fixed in time and space to evaluate the object's movements quantitatively. Nevertheless, the system's stability concept should consider different effects, depending on the spatial scale, since the territory itself can be exposed to relative movements.

In Geomatics, a Geodetic reference system (datum) is commonly represented by an oriented cartesian triplet with a defined origin and is related to the specific application, in particular:

- the complexity of the object to be monitored in terms of shape and dimensions;
- the magnitude of the expected deformations and coordinates variations, being the movements that one wants to be able to detect.

In practice, since it is hard to have a unique definition exploitable for different applications, several reference systems can be defined for different purposes or contexts. Then, these systems should be connected by defining their relative movements.

From a theoretical point of view, a suitable reference system could be quite easily defined. Contrarily, for its applicability in a natural context, there is the need for an arbitrary number of representative points responding to at least two different requirements: 1) they have to be directly measurable using one or more techniques, and 2) their associated coordinates have to be precisely defined. The illustrated requirements for practical use are actualised by the introduction of two different concepts, the Reference System (RS) and the Reference Frame (RF), so defined:

- The RS is the theoretical explanation of the system (mass centre, rotational axis, etc), which cannot be used at a practical level;
- The RF is the tangible materialisation of the RS, i.e. the coordinates of a chosen set of points distributed over the territory, allowing the link between the RS and the natural world and the practical use of the system itself.

Each RS requires the definition of the related RF, while the same set of points, i.e. the network, can be used to realise different reference systems. This means that the coordinates of a point can be defined according to multiple reference systems. This approach allows obtaining a set of parameters that can describe the relating position between the selected RSs and, therefore, the transformation to link one to the others.

Since the network which realizes the reference frame is distributed over physical objects, it could also be affected by the object's deformations/displacements over time. This aspect must be considered when choosing the maximum acceptable error for the coordinates related to a particular RS. The required precision in the definition of the frame depends on the RS specific use and impacts the techniques suitable to acquire the network's coordinates. Consequently, the reference frame must be adequately customized according to the magnitude of the expected detectable changes and the survey techniques employed. In fact, this latter aspect determines the practical design of the network's points in terms of localisation, materialization type, and density. Moreover, any inaccuracies affecting the RF's definition will affect all the measurements based on the frame's coordinates. In particular, the stability of the frame over time has to be ensured to avoid confusing points' movements with something related to the instability of the RF itself. Thus, the coordinates realising the frame can be redefined or updated, maintaining their connection with the system. The geodetic community is involved in the frames' maintenance, exploiting the available monitoring techniques to ensure an accuracy of one order of magnitude higher than the required for the related practical applications.

After these considerations, it is possible to classify the reference systems based on the techniques employed for their realization, classic or modern. Classic geodetic RS exploit observations obtained by traditional topographic instruments, i.e. angles and distances, gravimetrical and astronomical measurements. On the other hand, modern global RS are defined thanks to space geodetic techniques.

Classic RS need a separation between planimetric and altimetric aspects due to the inherent characteristics of the classical topographic techniques. This is mainly because, in practice, there is the need to use different instruments and techniques for the two aspects. Moreover, different specific requirements exist also in terms of supporting reference surfaces. Therefore, the definition of any point location is inherently distinguished between planimetric and altimetric features.

Concerning practical applications, the altimetric aspect, i.e. the problem of defining the height of points belonging to the Earth's surface, is commonly the most significant one since it is connected with the definition of the actual shape of the Earth. Nevertheless, the height concept presents several issues both in its analytical definition and measurement. Therefore, the concept of the altimetric reference requires a separate discussion, which becomes even more significant concerning coastal areas.

2.1 Altimetric reference systems

“Vertical reference systems, valid for regional parts of the Earth's surface, can be established in different ways, based on the type and availability of observational data” [70]. In particular, the practical use of a system typically requires the definition of a reference surface and its orientation in the space. On the other hand, the conceptualization of such a reference can be complex since no unique surface meets these requirements.

Concerning the Earth, the solution was found by considering the terrestrial mass, which leads to the presence of an associated gravity field (W). The link between the gravity force and some physical behaviour is also evident in many real-life situations. Since it is proved that this field allows an associated potential, equipotential surfaces (or level surfaces) of the gravity field can be defined, where $W = const$. The main characteristic of these surfaces is the fact of being point-by-point normal to the gravity vector [102]. Note that even if this definition can partly solve the problem, in practice,

it is not simple to perform precise and point-wise measurements of the gravity force to determine the related equipotential surface. At this point, in order to define a global vertical datum, a particular one of these surfaces can be distinguished (Eq 2.1):

$$W(x, y, z) = W_0 = \text{const} \quad \text{Eq 2.1}$$

This fixed level surface, called geoid, represents the equipotential surface of the Earth's gravity field passing below the topographic masses and approximating an average surface of the oceans (Figure) [146][102].

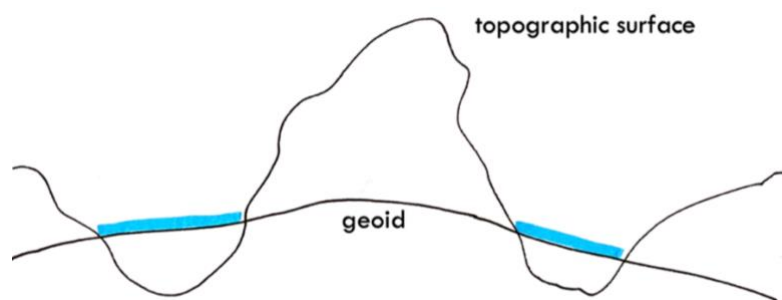


Figure 2.1 – Geoid surface definition with respect to the topographic surface and the average surface of the oceans.

Evidently, the geoid shape cannot be regular as a sphere due to the Earth's rotation around its axis, leading to differences in the force at the poles and the equator and the uneven distribution of the terrestrial masses (Figure).

Dealing with the altimetric aspect, it is essential to distinguish between the concept of height difference and the concept of height in absolute terms. In general, there are no particular issues in defining if a point is higher or lower than another, just considering that the water flows from higher to lower points by nature. For the same reason, the two considered points are characterised by the same heights if no water movement is present. This fact again is related to the gravity field; therefore, all the fluids that undergo a gravity potential tend to move toward higher potentials. Hence it is possible to obtain the first definition since if two points are located on the same equipotential surface, they also have the same associated height. Considering any equipotential surfaces, their lines of force are the orthogonal trajectories, and the tangent to a line of force at any of its points is in the direction of the gravity vector (g) [102]. Being P a

point located on the topographic surface (i.e. the physical Earth's surface), the orthometric height of P can be defined as the length of the line of force which goes from the point itself to the surface of the geoid, which is intersected in P_0 (segment PP_0) (Figure).

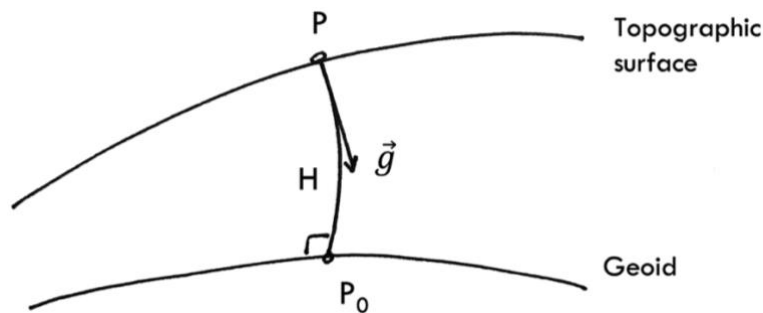


Figure 2.2 – Orthometric height (H).

Since the definition of the geoid is based on a specific value of the sea level, particular instruments, named tide gauges, are required to compute the zero level for the heights. These instruments can detect the sea level's position at a specific point, describing its variation over time. It is known that seas continuously undergo the gravity force; nevertheless their equilibrium is disturbed by irregular movements, such as winds and waves, and by cyclic oscillations, i.e. the tides, which depend on the interaction between the Sun, the Moon, and the oceanic masses. These effects are known as Sea Surface Topography, and combined with any variations in the water density, due to temperatures, currents, or salinity (local phenomena at tide gauge stations), result in different level surfaces corresponding to different tide gauges zeros [70]. Since the sea level's variation at different time scales can reach the centimetre or decimetre level, the precise location of the geoid must be estimated by analysing long time-series of tide gauges acquisitions of about a few decades. Commonly, each country's altimetric reference system is based on a single specific tide gauge, representing the starting point for the propagation of high-precision levelling networks.

Note that for the Italian peninsula, the fundamental tide-gauge, managed by Istituto Idrografico della Marina (IIM), is located in Genoa, while tide-gauges in Catania and Cagliari are used for Sicily and Sardinia islands, respectively. Therefore, the national

reference geoid for Italy is bounded to the sea level in Genova in 1942, computed by averaging ten years of observations between 1937 and 1946.

The considered tide gauge zero level for a specific country represents the starting points which allow the measurements' alignment to the geoid surface on the mainland. Levelling networks are defined starting from the selected reference tide gauges, thus defining the orthometric heights of several points distributed over the territory. The orthometric heights of these points are computed considering the differences in height (with respect to the zero level) from long-range spirit levelling measurements, and they realize the national altimetric reference system exploitable for the alignment of any performed local survey. The classic spirit levelling technique allows measuring differences in height with high associated accuracy, meaning distances along the same line of force, resulting in a fundamental instrument when dealing with the altimetric aspect. In Italy, the altimetric reference system was realized by the IGM (Istituto Geografico Militare) in 1950-1971, consisting of about 13.000 benchmarks, later increased to about 20.000.

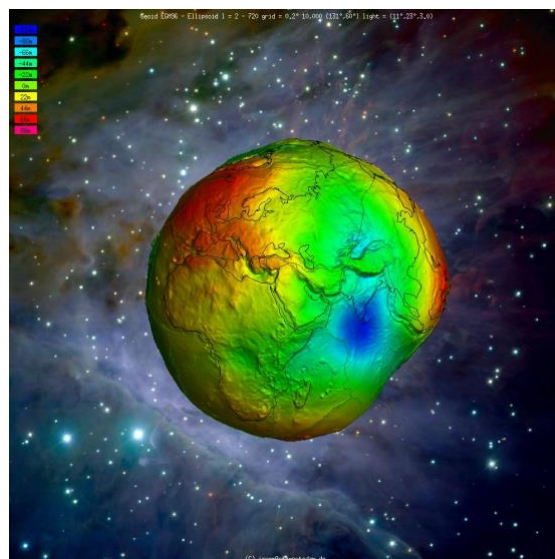


Figure 2.3 – Representation of the EGM96 geoid model. Source: [168].

Although the geoid is the fundamental surface for several applications in Geodesy, and it is the most suitable option to describe the Earth's physical surface, its shape is irregular, and it is impossible to describe it through a simple mathematical equation.

However, a reference surface’s suitability for practical applications is strictly related to the possibility of efficiently representing objects, allowing mathematical operations, and measuring angles, distances, and areas. Two are the main characteristics required in these terms: 1) to have a pretty simple definition expressible using a closed analytical form; 2) to adequately approximate the physical surface of the Earth, both in terms of shape and dimensions. In this regard, a simplification of the geoid has been introduced to solve this issue. The ellipsoid of revolution is generated by rotating an ellipse around the Earth’s z-axis, and it can be defined by using only two parameters (Figure). It represents the approximation of the geoid expression at the second magnitude order, and it can be analytically described in a cartesian reference system (Eq 2.2):

$$\frac{x^2+y^2}{a^2} + \frac{z^2}{b^2} = 1 \quad \text{Eq 2.2}$$

Where *a* and *b* are major and minor semi-axes of the ellipse, and the intersection between the positive and negative z-axis are named North Pole and South Pole, respectively.

Even if such a simplification leads to the loss of the physical meaning related to the gravity field included in the geoid’s definition, the ellipsoid of revolution can adequately describe the compression at the poles typical of the Earth due to the inertial forces caused by the rotation around the z-axis.

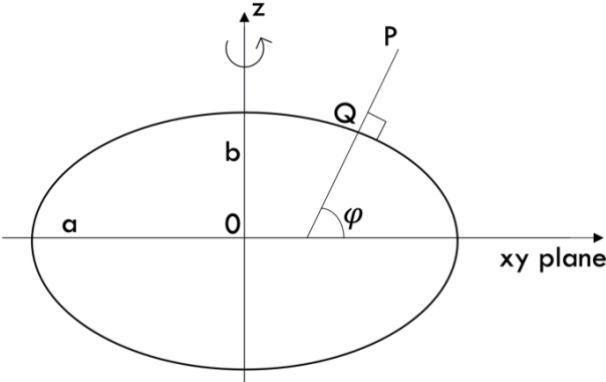


Figure 2.4 – Cartesian triplet and related ellipsoid.

At this point, the height with respect to the ellipsoid surface can also be defined. To do this, the considered point P is projected onto the ellipsoid by the straight line normal to its surface, intersecting with point Q (Figure). Thus, the segment QP represents the ellipsoidal height (h) of point P , being the distance from the point itself to the ellipsoid's surface. Since the ellipsoidal height comes from a geometrical-based definition and is not bounded to any physical constraint, typically, it is not used for all surveying applications, especially water management.

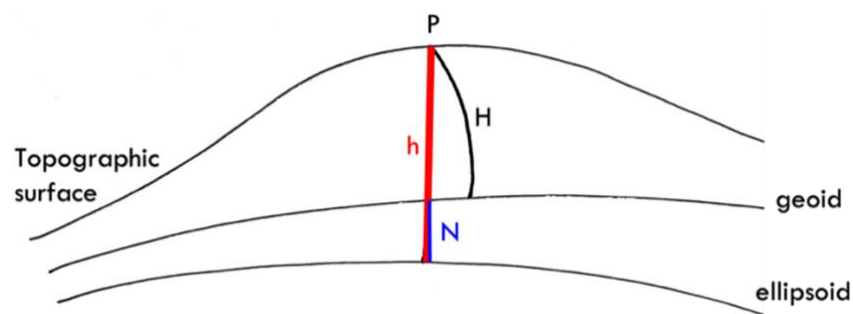


Figure 2.5 – Orthometric and ellipsoidal heights and geoid undulation.

Due to the complexity of the geoid's shape, the mathematical approximation realized by the ellipsoid can lead to different levels of coherence between the two surfaces depending on the observed area. This coherence is meant to be the deviation between the local vertical with respect to the geoid and the straight line normal to the ellipsoid. In order to reach better coherence in specific areas for practical survey applications, different computations of this mathematical surface have been developed depending on the chosen extension and location. According to this, the geoid itself can be defined as the altimetric correction to be applied at any point of the ellipsoid surface: this correction is named geoid undulation (N) (Figure).

Reasonably, a single definition of the ellipsoid of revolution can be used globally, while dealing with specific regions, it is possible to consider different local ellipsoid shapes and orientations. In fact, the interrelationship between the geoid and ellipsoid surfaces depends on the shapes and dimensions and their relative orientation. Classical Geodesy addresses this problem by defining the so-called Geodetic Datum,

the set of parameters describing the ellipsoid's dimensions and position with respect to the geoid. In particular, different datums can use the same ellipsoid's shape by changing its orientation [145]. Operatively, any Datum has to distinctively fix the ellipsoid's position with respect to the topographic surface using a set of constraints:

- the relative deviation between the ellipsoid and the topographic surface is bounded at a specific point (origin) of known coordinates, where the local vertical is assumed to coincide with the straight line normal to the ellipsoid;
- the ellipsoid's direction is fixed by making the ellipsoidal azimuth between 2 points (i.e. the origin and an additional one of well-known coordinates) coincident with the astronomical one;
- the ellipsoidal and orthometric heights are made coincident at the point of origin.

Reasonably, this coherence ensured at the origin of the specific Datum gradually decreases with the increasing distance from it, leading to possible higher values of the vertical deviation. For this reason, the extent of the considered area represents the most impacting factor on the proper choice of the orientation's parameters, thus on the reached values of geoid undulation [145].

2.2 Geoid undulation

As mentioned, the geoid undulation (N) represents the separation between the reference ellipsoid and the geoid itself [125]. The accurate estimation of the geoid undulation has become fundamental, especially in the last decades, with the increasing use of GNSS and other spatial techniques for surveying and monitoring. In fact, all the techniques that use satellite orbits as constraints for their measurements are bound to relate the height component to the geometric surface of the reference ellipsoid, thus directly providing the ellipsoidal height only [146]. Orthometric height can be determined using geoid undulations in the case of points surveyed using a space technique, especially in those areas where levelling measures suffer from logistic

problems. In general, different techniques allow computing geoid models, such as gravimetric measurements, astronomical measures of the vertical deviation, satellite orbits and point-wise differences between GNSS and levelling heights.

To date, several models of geoid undulation are available both at the global and regional scales. These models have been developed over time, starting from satellite gravimetric measurements (Gravity Recovery and Climate Experiment (GRACE) by NASA and DLR, and Gravity field and steady state Ocean Circulation Explorer (GOCE) by ESA) and modelling the geoid's shape using a series of a certain number (up to 2.190) of spherical harmonics cut at a defined degree. Moreover, global models can be locally adapted, having available a suitable number of points whose heights are known in both the altimetric systems [51]. Different geoid undulation models usually show biases due to the specific choice adopted in reference datum [11]. In general, local models can be more reliable with respect to global ones, especially where particular morphologies are present, so they can be missed at a global level without using local data [111].

The official geoid model in Italy is the ITALGEO2005, computed by the Politecnico di Milano in collaboration with the Military Geographical Institute (IGM) of Florence [14]. This model is usable for the Italian peninsula, islands, and immediately adjacent areas (Figure). The area covered by the estimate is $35^\circ < lat < 48^\circ$, $5^\circ < lon < 20^\circ$, with a grid spacing of 2' both in latitude and longitude [219]. The model has been computed using gravimetric observations integrated with GNSS and spirit levelling measures on selected points belonging to the national geodetic levelling network (IGM95), astronomical measures, and considering the local topography. The declared accuracy is around 4 cm for the mainland and 5 cm for Sicily and Sardinia [15]. The ITALGEO2005 model is available in the form of IGM. (gk2) grids, and a customized software can also manage it, ConvER3_2013 [190], which allows different processing [11].

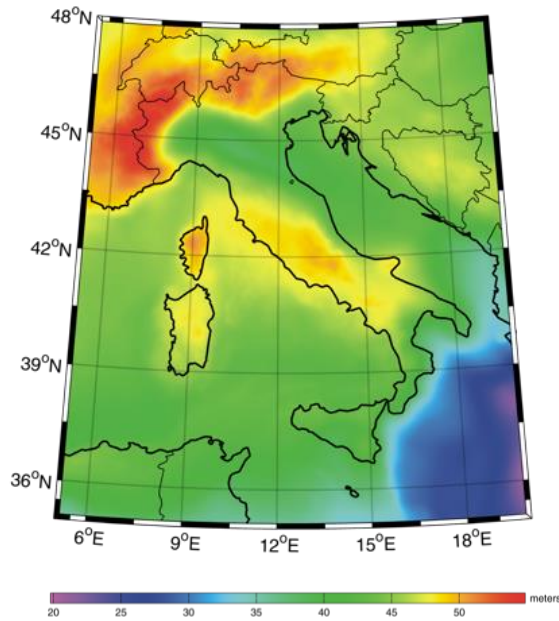


Figure 2.6 – Geoid undulation model ITALGEO2005. Source: [219].

The latest geoid model available for the Italian region is the ITG2009 (Figure). The area covered by this geoid estimated is $37^\circ < lat < 48^\circ$, $6^\circ < lon < 19^\circ$, with a grid spacing of $1.5' \times 1.5'$ [220]. This gravimetric geoid was computed based on the EGM2008 (Earth Gravity Model released by the U.S. National Geospatial-Intelligence Agency (NGA) EGM Development Team in 2008) geopotential model, using the digital terrain model SRTM90m [109]. This choice was because the EGM2008 global model proved to be very effective in fitting data, especially in the central Mediterranean area.

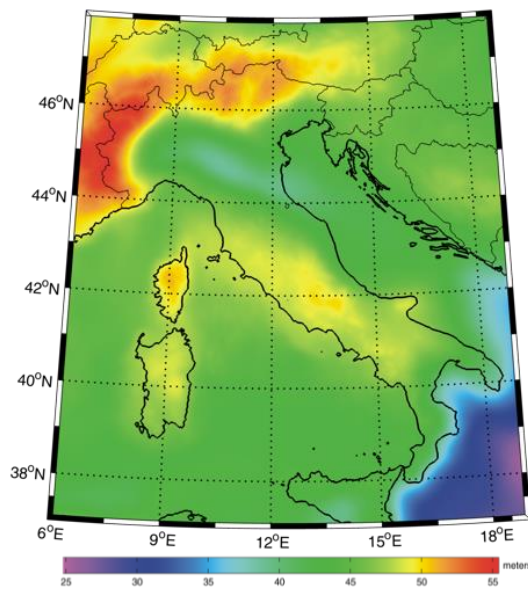


Figure 2.7 - Geoid undulation model ITG2009. Source: [220].

The study by [32] checked the ITG2009 model's accuracy by comparing its values with geoid undulations computed on validation points located within the study area. This analysis confirmed an improvement in precision and reliability and a better fit of the point-wise undulation values with respect to the EGM2008 over the Italian area.

As said, a possible way to compute the geoid undulation could be to compare over common points the ellipsoidal height defined through GNSS positioning and the orthometric height measured through spirit levelling [139][21][106]. Reasonably, this approach cannot be globally applied because of the logistic limitations in the application of spirit levelling, but it can be helpful at the regional scale [146].

In the article *"Definition of the Local Geoid Undulation Using Non-contemporary GNSS-Levelling Data on Subsidence Area: Application on the Adriatic Coastline"* [146], of which I am co-author, we investigated the possibility of calculating a GNSS-levelling derived model for the local geoid undulation along the coastal area of Emilia-Romagna, in Italy. This model could provide a way to correct the ellipsoidal heights more consistently with the orthometric data already available. One of the critical points in this work is the unavailability of contemporary measurements with both GNSS and spirit levelling, combined with the fact that the whole area is affected by significant subsidence phenomena [1][93][148]. Hereafter, the main results of this study will be described, including the proposed strategy to deal with non-contemporary height values, together with a discussion on the expected accuracy of the geoid undulations estimated on-site.

Fifty-one benchmarks along the coast of the Emilia-Romagna region were chosen, whose orthometric and ellipsoidal heights were not referred to the same epoch (see Chapter 4.1). The methodological approach considers the undulation value as invariant to the subsidence phenomenon, while the subsidence's impact on the calculation in non-contemporary measurements is considered. For this reason, the computation of the local geoid undulation N needed for the updating of both the

height values to a common epoch. Piecewise linear models of height variations were used to compute the contribution of the subsidence phenomena, and the chosen epoch to update the height components was 2018.0, being it about in the middle of the GNSS surveying campaigns and relatively recent time.

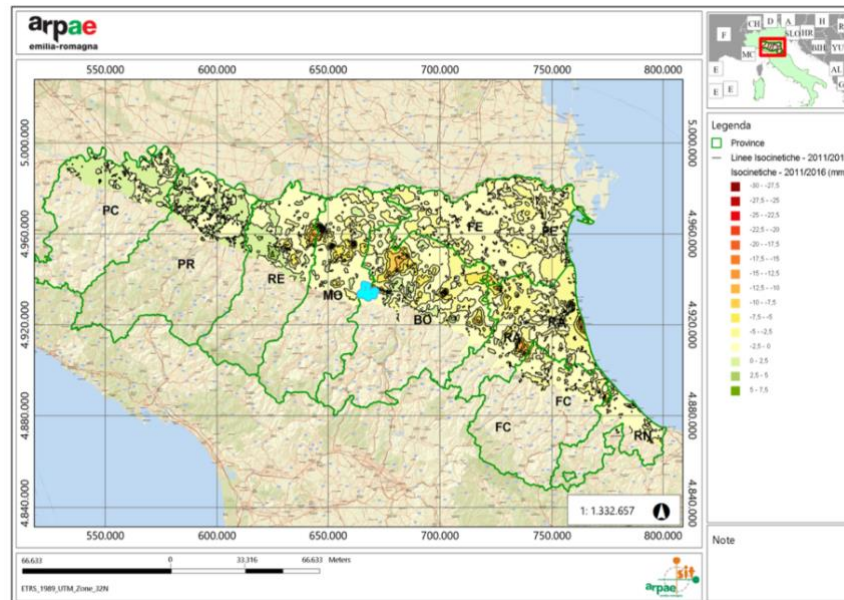


Figure 2.8 – Subsidence model for the period 2011/2016 extracted from the cartographic website of Arpae. Source: [205].

To do this, Subsidence Models provided by the Emilia-Romagna region have been used: these have five-year validity and are based on InSAR data [20][45][46] (Figure). Official models for the periods 2006-2011 and 2011-2016 were used for the analysis, whereas values for the later period have been extrapolated at epoch 2018.0 (the up-to-date model was not already available). Note that Chapter 4 will address this topic with a higher level of detail.

As for ellipsoidal heights, values for each benchmark were updated at epoch 2018.0 following the formula:

$$h_{2018.0} = h_t + \Delta t * v_s \quad \text{Eq 2.3}$$

Where h_t is the ellipsoidal height at the measurements epoch, Δt is the period ranging from the such epoch and 2018.0, and v_s is the subsidence rate provided by the most recent model in the corresponding location of the considered point.

The orthometric heights were updated at 2018.0 by applying the formula in Eq 2.4:

$$H_{2018.0} = H_t + \Delta t_1 * v_{s1} + \Delta t_2 * v_{s2} \quad Eq\ 2.4$$

Where H_t is the orthometric height at the measurement epoch (mostly 2005, while 1999 in a couple of cases). Δt_1 and v_{s1} are the period and related subsidence rates valid before 2012, whereas Δt_2 and v_{s2} are related to 2012–2018.0.

Starting from the height values referred to the 2018.0 epoch, the experimental undulation for each point has been calculated through the simple equation:

$$N = h - H \quad Eq\ 2.5$$

Table 2.1 reports the values in the calculus for each of the considered benchmarks, being the ellipsoidal and orthometric heights and the obtained geoid height.

Intending to estimate the a-priori accuracy of the experimental values of geoid height, we combined the uncertainties of all the measures by applying the covariance propagation law. Because of the poor knowledge about the considered uncertainties, we focused on defining a single value suitable for all the points. The accuracy for the subsidence models (σ_{subs}) can be considered about 2 mm/year for both the selected periods, as stated in [45][46]. The accuracy of the orthometric heights (σ_{Hi}) provided by spirit levelling campaigns can be considered about 7 mm, as declared by the involved authorities [44]. For what concerns the levelling measures carried out in 2019, we considered an accuracy equal to 1 mm (σ_{lev}), being the involved distances of a few hundred meters. The last uncertainty to be considered is that of the ellipsoidal height (σ_h) obtained from the GNSS measures. For this evaluation, we considered the a-posteriori standard deviation obtained in the network adjustment, whose average value over the 51 benchmarks is about 32 mm.

Table 2.1 - Ellipsoidal heights (Columns 2, 6) and orthometric heights (Columns 3, 7) at 2018.0 epoch. Columns 4 and 8 report the experimental undulations in the chosen benchmarks.

| RGC id | h (m) | H (m) | N (m) | RGC id | h (m) | H (m) | N (m) |
|----------|-------|-------|-------|----------|-------|-------|-------|
| GABI0100 | 45.33 | 4.88 | 40.45 | SAPC0400 | 40.35 | 1.17 | 39.18 |
| CARI0100 | 42.84 | 2.40 | 40.44 | SAPC0500 | 40.56 | 1.38 | 39.19 |
| CARI0010 | 42.81 | 2.38 | 40.43 | SAPC0600 | 43.34 | 4.17 | 39.17 |
| CARI0200 | 42.32 | 1.91 | 40.41 | SAPC0650 | 39.97 | 0.71 | 39.25 |
| CARI0210 | 42.27 | 1.88 | 40.38 | SAPC0700 | 41.33 | 2.05 | 39.28 |
| CARI0300 | 43.46 | 3.15 | 40.30 | PCPG0020 | 41.96 | 2.58 | 39.39 |
| CARI0400 | 43.69 | 3.49 | 40.20 | PCPG0010 | 40.93 | 1.49 | 39.44 |
| CARI0500 | 43.10 | 3.01 | 40.08 | PCPG0100 | 41.08 | 1.64 | 39.44 |
| CARI0600 | 42.94 | 2.96 | 39.98 | PCPG0200 | 41.68 | 2.11 | 39.57 |
| CARI0700 | 41.72 | 1.83 | 39.89 | PCPG0300 | 40.36 | 0.68 | 39.68 |
| RICE0100 | 42.68 | 2.81 | 39.87 | PCPG0400 | 41.51 | 1.68 | 39.82 |
| RICE0200 | 42.57 | 2.77 | 39.80 | PCPG0450 | 41.57 | 1.69 | 39.88 |
| RICE0300 | 42.33 | 2.57 | 39.76 | PCPG0500 | 41.56 | 1.58 | 39.98 |
| RICE0400 | 42.85 | 3.29 | 39.56 | PCPG0600 | 41.93 | 1.78 | 40.14 |
| RICE0500 | 41.55 | 1.97 | 39.58 | PGFV0100 | 42.08 | 1.82 | 40.26 |
| RICE0550 | 41.01 | 1.49 | 39.51 | PGFV0200 | 44.11 | 3.74 | 40.37 |
| RICE0600 | 41.83 | 2.36 | 39.47 | PGFV0300 | 43.14 | 2.53 | 40.61 |
| RICE0700 | 42.01 | 2.54 | 39.47 | PGFV0400 | 42.73 | 2.08 | 40.65 |
| CESA0100 | 40.99 | 1.60 | 39.39 | PGFV0500 | 41.06 | 0.20 | 40.86 |
| CESA0200 | 41.40 | 2.10 | 39.30 | FVFG0500 | 42.20 | 1.43 | 40.77 |
| CESA0300 | 41.17 | 1.96 | 39.21 | PGFV0600 | 43.58 | 2.61 | 40.97 |
| CESA0400 | 40.74 | 1.63 | 39.11 | FVFG0400 | 43.07 | 2.00 | 41.07 |
| SAPC0100 | 43.01 | 3.90 | 39.10 | FVFG0300 | 42.44 | 1.30 | 41.14 |
| SAPC0150 | 40.58 | 1.50 | 39.08 | FVFG0100 | 41.77 | 0.55 | 41.22 |
| SAPC0200 | 40.49 | 1.39 | 39.10 | FVFG0200 | 39.35 | -1.92 | 41.27 |
| SAPC0300 | 41.41 | 2.24 | 39.17 | | | | |

Due to the error propagation, combining Eqs. 2.3, 2.4 and 2.5, we obtained the accuracy associated with our experimental undulation values:

$$\sigma_N = \sqrt{(\sigma_h)^2 + (\sigma_{H_i})^2 + (\sigma_{lev})^2 + (\Delta t_H + \Delta t_h)^2 * (\sigma_{subs})^2} \quad Eq. 2.6$$

Where Δt_H is the period between the measuring epoch (assumed to be 2005) of the original orthometric heights and the final epoch 2018.0, and Δt_h is the period between the average measuring epoch for the GNSS measures (2017.08) and 2018.0, both expressed in years. It is essential to underline that for simplicity, the levelling measures have been considered for all the benchmarks while actually involving only 11 points,

thus obtaining a slightly overrated final value. Using the listed values within Eq 2.6, the estimated a-priori accuracy of the undulation was about 4.3 cm.

The experimental undulations have finally been compared with the point-wise values extracted from different geoid models, the Italian official ITALGEO05, the more recent ITG2009, and the EGM2008 global model. Because of the particular geometry of the chosen benchmarks, which are mostly aligned along a straight direction, we have chosen to solve the biases between the four considered realizations of geoid undulations using linear regression.

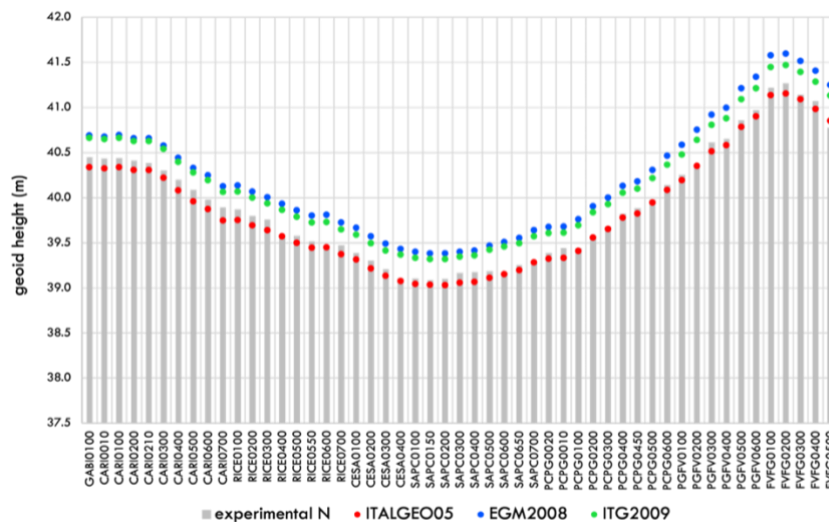


Figure 2.9 – Geoid heights computed over the benchmarks positions: experimental GNSS-levelling values (grey bars), ITALGEO05 (red dots), EGM2008 (blue dots) and ITG2009 (green dots).

Figure shows the experimental values of geoid undulation and the extrapolated values in the corresponding positions for the three employed geoid models. A general agreement between the estimations can be noticed, with a better alignment between ITALGEO05 and the experimental values, whereas EGM2008 and ITG2009 values are higher and close to each other. This result is not surprising: ITG2009 and EGM2008 are based on the same computation with a difference in the fitting area [32], and the ITALGEO05 is the official reference for Italy.

The straight regression lines for each set of geoid heights were computed and are reported in Figure . A general tilt is present, moving along the coastline from South to

North. The geoid height differences from South to North are 70 cm for the experimental geoid height (m) data and 76.5 cm, 74 cm, and 82 cm for the ITALGEO05, ITG2009 and EGM2008 respectively.

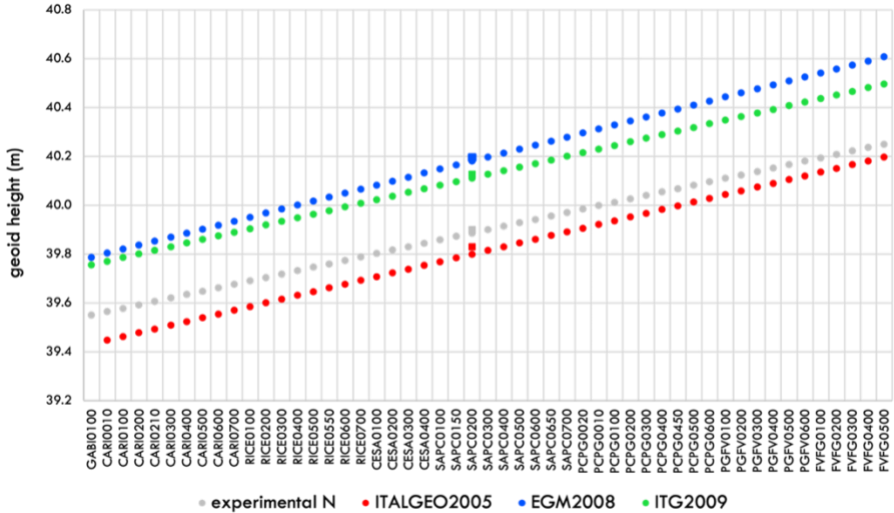


Figure 2.10- Regression lines used to define and remove biases between the three sets of geoid heights: experimental GNSS-levelling values (grey dots), ITALGEO05 (red dots), EGM2008 (blue dots) and ITG2009 (green dots).

The ITG2009 geoid model, the most recent and refined Italian model, shows the tilt closer to the experimental data. The mean biases between the experimental data and the geoid models are -7 cm, 23 cm and 30 cm for the ITALGEO05, ITG2009 and EGM2008, respectively. All these values can be considered significant for the GNSS and spirit levelling precisions in measuring the height. Therefore such biases have to be taken into account. Regarding the 7 cm bias with respect to the Italian official model, this could be due to possible mistakes in the definition of the origin of the Levelling Network considered in the computation of the experimental value of N. In fact, some discrepancies are known to affect the heights of reference benchmarks belonging to networks for monitoring applications [110].

In any case, the obtained differences between the regression lines can be explained as the difference that could result from applying one of the models with respect to another to correct ellipsoidal heights measured along the coastline.

However, the coherence of the experimental geoid heights has proven to be in line with the expected accuracy of the available data. Widespread biases of several centimetres between the experimental data and the models have been found because of the different references used to identify the geoid itself. Therefore, we eliminated these biases for further analysis by subtracting the straight regression lines from each geoid model.

In order to eliminate biases and trends from each dataset, residual values between each geoid undulation dataset and its associated regression line were computed. Assuming the averaged value of these residuals as a reference, the differences between each set of residuals and this mean were calculated. Figure shows the computed differences, where zero is the average of the 3 models residuals. The geoid models are scattered around their mean value with an RMS at the 1 cm level, which is within the accuracies declared for their determination [123]. Nevertheless, local differences higher than 4 cm can be found over specific points, particularly between the ITALGEO05 and the EGM2008. GNSS-levelling geoid heights are more scattered with respect to the reference, meaning 3.4 cm in terms of RMS with a couple of data up to 11 cm far. Considering a normal distribution of the measuring errors and a three-sigma confidence interval, all these data are compatible with the a-priori uncertainty of 4.3 cm. Differently, considering the measures' a-posteriori dispersion, two points (-11.2 cm, -9.9 cm) are not compliant with the measuring errors. These differences can lead to different possible interpretations: on the one hand, they can be due to gross errors in the measures, but they can also be related to local deviations of the geoid due to particular conditions that cannot be modelled by gravimetric data at the national/global scale. The latter hypothesis does not seem to apply to one of the points since the area surrounding it is similar to the neighbouring coastline. Differently, the other point is located in a very particular area in the North of the regional coast, the Sacca di Goro lagoon, at the extremity of a small peninsula. This might induce a

gradient in the gravity field close to the area, which is hardly unrecognizable by large-scale data.

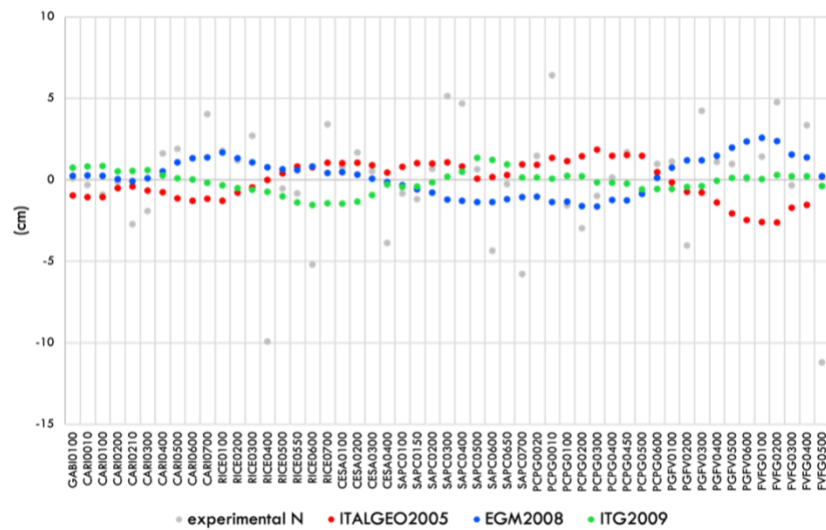


Figure 2.11 - Local differences between each geoid height determination and the reference defined as the mean value of the three considered gravity models: experimental GNSS-levelling values (grey dots), ITALGEO05 (red dots), EGM2008 (blue dots) and ITG2009 (green dots).

The last discussion concerned the possibility of using already existing geomatic data to estimate local models for the geoid heights. Therefore, the opportunity to extend the adopted approach was taken into account by analysing the requirements necessary to reach an accuracy sufficient to obtain a trustable reference and a real improvement with respect to global/national geoid models. In fact, due to the obtained values in terms of a-priori and a-posteriori uncertainties, it is not fair to use the experimental data as a local correction of the geoid's shape. Hence, we analysed the possible way to enhance the measurement accuracy in detail. As a first component, the uncertainty related to the spirit levelling did not significantly impact the final result given by Eq 2.6. Therefore we examined how the a-priori accuracy would have improved in the case of contemporary measuring campaigns for GNSS and spirit levelling, obtaining a successful variation from 4.3 to 3.2 cm. Reasonably, this hypothesis leads to the same results of considering the subsidence models as not affected by any uncertainty. When varying the other inputs, the ellipsoidal height given by the GNSS measurements was the most impacting source of error: by reducing its uncertainty from 3.2 to 1 cm, the final uncertainty of the model results equal to 3 cm. Finally, the best scenario

considered the combined use of contemporary acquired data and ellipsoidal height defined with 1 cm uncertainty, resulting in estimating the geoid height accuracy of about 1.2 cm. Nevertheless, the only way to reach this accuracy in the GNSS height definition requires performing observing sessions much longer than 1-2 hours.

Despite the considerations mentioned above, the computed experimental geoid undulation can be used to transform ellipsoidal heights measured using satellite systems into orthometric heights more coherently with the reference already defined in the considered area.

2.3 Sea level reference

When dealing with surveys in the submerged beach, i.e. depth measurements at sea, it is necessary to have awareness about the sea level reference used. In fact, detected depth values refer to a specific sea level, commonly known as *chart datum*. Existing sea level references are primary related to marine applications, which rely on different datums depending on the area of interest and specific purposes. Each nautical chart states the datum used for the alignment, which can be either local or regional and refer to different tidal conditions.

In particular, the standard datum for nautical charts is the Lowest Astronomical Tide (LAT). This value represents the lowest possible sea level due to the astronomical tidal movements caused by lunar and solar gravity, typically the most dominant components affecting the level's changes [189]. Otherwise, the meteorological tide is the component governed by the weather, in particular wind and pressure variations.

Using the LAT allows for being conservative, as it ensures that the actual sea level at the moment is always equal to or higher than the one stated in the chart (Figure). In fact, it is only possible to have water levels below the LAT due to weather influences, such as high air pressure or seaward breeze [187]. For this reason, the LAT can be

referred to as the lowest theoretical water level, and it may not be actually reached every year. It is computed by considering the lowest tide levels predicted during a period of about 19 years. To be exact, the acquisition period is 18 years and seven months, equal to the time required for the Moon to repeat its complete path relative to the Earth. This calculus allows considering the change in tilt and orbit of the Moon's movement around the Earth due to the Sun's gravity action [208].

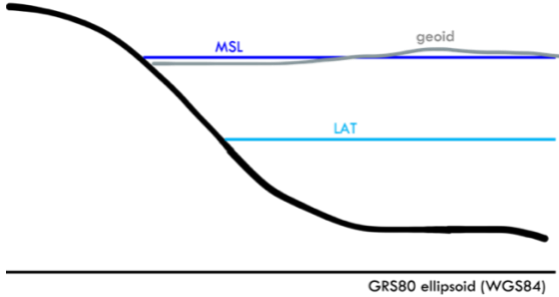


Figure 2.12 – Graphical representation of the Low Astronomical Tide and the Mean Sea Level with respect to the geoid and ellipsoid surfaces.

The use of the Low Astronomical Tide as zero-level for nautical maps is based on international standards shared worldwide: the International Hydrographic Organization (IHO) guideline states the LAT as a chart datum where tides have an appreciable effect on the water level [194]. For this reason, most publicly available bathymetric maps are commonly defined with respect to the LAT.

The other standard used as a vertical datum is the Mean Sea Level (MSL), often called *sea level*. The MSL generally represents the average surface level of one or more of Earth's coastal water bodies from which heights such as elevation may be measured [186]. This is commonly used as a vertical reference for modelling in shallow coastal waters, offshore industry applications and oceanography. It is not straightforward to obtain a precise and reliable determination of the MSL because its value can be affected by several factors, such as tides, winds, temperature, salinity and local gravity differences. Moreover, it naturally varies in time and space due to several factors, such as glacial activity, meteorological effects, tectonics, and astronomical effects. For this reason, talking about the MSL, it is necessary to refer to a specific location chosen as a

reference for a particular datum. On the other hand, to consider and include the inherent variations over time, MSL is obtained by computing the mean of 19 years of hourly level observations [208].

Concerning the global MSL, it refers to a spatial average over the entire ocean and corresponds to the Earth' equipotential surface as described by the EGM2008 geoid (Figure). Conversely, at a local scale, the sea level can be measured through continuously acquiring tide gauges. In particular, each country selects a specific location for its measurements and uses the obtained value as a national reference. The Permanent Service for Mean Sea Level (PSMSL) deals with the collection, publication, analysis and interpretation of sea level acquisitions from worldwide tide gauges [226]. The PSMSL archive is a fundamental source of helpful information regarding sea level changes. Thus this dataset is used for the IPCC (Intergovernmental Panel on Climate Change) studies.

The existing separation between MSL and LAT levels should be determined locally for their inherent definitions. The difference can be computed by considering tide-gauges measurements, but this approach would require extrapolating values to the whole grid based on unevenly distributed point-wise acquisitions. About this, the Global Storm Surge Information System (GLOSSIS) of Deltares developed a numerical model to produce a 10-day water level and storm-surge forecast, named GTSM (Global Tide and Surge Model). The GTSM development is still ongoing, but it can be employed to convert depth data from LAT to MSL reference, at least for large spatial scales [212]. This is the case of EMODnet Bathymetry, available both according to the LAT and the MSL for the European sea regions [47][214]. In particular, analysing EMODnet-LAT and -MSL maps along the Adriatic coast of Emilia-Romagna in Italy, an average bias of about 60 cm has been found. Chapter 5.1 will provide further discussions about this data source. In any case, when dealing with publicly available maps, such as bathymetries, identifying the sea level used as reference is mandatory and must be specified within the associated metadata in the "Depth datum" field. However, it is

known that the two surfaces identifying the LAT and the MSL converge when approaching deep waters (more of 20 m of depth) and in some areas, such as the closed Mediterranean sea, where their separation is less significant due to lowest characteristic tidal amplitudes [187].

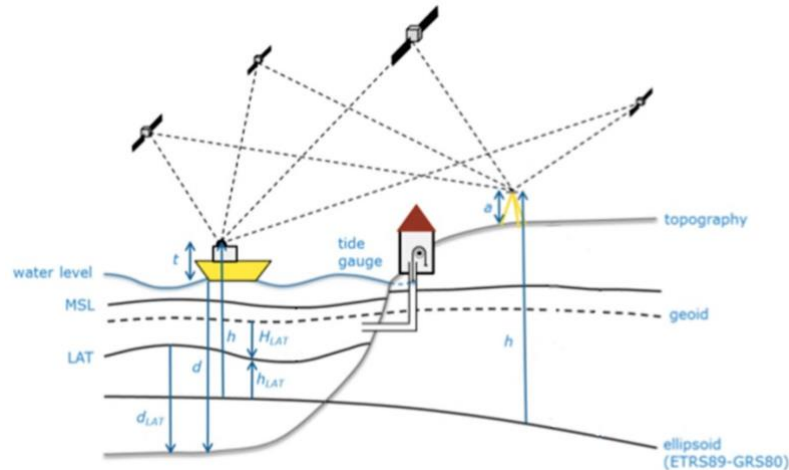


Figure 2.13 – Practical view of different parameters entering the discussion about the altimetric reference.
Source: [171] (modified).

In Italy, the national altimetric reference is based on the tide gauge of Genova, which is used both for heights and depths. In particular, the sea level reference dates back to 1942: “Genova 1942” is the average of annual sea levels measured during ten years (1937-1946) of acquisition [221]. Therefore, the zero-level used for the orthometric heights on the mainland is commonly aligned with the MSL in Genova. Conversely, the depth measurements require different considerations, mainly depending on the employed technique and the specific application. Without going into the details of the surveying techniques’ specifications (later described in Chapter 3), the measured values of height or depth are typically referred to different references, which are graphically shown in Figure . Commonly, considering the most widely used surveying techniques, we could refer to:

- orthometric heights – MSL (H);
- ellipsoidal height (h);
- distance from the acquiring system to the topographic surface (d);
- d_{LAT} .

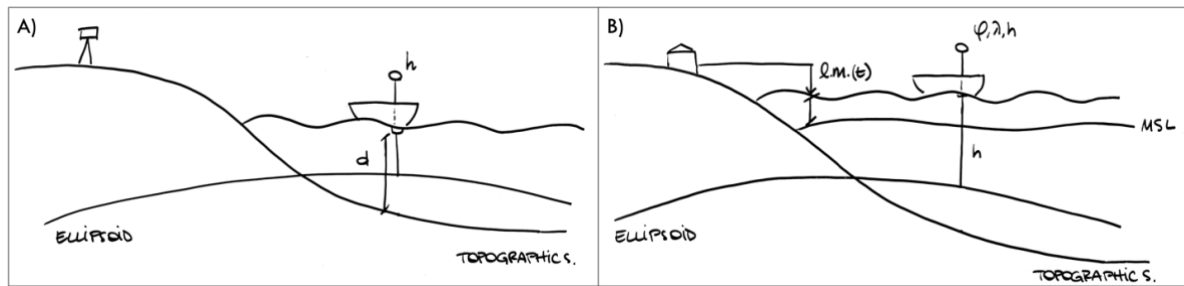


Figure 2.14 – Possible approaches to obtain the depth value.

Figure shows two possible approaches to measure the depths of the points. Figure -A is the classical technique that combines the ellipsoidal height and the distance from the acquiring system to the topographic surface. This method requires a link for the MSL alignment since depth values refer to a local sea level. Figure -B refers to another possible approach that relies only on ellipsoidal heights without considering the tidal effects. Even though theoretically, it could provide repeated values of the depths always referred to the same reference, this second approach finds complex application in nautical contexts.

Dealing with topographic applications, we commonly consider the sea surface as something stable, assuming an isostatic point of view. This is related to the fact that a defined value of the MSL in a specific location is used in connection with the geoid surface. Actually, the sea level is exposed to changes which are addressed by particular studies in the context of satellite altimetry. Several satellite missions have been launched to measure the sea level surface at a global scale, starting with the TOPEX/Poseidon in 1992, followed by Jason-1 in 2001 and Jason-2 in 2008 [204]. These spacecrafts are equipped with radar altimeters and radiometers, which, combined with other ground information, can provide the height of the sea surface. We will not enter the details of this matter, but in the following paragraph, some significant definitions are reported.

Basically, a separation between the oceans' mean and variable parts is introduced by considering two different contributions: the Mean Sea Surface (MSS) and the Mean Dynamic Topography (MDT). The MSS represents the level due to constant

phenomena, i.e. the averaged shape of the ocean surface considering a specific period so that annual, semi-annual and seasonal signals are removed. On the other hand, the MDT contribution considers the permanent stationary component of the oceans' dynamic topography [169] (Figure).

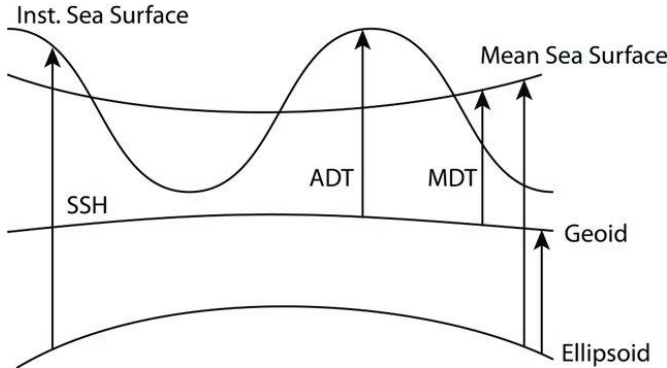


Figure 2.15 - Schematic illustration of the relationship between the mean dynamic topography (MDT), the mean sea surface and the geoid referenced to the same ellipsoid. Source: [124].

Satellite altimetry can measure the Sea Surface Height (SSH), the height of the instantaneous sea surface with respect to the reference ellipsoid. Having the SSH and the MSS, it is possible to obtain the Sea Level Anomaly, representing the sea surface height with respect to the Mean Sea Surface. Finally, Absolute Dynamic Topography (also named Sea Surface Topography) is the sea surface height above the geoid [5][182] (Figure).

Chapter 3

3 Geomatic Techniques for coastal monitoring

Operatively, coastal monitoring is realized through analysing multitemporal geomatic surveys repeated over common areas. This means that the reachable effectiveness associated with a monitoring plan is dependent on the accuracy of the employed surveying technique, on the management of different data sources, and on the post-processing adopted [30][24][165]. This Chapter will address the analysis of the surveying techniques and how their characteristics and application can affect the measurements' accuracy.

To date, several different geomatic techniques are available for coastal applications, each with inherent characteristics, both regarding the obtainable precision and accuracy and the practical operations required on the field. Moreover, from previously explained considerations, it is known that the obtained results of coastal analysis are strictly connected with the measurements' accuracy and the proper definition of the supporting reference system.

Therefore, the choice of the adopted surveying technique depends on several aspects, such as:

- required precision and data accuracy;
- morphological characteristics of the specific area;
- expected variations to be detected;
- extension of the surveyed area;
- desired spatial resolution, i.e. density of the acquired points;
- required frequency of the survey campaigns;
- practical operations performed on the field;
- available instruments;
- costs employable in the survey;
- specific characteristics of the phenomenon to be investigated;
- objective of the study.

It is essential to underline that each of these aspects cannot be considered independently, as the underlying considerations which lead to the identification of suitable parameters are typically based on common or related arguments. This means that, in this context, complex evaluations are required, usually leading to subjective decisions which are inevitably governed also by the possible already validated procedures for a particular environment. For example, considering the surveys' repetition rate, this depends on the expected variations to be detected and, therefore, on the specific phenomenon to which the survey is addressed. In the case of ordinary monitoring activities, which commonly involve vast areas, reasonably, the survey campaigns cannot be repeated at high time-frequency or cannot be realized at very high spatial resolutions. In turn, these aspects are connected with considerations about the field time and, thus, the related costs. The applicability of a particular technique is also dependent on the area's specific characteristics, as different methods can better perform in some environments rather than others. In order to monitor rapid changes or variations over limited areas due to specific interventions (e.g. defence structures), it would be necessary to perform high-frequency surveys with reasonable accuracy to detect the changes. Even the computational effort must be considered since an increase

in the measurements' spatial resolution, and thus the reachable accuracy of the final products results from a high amount of data to be processed. Furthermore, monitoring activities generally have to deal with economic considerations since they are strictly related to the touristic management plans in the interesting areas. In fact, "the need to monitor, analyse, and model processes is recommended to determine suitable interventions on the coast in the present and immediate future" [36]. This is particularly true when the investigated phenomenon is part of a rapidly evolving system, leading to a particular urgency in the related decisional policies. These arguments could continue considering each aspect individually or trying to connect all of them, but either way, there would be no objectivity in the discriminating of one technique over the others [24][118][75]. What is certain is that it is not possible to identify a single technique that is suitable and better performing for every application [35].

Moreover, in the case of coastal monitoring, it is not sufficient to consider how each technique works and its inherent characteristics, but each argument should be addressed to their particular application in coastal areas. This is undoubtedly one of the main issues, as the sandy coast represents a complex area from different points of view. Firstly, for their inherent definition, coasts are the interphase areas between land and sea, and thus all the considerations about the usable techniques have to take into account these two environments simultaneously. On the other hand, dealing with sandy coasts, which are the ones addressed by all the analysis of the present study, one has to be aware of the possible sources of error or inherent uncertainty which cannot be avoided due to the natural movements of the material.

One approach to allow more straightforward evaluations, and especially a close link with the practical operations, could be to consider the products one wants to obtain from a specific surveying activity. This means that all the previously listed parameters can be considered in terms of how they impact on the final results, representing the starting point for all the coastal studies. In fact, a fair trade-off between lower costs

and proper representativeness of the collected data should always be respected. In particular, the proper analysis of the processes and their evolution can be ensured only by a reliable level of measurement accuracy and by suitable values of spatial resolution and frequency according to the investigated phenomenon [30].

Thanks to technological development, several different geomatic techniques are currently available and employable for coastal surveying, apart from the consolidated classical topographic techniques. First of all, “existing geomatic techniques used for coastal applications can be divided into those focused on measuring a limited number of feature points or techniques acquiring massive data (i.e. point clouds)” [158]. Traditional topographic instruments and techniques, such as the Total Station (TS) and the spirit levelling measurements, belong to the first class, with the additional characteristic of allowing measurements of distances, angles, or height differences. These techniques are always helpful, at least as a support for other instruments, thanks to their associated high precisions, but they are increasingly less used in favour of others due to their associated costs and time efforts. Therefore, the primary technique mentioned in the first class is the Global Navigation Satellite Systems (GNSS), which allows for obtaining 3D coordinates on the points. On the other hand, the most common methods to obtain point clouds in the surveying context include photogrammetry (close-range or aerial) and Laser Scanning (LiDAR), and both have demonstrated promising results when applied to coastal areas [35]. It should be stressed that when applying methods which collect data at different spatial scales, possible comparisons must consider these differences [35]. Moreover, another distinction about emerged and submerged beach must be considered. Some of the mentioned techniques can be applied in both environments. Others present significant issues specifically in the submerged areas or are specific for some applications (such as echo sounders for depth measurements).

Among the available techniques, the main discriminating parameters for the present study are cost sustainability and the possibility of obtaining three-dimensional data.

For example, the spirit levelling technique allows measuring altimetric variations with very high associated accuracy, but it is inapplicable as a single technique for coastal monitoring purposes for its related high costs. It should be mentioned that, actually, particular coastal studies could be based not on the morphological variations of the littoral (3D representation). However, conversely, they could aim at evaluating only some other aspects, such as the advancement or retreat of the coastline. In these cases, single-scope images from fixed cameras or satellites can be employed [7][67][159]. These techniques can provide other information sources for coastal analysis and eventually complement other products.

The following paragraphs will address the analysis of the main geomatic techniques considered in this study, i.e. the most well-established for the monitoring activities performed in the Emilia-Romagna region. The techniques' analytical principles are beyond the scope of this analysis and will be therefore addressed in a summarised way, focusing on the more functional characteristics.

3.1 Global Navigation Satellite Systems (GNSS)

Global Navigation Satellite Systems (GNSS) are flexible systems allowing for a wide possibility of applications in several different contexts. This is primarily because they can be employed using different methodologies, approaches, and instruments which can result suitable for very different applications. The following paragraph will briefly describe the basic functioning and characteristic of this technique, later focusing on the two main approaches used for coastal surveys.

Using GNSS systems, it is possible to realize the three-dimensional positioning of objects throughout the Earth, independently from the weather conditions. This is obtained by receiving radio signals sent by artificial satellites which move on defined quasi-circular orbits (about 26.500 km of radius). These satellites are continuously orbiting around the Earth. Therefore their position changes over time and can be

deduced by knowing their orbits. Since the transmission of the satellites' signal works in a unique direction, the number of users exploiting the system is theoretically unlimited.

During the '70, the U.S. Department of Defense launched the first constellation of satellites, named NAVSTAR GPS (NAVigation Satellite Timing And Ranging Global Positioning System), which was initially used only for military applications. Lately, its use has been made available also for civil applications, leading to the rapid development of the so-called GNSS (which involve all the available constellations). To date, in fact, the GNSS include other constellations besides the GPS: the Russian GLONASS (Global' naya Navigastionaya Sputnikovaya Systema), the Chinese BeiDou and the European Galileo. The working principle is the same for all the available constellations, and it is related to three components:

- Spatial segment: is the constellation itself, i.e. the satellites orbiting at a certain distance from the Earth's surface.
- Control segment: it consists of stations distributed around the Earth and continuously monitoring the satellites. In particular, the station in Colorado Springs is the master station for the GPS which manages and processes all the acquired data.
- User segment: all the users equipped with a GNSS receiver acquiring the satellites' signals belong to it.

Each GNSS receiver is composed of different elements that determine the positioning: an antenna, a microprocessor, and a radio frequency section. Actually, the obtained positioning always refers to the phase centre of the receiver's antenna, which represents the instrumental centre. The satellites' orbits are aligned to the WGS84 (World Geodetic System 1984) reference system, i.e. a geocentric system where the ellipsoid's rotational centre coincides with the Earth's centre (in particular to the centre of the mass). Since the satellites' ephemeris are known and included in the received

signals, the absolute position that any user can receive in real-time is aligned with the WGS84 system. The main parameters describing the WGS84 ellipsoid are listed in Table . According to this, the altimetric component obtained employing GNSS systems is always bounded to the ellipsoidal surface (ellipsoidal height).

Table 3.1 – Parameters characterizing the WGS84 ellipsoid.

| Semi-major axis a | Semi-minor axis b | Flattening f | Gravity constant u |
|-------------------|-------------------|-----------------|--|
| 6378137.000000 m | 6356752.314245 m | 1/298.257223563 | 3986004.418×10 ⁸ m ³ /s ² |

The analytical dissertation of the GNSS signals and how they are employed to obtain the actual positioning is a complex matter beyond the scope of this analysis; therefore, these aspects will be briefly addressed only to introduce the following discussions. Each satellite transmits navigation signals modulated on two carrier phases, L1 and L2, both obtained as multiple of the fundamental frequency characteristic of the on-board oscillator ($f_0 = 10.23 \text{ Mhz}$, $L_1 = 154 * f_0$; $L_2 = 120 * f_0$). Moreover, the satellites' signal includes the pseudo-random codes (C/A, P, W), i.e. pseudo-random binary sequences which repeat after a certain time interval, and a navigation message (D) which includes useful information about the satellites and their orbits. This fact is significant as it leads to two possible measurements made by the GNSS receivers, named *observables*, using only one or both carrier phases: pseudo-range (codes) or carrier phases. Table lists the most used approaches for surveying applications, including their characteristics in acquired observables and associated accuracies, which are also related to instrumental performances. Absolute and relative methods are distinguished based on the need for one or more receivers to perform the survey. A fundamental consideration to be done is related to the acquired observables, as higher levels of accuracy can be obtained only if the carrier phases are employed.

Table 3.2 - Summary scheme of the most commonly used GNSS surveying techniques: acquired observables, approach (whether absolute or relative), kind of acquisition (in real-time or post-processing), level of accuracy, and impacting factors on the reachable accuracy.

| Approach | Acronym | Observable | Absolute/ Relative | Post Processing required | Accuracy | Accuracy dependent on |
|---------------------------|---------|-----------------------------|-----------------------|--------------------------------|---------------------------|--|
| Single point positioning | SPP | Code (C/A or P) | Absolute | No | 10-20 m | Geometry constellation |
| Differential GNSS | DGPS | Code (C/A or P) | Relative | No | 2-3 m | Distance from master station |
| Static | Static | Carrier phases | Relative | Yes | Up to a few mm | Distance among receivers, time observation window |
| Precise Point Positioning | PPP | Carrier phases and Codes | Absolute | Yes | Up to a few mm | Time observation window |
| Real-time Kinematic | RTK | Carrier phases | Relative | No | A few cm (2/3 cm) | Distance among receivers, time observation window |
| Wide area Augmentation | SBAS | Codes or carrier phases | Relative ?? | No | From 2-3 m to a few cm | |

Concerning the technical applications, the techniques allowing for real-time positioning, Real-time Kinematic (RTK) [161][85] and Network RTK (NRTK) [73][28] have nowadays become a standard, even if they are both bounded on the support of ground-based infrastructures, though they rely on them in different ways (see Chapter 3.1). This fact could represent a limit, especially in offshore or mountain areas, characterized by a lack of control points or internet coverage [147]. In these contexts, the recently implemented Satellite-Based Augmentation Systems (SBAS) could be a possible solution (Table). In fact, using these systems, it is possible to realize the positioning thanks to the support of geostationary satellites coupled with a network of continuously operating reference stations (CORS) for the corrections estimation [147][160][27][162][86]. This way, the limitations in terms of coverage can be solved, and the broadcast GNSS corrections can be sent to many users. To date, SBAS have been developed by countries as global public services and by private companies at a commercial level: the main differences lie in the acquired observables and associated accuracies. A deeper description of these services is not relevant to this study and can

be found in the paper *Performance of Atlas GNSS Global Correction Service for High-Accuracy Positioning*, of which I am a co-author [147]. After a description of the available SBAS and their main characteristics, this paper addresses, in particular, the Atlas correction service managed by Hemisphere GNSS [218]. Two different contexts of the acquisition have been analyzed and compared, one with long observing sessions on a fixed point in ideal conditions of sky visibility and the second representing actual survey conditions along the Adriatic coast of Emilia-Romagna, with the primary purpose of evaluating whether this technique could be an effective approach for practical monitoring applications.

As already mentioned, “the most widespread approaches used in GNSS coastal surveys are those enabling real-time results: RTK and NRTK” [30][61][119][40][143][158]. These two approaches share the advantage of not requiring a post-processing phase, which means that they both allow indications about the actual survey performance immediately, avoiding understanding any critical issues only once the measurements are already concluded. In fact, the state of ambiguity fixing can be checked contemporary to the survey itself, having essential information about the final reachable quality of the measurements. Moreover, as the post-processing phase is not required, the collected 3D coordinates can be directly obtained without needing specific and complex processes or software, making these techniques particularly suitable for users outside the scientific field. Both RTK and NRTK methods allow reaching centimetre level accuracies with differences due to their specific characteristics.

In the following paragraphs, RTK and NRTK techniques will be described, considering their main differences and focusing on cinematic positioning since it is the one commonly applied for coastal surveys.

3.1.1 Real-time Kinematic

The Real-time Kinematic (RTK) method can be seen as an evolution of the classical cinematic positioning, which allows for real-time data acquisition directly on the field. Since it relies on the carrier phases as the main observables (Table), it ensures obtaining centimetre-level accuracy in the positioning, making it an advantageous technique. Considering employing the RTK approach for kinematic positioning, in general, it is possible to save much time on the field with respect to a static approach when dealing with high amounts of points to be collected.

The main requirements to perform an RTK survey are:

- Two geodetic receivers contemporarily acquiring;
- two surveyors working on the field;
- internet or radio connection between the two receivers.

The first receiver is called *master*, and it has to be located in a well-known and fixed position for all the acquisition sessions. The second, named *rover*, moves in the surrounding area, performing a sort of relative positioning with respect to the master receiver. Note that the need for at least two surveyors on the field is primarily due to practical considerations since the master station does not require any field operations apart from the stationing. The master position is one of the main aspects to be considered when an RTK survey is performed, which is inherent in the working's principle of this technique. On the one hand, the master's coordinates have to be known, but at the same time, this receiver is continuously acquiring codes and carrier phases signals from the satellites (Figure). This fact allows the master to compute in real-time the differential phase corrections mainly due to distance-related errors, i.e. the discrepancy between its known position and the one obtained from the acquisition. Considering that the rover moves within a certain distance from the master, these corrections are also valid for its measurements. Hence comes the need for a data transmission system between the two receivers, allowing the rover to receive the

differential phase corrections in real-time. In fact, since also the rover is continuously acquiring from the satellite constellations, it can correct its position without any post-processing phase. Thus, unlike the cinematic post-processing positioning, the RTK survey is possible only if both the master and the rover are equipped with a data transmission system. A good signals reception has to be ensured, usually choosing for internet or radio connection depending on the specific situation. For example, some remote areas cannot ensure good internet coverage, leading to the choice of a radio system for data transmission.

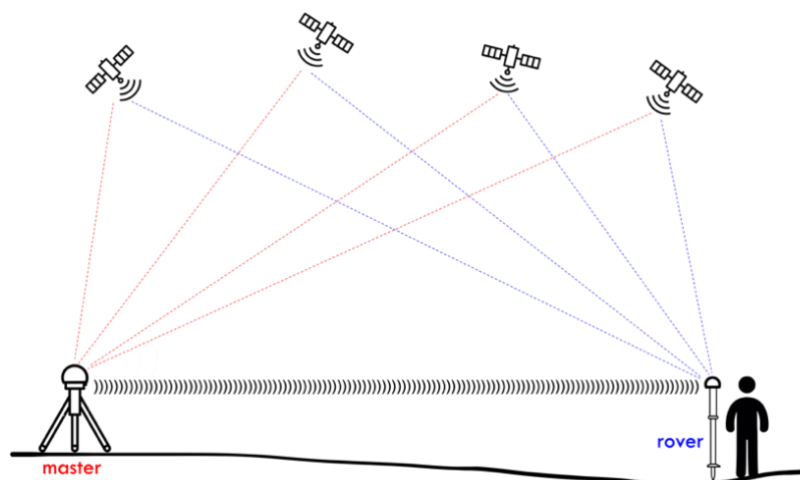


Figure 3.1 – Working principle of the RTK technique.

As a result, the rover's coordinates are always aligned with the same reference system in which the master's coordinates are known. This is another great advantage of this technique, since the reference system of the whole measurements is always known and can be defined by the user, depending on the specific purpose of the survey. In order to have reliable coordinates of the master station, usually, this receiver is located on a benchmark or vertex belonging to a specific network, having available its coordinates from existing monographs.

Before starting operatively with the measurements, the computation of the initial set of phase ambiguities from all the visible satellites is required in order to have only the position as unknown. For this purpose, commonly, algorithms based on all the acquired observables are employed, named On The Fly (OTF). OTF algorithms can

initialise the survey very rapidly under the condition of having more than four contemporary visible satellites, though they suffer when frequent signal interruptions occur. In this case, their functioning is not ensured, and a new initialisation process is required due to the phase's ambiguities change.

RTK surveys can reach centimetre-level accuracies (2/3 cm) both for plane and height, even if the height component is typically worse [63][8]. Nevertheless, these values refer to the so-called "fixed" situation, i.e. the positioning performed with ambiguities fixed as integer numbers, while if they are fixed as real numbers ("float"), the reachable accuracy can decrease up to 20-150 cm. Moreover, the obtained accuracy is always connected with the distance between the master and rover receivers: as this inter distance increases, the hypothesis of having the same corrections valid for the rover loses its significance. In fact, the assumption underlying these corrections is that the spatially correlated errors can be strongly reduced by means of a differential approach, but this is not true over a certain distance. In particular, over 10/15 km of inter distance between master and rover receivers, the correlation's degree between the spatially-dependent errors is too low, and the RTK approach cannot ensure high levels of accuracy (Figure 3.2 3.2).

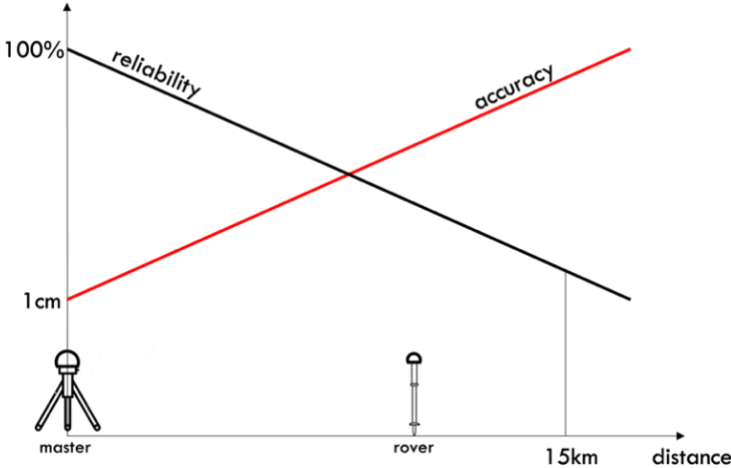


Figure 3.2 – Existent relationship between master-rover interdistance and reachable accuracy when working in RTK mode.

3.1.2 Network Real-time Kinematic

The NRTK technique allows a precise positioning (< decimetre level) performed in real-time with only one receiver on the field. This approach solves the main drawbacks of the RTK technique, i.e. the short range of distances to obtain high accuracy and the need to have known coordinates for the master's position. The network itself consists of a certain number of GNSS permanent stations, which are double-frequency receivers continuously acquiring 24h/24 on fixed positions whose coordinates are defined according to a known reference system. All the stations considered within a network must be equipped for sending their acquisition to a control centre. In particular, the working principle is similar to the one of the RTK approach, while in this case, the computed differential phase corrections are firstly sent in real-time from several different stations to a single receiving object. Therefore, the control centre can interpolate these biases, computing a model which describes the spatial-related errors affecting the whole area at a specific epoch (Figure).

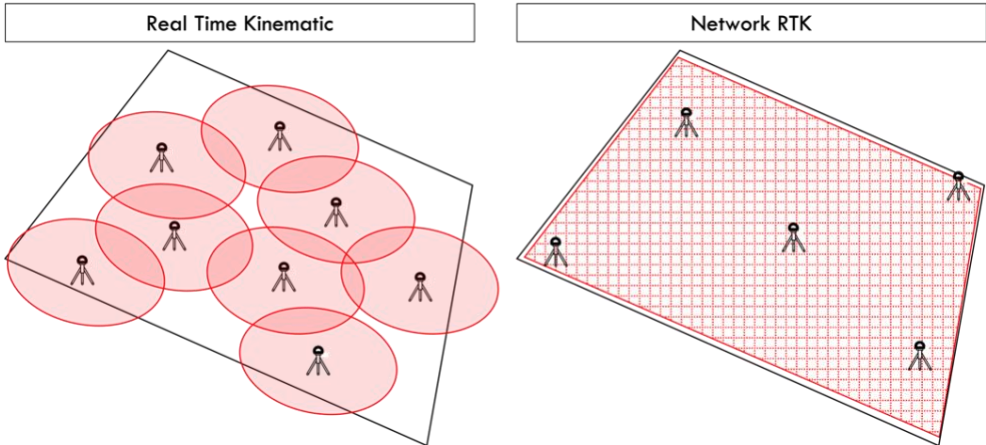


Figure 3.3 – Working principles of RTK (left) and NRTK (right) approaches with the different ranges of distance.

Each user operating within the network receives the correction's model computed for its location in real-time, thanks to the knowledge of its approximate position. Hence, all the receivers that exploit this service can perform a precise positioning in real-time, obtaining their coordinates in the same reference system in which the permanent stations are aligned. However, this is possible only if the users subscribe to a paid

service, and the functioning is ensured inside the area covered by the network. In particular, the NRTK approach allows increasing the maximum inter distance between the master station and the rover receivers (15 km for the RTK), supporting the real-time positioning through GNSS stations distant up to 50/60 km (Figure). The calibrated corrections can be sent to the user receivers through three different approaches: Virtual Reference Station (VRS), Flächen-Korrektur-Parameter (FKP), Master Auxiliary Concept (MAC). These methods will be briefly described in the paragraphs below. The VRS approach provides one correction “ad hoc” for each user. This fact is obtained through the simulation of a virtual station located nearby the rover, and it requires a bidirectional communication system between the control centre and the rover itself (Figure).

The VRS corrections are computed using an interpolation process which considers the data from the surrounding stations applying weighted least squares methods. Thus, these calibrated corrections can be computed within the network’s area or in the immediate proximity of its borders. According to the FKP approach, the control centre generates a model of errors correction, which is made available for all the users, independently from their specific receiver. In this case, monodirectional communication is applied since the centre sends the computed corrections to all the rovers in the form of a regular grid, including the whole network area. The last approach, MAC, requires a much lower effort with respect to the first two in terms of data used for the computation and transmission. The users on the field receive the corrections from a single permanent station selected as master, while the others are used only as auxiliary stations for differential information with respect to the master. Thanks to the lower requirements in the transmission band, this method can be affordable even for users without a broadband connection. It is essential to mention that using the NRTK approach, users are bounded to the reference system used for the alignment of the network’s stations. Thus they always have to be aware of this before starting the survey, and in particular when they process the acquired data.

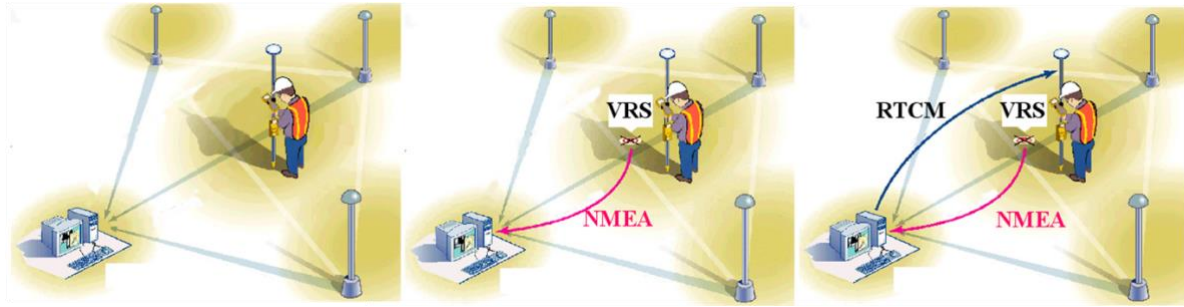


Figure 3.4 – VRS working principle. Source: [84] (modified).

Moreover, the NRTK technique cannot ensure reliable accuracies if the user is located outside the network. Nevertheless, using such an infrastructure, allowing users to perform precise surveys independently, is a topic of great interest both from scientific and professional points of view. For this reason, to date, many networks of GNSS permanent stations for NRTK positioning are present, mainly managed by geomatic instruments manufacturers and technical institutes for surveyors. Among them, we can mention, for example, the Leica Smartnet Italpos and the Topcon NetGEO, in Italy [193][173].

In the specific context of coastal areas, GNSS surveys result particularly suitable according to two main aspects: 1) the satellite coverage is commonly verified in these areas, thanks to the generally ensured sky visibility in such open environments; 2) the absence of obstacles and building ensures very low multipath effects [157]. Moreover, in this environment, the great flexibility and the high levels of accuracy of the GNSS make its use possible both as the primary survey technique and as a support for other instruments according to different sensors' combinations. In particular, GNSS auxiliary measurements are usually performed to survey ground points required for a proper georeferencing of other techniques on the emerged beach (e.g. aerial photogrammetry). Concerning the submerged beach, they commonly serve for the planimetric georeferencing of the depth measurements obtained by echo sounders, while they could be applied for the whole survey in the case of using ellipsoidal heights only (see Chapter 2.3 - Figure).

As already mentioned, typically, beach areas are surveyed employing the RTK or NRTK approaches, and this is due to two main reasons. Firstly, these methods provide proper accuracy for the specific purpose of coastal monitoring, considering that in such an environment, it is commonly not required to increase the precision over the centimetre level. Secondly, they both allow for cinematic positioning without post-processing, which is the ideal working mode for GNSS when many collected points are required. Moreover, using these approaches allows for acquiring additional denser areas if any particular morphologies are observed during the survey.

A pretty standard surveying procedure on beach areas involves acquiring a certain number of points along defined transects, i.e. cross-shore or along-shore sections to the coastline (Figure 3.5).



*Figure 3.5 – Typical configuration of GNSS-multibeam acquired profiles, cross-shore and along-shore.
Base map: Google satellite.*

Typically, three options are possible for this kind of survey, with the standard requirement of relatively slow movements:

- use of a GNSS pole: the surveyor moves, paying attention as far as possible to the level to avoid tilt movements on the top and trying to stay at about the same height from the ground throughout the survey;

- use of an equipped backpack: same considerations of the first case, with more simplified movements of the surveyors;
- use of an equipped vehicle: indeed this option allows for easier and faster surveys, while it leads to an inevitable loss of accuracy due to the caused movement of sand.

The spatial density of the acquired points can be subjectively defined according to the final aim of the survey. Typically, for flat areas, such as sandy beaches, it could be sufficient to collect points with an inter distance of a few meters along sections spaced out of about 100m (or 500m for regional-scale monitoring) to obtain a proper representation of the shape of the whole area [158]. However, the choice in terms of spatial resolution has to take into account possible interpolation errors in the following data processing, as “GNSS sparse data are to be interpolated to obtain Digital Terrain Models (DTMs), under the assumptions of continuity between different sections” [30].

On the other hand, this functional approach can become time-consuming if performed on vast areas or whether the terrain’s complexity requires a very high density of points [158]. Finally, by definition, GNSS surveys require physical contact of the instrument with the area to be surveyed, so they cannot be applied where this is not allowed [165].

3.2 Singlebeam and multibeam echo sounders

Considering the submerged beach, bathymetric surveys are typically performed by echo sounders, i.e. specific instruments that rely on acoustic measurements, such as SONAR (Sound Navigation And Ranging). The working principle of the echo sounders is based on transmitting a signal (sound waves) from the ship’s bottom to the seabed and measuring the return time of the echo (Figure) [180]. The principle of ranging is the same whatever the kind of signal used. Considering the case of the water, neither the use of an electromagnetic signal nor a light-based one is possible since the first would be attenuated and the second is not usable since the water is not

transparent and there is no mirror-like reflecting surface at the seabed. Thus, using acoustic signals is the most suitable option, bearing in mind also that in this context small magnitude's vibrations can travel long distances [180].

Echo sounders systems have three main components: a transducer, a transmitter and a receiver/amplifier. Firstly, the transducer receives electric energy and transforms it into sound energy in order to be able to send a sound pulse to the seabed. Once the pulse strikes the ground, the sound pulse is reflected to the transducer and the time taken by the waves (echo) is recorded (Figure).

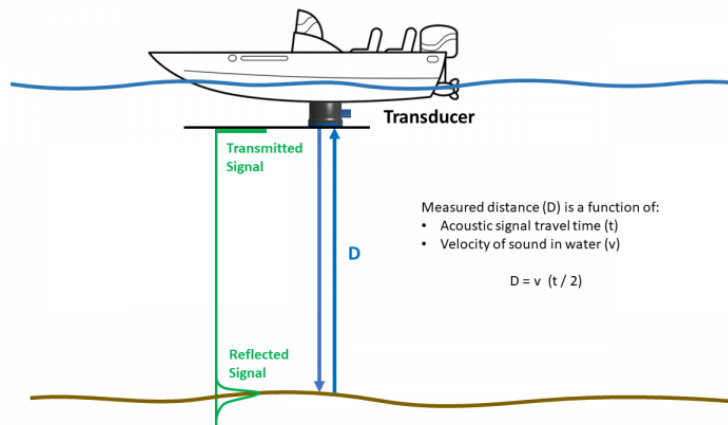


Figure 3.6 – Echo sounder's working principle. Source: [179].

Therefore, the points' depth can be determined by considering the simple formula in Eq 3.1:

$$D = v * \frac{t}{2} \quad \text{Eq 3.1}$$

Where D is the distance from the sensor to the seabed; v_w is the speed of sound in the water; t is the measured return time of the echo; all is divided by 2 to consider the double travel made by the signal.

Therefore, a point-wise measure of the depth under the ship's trajectory is obtained, thanks to the proportionality relationship between the velocity and the time. In particular, the speed of the sound in the water depends on the temperature, the presence of dissolved or suspended materials and the salinity. For these reasons, for

precise applications, a preliminary operation is required in order to calibrate the instrument [62]. In practice, this is realized by performing the measurement of an artificial target (a steel plate) located at a known depth. Two sensors are employed for this purpose, a Sound Velocity Probe (SVP) and a Sound Velocity Sensor (SVS). The SVP provides the profiles of sound's velocity along the water column (from the sensor to the seabed), making it possible to adequately compensate for the reflection effect of the acoustic beams (Figure). On the other hand, the SVS mounted on the transducer performs a continuous measurement of the sound's speed at the top of the system in real-time [62]. Note that the SVS measurements are commonly required only for some specific echo sounders (multibeam wide swath), which will be described in the paragraphs below. It is a good practice to perform the velocity calibrations each time possible changes in the chemical/physical parameters are supposed to occur and thus affect the speed of the sound propagation leading to uncertainties higher than the maximum allowable ones expected for the survey [222]. Moreover, modern instruments can be equipped with specific software and tools for measuring and managing the sound's velocity. Typically, considering the seawater, the velocity of acoustic signals ranges between 1.400 m/s and 1.600 m/s.

Apart from the value of the velocity of sound's propagation in water, different sources of error can affect the echo sounder measurements, impacting the final confidence level associated with the depth value [180]:

- multipath echoes: potentially, the signal can be reflected multiple times from the keel to the seabed, leading to multiple different values of the depth associated with one single point. Commonly in these cases, the first path is considered the correct depth;
- Pythagoras error: it happens when different transducers are used for the transmission and the reception;
- thermal and density related errors: water density can change with variations in temperature and salinity, causing several layers which the signal can strike;
- errors in the offset measures;

- errors due to the weather conditions.

Furthermore, to avoid other possible errors, reasonably these surveys must be performed with calm sea conditions.

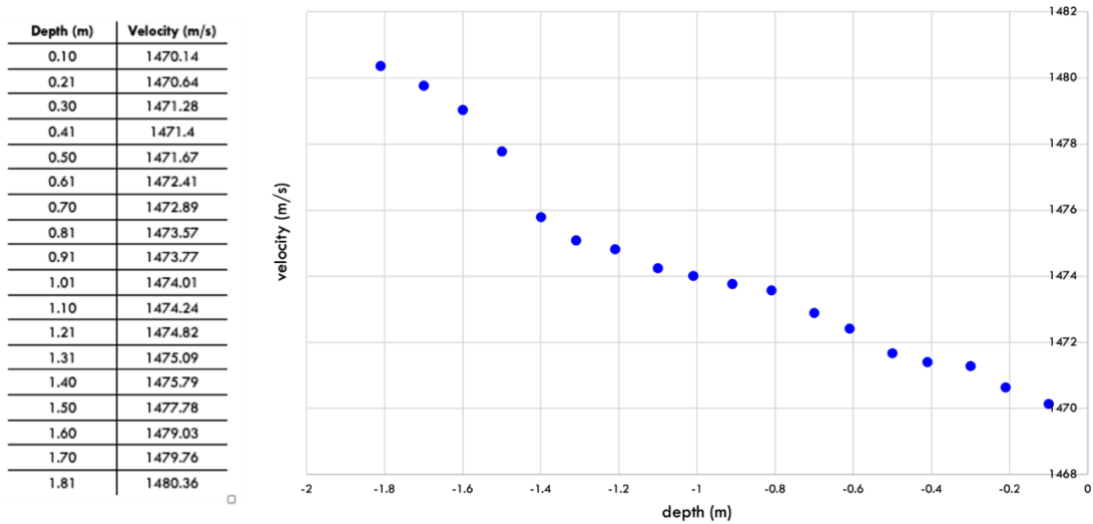


Figure 3.7 - Example of measured sound velocity with increasing depth.

According to the specific characteristics of the instrument, in terms of signal power, they can be able to measure at different depths: the higher the frequency, the more reliable they will be the measure since the signal’s penetration across the sand is strongly reduced, together with the error of the depth value. The geometric resolution associated with these measurements depends on the footprint created on the seabed by the conic beam. Reasonably, smaller footprint areas allow better discriminating between close points, avoiding a smoothing effect even when discontinuities in depth are present [172].

For what concerns the vessel position, this is commonly determined with a centimetric accuracy by means of a geodetic GNSS receiver working in a real-time mode (see Chapter 3.1). To this end, to ensure coherence with the reference used for the topographic surveys, a good practice could be to work in RTK mode, placing the master station on the same benchmark used for the emerged beach. On the other hand, the rover receiver is placed on the vessel; thus the obtained coordinates refer to the antenna’s position on the ship and not to the transducer itself, which is the actual

reference for the depth (Figure). Thus, the offset between these two sensors has to be precisely determined to be able to combine their measurements. Moreover, a possible way to minimize the uncertainty of the measured offset could be to install the GNSS antenna and the transducer along the same vertical direction.

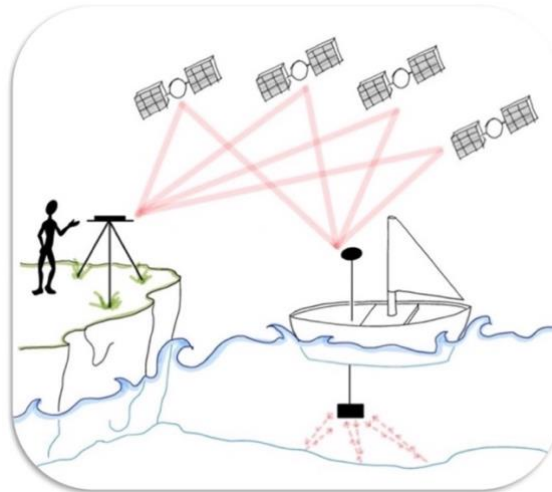


Figure 3.8 – Scheme of the vessel's positioning using the GNSS-RTK technique.

Besides the GNSS receiver, another electronic sensor is required to perform precise depth measurements through echo sounders: the Inertial Measurement Unit (IMU). This system consists of different sensors that work individually and then combine their data to obtain information about the motion of the platform they are mounted on. IMUs are commonly used when measurements are taken from vehicles, vessels, unmanned aerial vehicles (UAVs), missiles, aircrafts, and satellites. These sensors include accelerometers, gyroscopes, and sometimes magnetometers.

A short description of the three different components is addressed in the paragraph below [230].

- Accelerometers: these instruments can measure the gravity forces in a defined reference system. If the platform is moving, they will also record the measure of the existing inertial forces. Thus, they detect the linear acceleration of the object.
- Gyroscopes: they are commonly composed of a spinning disc and a sensor which registers the changes in the orientation, providing the measure of the angular velocity.

- Magnetometers: they measure the local magnetic field, i.e. the direction of the Earth's magnetic field in 2D or 3D.

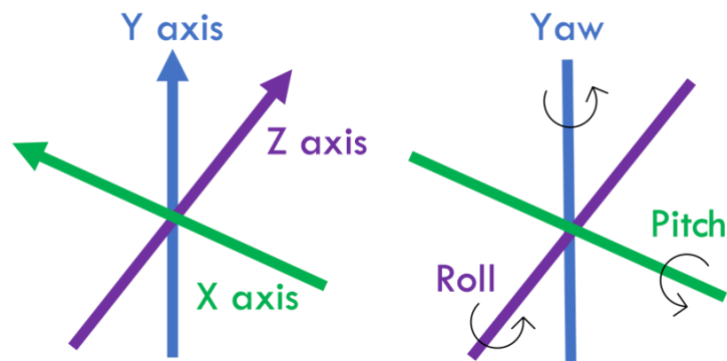


Figure 3.9 - X, Y, and Z axis and related attitude angles, pitch, yaw and roll.

If the platform can move throughout the 3D space, six degrees of freedom can be considered, being the number of different movements the object can experience. Three degrees include the translation along each axis (front/back, right/left, up/down), and three degrees refer to the rotational movement around the x, y and z axes [230].

The values obtained from accelerometers and gyroscopes can be therefore used to describe the overall dynamic of the object, being its position, attitude, and velocity. Moreover, measured data are usually fused to infer three fundamental angles, roll, pitch, and yaw, able better to describe the navigation's state (Figure). A Central Processing Unit (CPU) is employed to process the raw data collected from the IMU's sensors by applying different algorithms [211].

In order to obtain reliable depth measurements, the known effects of pitch, yaw and roll have to be compensated. Furthermore, to refer all the measurements from GNSS, transducer and IMU to the same local reference system centered in the centre of the IMU platform, the offsets between any sensors must be precisely measured.

Knowing the existing offsets and having the GNSS coordinates of each vessel's position, the employed navigation software can combine them to the IMU corrections and to the transducer measures directly on-board, exploiting the time information associated with each measure (Time Synchronization System). Thanks to this

approach, the 3D coordinates of the seabed are obtained following the vessel's route with a regular period depending on the cruising speed. The on-board workstation automatically registers all the collected data in the specified reference system, also allowing some editing operations (e.g. identification of possible spikes) and directly exporting the points in digital format [98]. This way, the on-board surveyors can follow defined monitoring sections uploaded within the navigation software [58][175], although the possible precision in following a sea route is reasonably different from the one obtainable on the land.

Monitoring sections on the submerged beach are generally realized as extensions of the cross-shore topographic sections acquired on the emerged beach (see Chapter 1). Besides, additional sections in the alongshore direction can be required where particular patterns are expected or where defence structures are present.

An example of a set of limit conditions is reported below (the one defined by Arpa), considering that they can vary depending on the specific area and application:

- maximum speed of the vessel during the survey: 4 kn;
- wind speed: lower than value 2 according to the Beaufort Scale (lower than 4-6 kn);
- waves significant height: lower than value 2 according to the Douglas Scale (0.10-0.50 m);
- absence of strong precipitations.

As for the absolute accuracy related to the echo sounders' measurements, usually, it cannot be precisely estimated since there is no prior knowledge of the seabed surface, thus, no reference data can be used for the estimation [91][39]. Therefore, the approach to identify the uncertainty commonly assumes the instrument's accuracy, i.e. the one declared by the manufacturer, as depth error. Nevertheless, this is a simplified analysis, as this averaged value cannot represent how the measures' errors are distributed. In fact, the final error related to each depth value is strictly related to the employed instrument, the frequency of measurements, the seabed's typology, the beam angle (i.e. the one between the beam ray and the vertical line - Figure), and

especially to the depth itself. This means that as the depth at the surveyed location increases, the measurement error increases, too. A study by [90] proposed a method to estimate the accuracy of multibeam echo sounders measurements, capable of being applied to any instrument and surveyed area. The selected case study in [90] found an overall accuracy at 5 cm level, with specific values of 3 cm and 4 cm, at 2-8 m and 8-16 m of depth respectively. The paper by [39] analyzed a possible way to evaluate MBES accuracy under plausible survey conditions for littoral applications, considering, in particular, harbour and port areas. Their approach was based on varying some boundary conditions of the survey, such as the speed, the orientation and the range. The results in [39] showed horizontal and vertical RMSE equal 2 cm and 3 cm, respectively. The proposed method can be further implemented, including other significant conditions which can affect the obtained accuracy. Thus it allows for avoiding working in conditions which can lead to uncertainties out of tolerance.

The new official document published by Istituto Idrografico della Marina states the new shared requirements for all the hydrographic surveys. Here, the TVU (Total Vertical Uncertainty) is considered a fundamental one-dimensional parameter, describing the contribution of all the sources of uncertainties (different combined instruments, parameters, measures) on the vertical component.

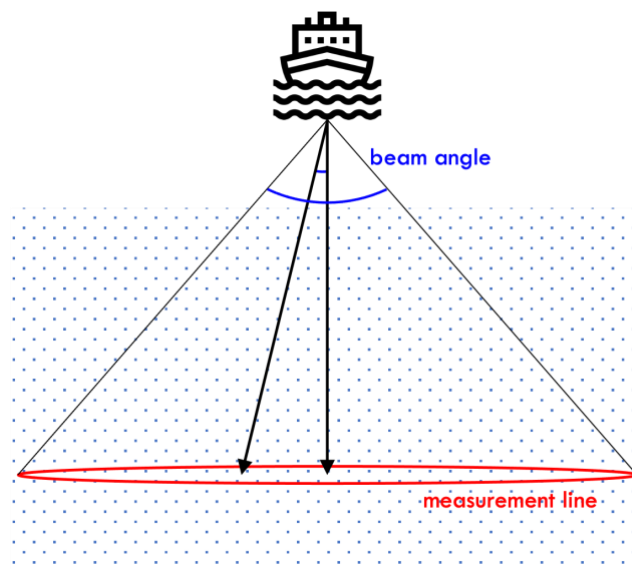


Figure 3.10 – Working principle of the multibeam echo sounder with reference to the beam angle.

In particular, the following formula has to be applied to provide the maximum TVU at a 95% confidence level (Eq 3.2) [222]:

$$\pm\sqrt{a^2 + (b * d)^2} \quad \text{Eq 3.2}$$

Where: a is the uncertainty's contribution which is not dependent on the depth; b is the coefficient representing the uncertainty related to the depth value; a and b are given for different kinds of surveys; d is the considered depth.

Depending on the depth where the survey is performed and on the required spatial resolution on the seabed, two typologies of echo sounders can be employed for the survey: singlebeam (SBES) or multibeam (MBES) [16][96] (Figure). The working principle of these two techniques is the same as described in the previous paragraphs, while their specific differences will be explained below.

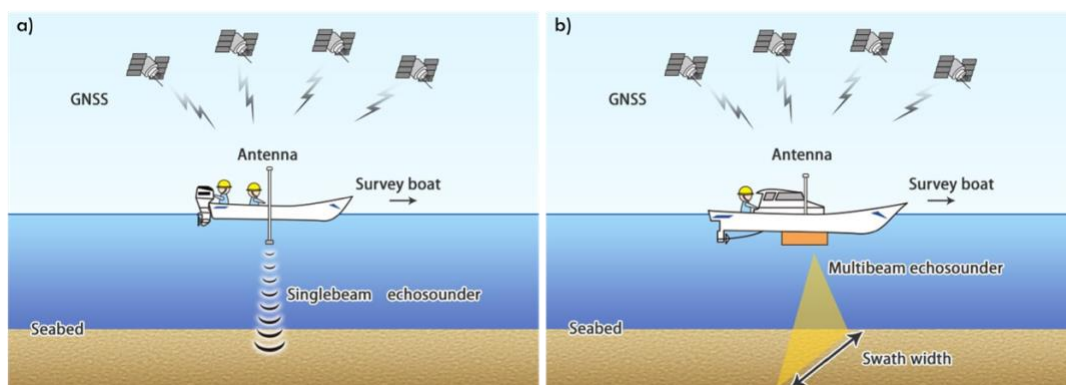


Figure 3.11 – Echo sounder's coupling with GNSS antenna: a) singlebeam, b) multibeam. Source: [197] (modified).

Reasonably, shallow water areas require the bathymetric survey to be performed using low draught vessels. Here singlebeam echo sounders are commonly employed, i.e. instruments allowing for the collection of single points beneath the transducer which follow the track line of the vessel [78]. The survey of shallow water represents the link between the topographic survey and the deep water. Therefore it is fundamental to ensure a proper coherence between the two environments, emerged and submerged beach. About this, it is good practice to perform singlebeam surveys with high tide conditions, completely calm sea and weak wind. Compared to the MBES, SBES

instruments are commonly cheaper, and this is true also considering the overall costs of the survey, as they require the use of small rubberized vehicles.

Typically, multibeam systems are employed in deeper water. These echo sounders are composed of several probes, allowing the acquisition of a band of points under the vessel's trajectory. For this reason, they provide very detailed information about the seabed's morphology, detecting even limited morphological variations and ensuring the possibility of acquiring points nearby hard structures. On the one hand, with an equal surveyed area, using MBES indeed leads to less time-consuming surveys. Moreover, the reachable spatial density of the collected points provides detailed measurements, also considering the possibility of avoiding possible interpolation errors in the post-processing phases. In the case of multibeam wide swath systems, SVS measurements are required to properly track the acoustic bands.

Since the existing differences in terms of costs associated with these two instruments, the choice relies on the specific context and the required detail level. Usually, when coastal monitoring surveys are repeated after years to compute volume variations, MBESs are employed.

3.3 Unmanned Aerial Vehicles (UAV) photogrammetry

In general, photogrammetry is the process of reconstructing the shape, size and position of areas or objects (all the metric information) starting from photographs with the main requirement of having the same object visible in more than one frame. This chapter will specifically address the description of aerial photogrammetry, which typically uses images taken from above by unmanned aerial vehicles (UAVs). UAV photogrammetry technique has to be considered within the context of digital photogrammetry, which represents the technological evolution of classical photogrammetry, even if their working principle is the same. Moreover, when a 3D

model is obtained starting from a set of two-dimensional images, we refer specifically to automatic digital photogrammetry.

Structure from Motion (SfM) is the employed technique for this purpose, allowing to reconstruct the shape of objects and extract 3D information by means of automatic collimation of points from a large set of uncalibrated frames [131][26]. SfM process is based on computer vision's algorithms, with the main requirement of having a large set of images acquired on the same area and with high overlap. This technique is characterized by high flexibility, as the images can be acquired by moving sensors (as UAVs) or by surveyors changing their position and angle with respect to the surveyed object. Moreover, for this application, common consumer-grade cameras can also be used. The process of Structure from Motion is structured into different steps, and it requires quite a high computational effort in terms of processing time (Figure).

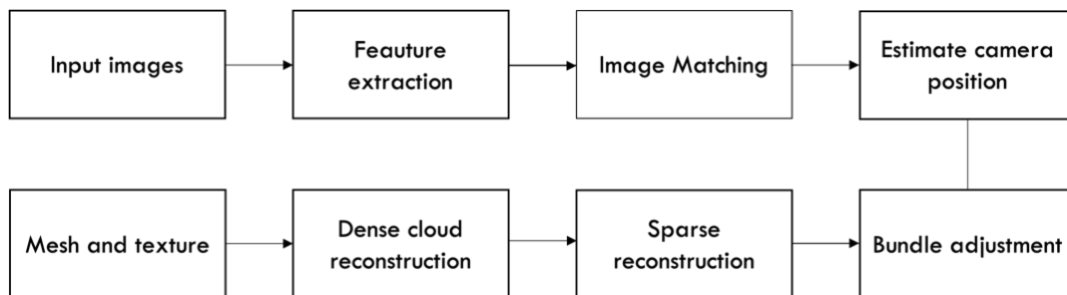


Figure 3.12 – Structure from Motion pipeline.

First of all, the geometry of acquisition of each single frame has to be determined in order to be able to infer the position of all the objects in the photographs. To do this, SfM aims at automatically identifying a certain number of key points which are contemporarily visible in at least three images. These points allow realizing the automatic alignment of the different frames, i.e. the Image Matching, representing the starting point for the following phases. The Bundle Adjustment is an operation of triangulation, which leads to the calibration of the camera (internal orientation) and the reconstruction of the camera's position during the acquisition of every single frame (external orientation). Therefore, during this phase, all the camera calibration parameters are estimated. After this operation, it is possible to obtain the first

intermediate product, i.e. a sparse point cloud, representing the 3D coordinates of the key points. The following step addresses the densification of the sparse cloud: the 3D coordinates of the key points are used to extract the positions of neighbouring elements, leading to the so-called dense point cloud. The dense point cloud represents the raw data of the photogrammetric process, allowing the description of the surveyed object or area through a large set of 3D coordinates. Afterwards, this dense cloud can produce a continuous surface, the mesh, a solid 3D model composed of several polygons built using the clouds points as vertexes (Mesh Reconstruction). A possible additional step is the colouration of the mesh, which can be applied following two different approaches: colour-per-vertex, when the colour of the dense cloud's points is used to extract the colour of the corresponding polygon; or texture mapping when the original frames are used for the same purpose. Finally, a proper scale has to be assigned to the 3D model since it is impossible to infer metric information from the images. This operation requires at least one reference distance within the model, which allows the software to accordingly rescale all the objects [211][209].

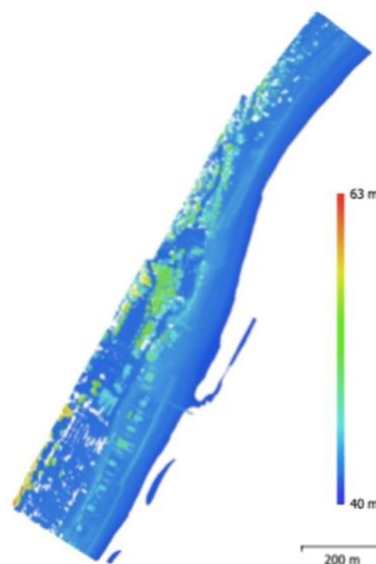


Figure 3.13 – Example of a Digital Surface Model obtained from the SfM process.

SfM technique is commonly applied to create high-resolution Digital Surface Models (DSMs) as final products, which are helpful for a wide range of applications, also considering their low requirements in terms of specific expertise (Figure).

A general rule in photogrammetry is that the greater the detail of the photographs, the higher resolution can be reached in identifying and reconstructing the features acquired during the survey. Therefore, the desired detail level at the ground is the fundamental value to be defined to properly select all the related design parameters, such as camera, sensor, and distance of acquisition. In digital photogrammetry, all the considerations are related to the pixels, which represent the single elements of the images, each one with its specific information. For this reason, the fundamental issue is that of describing the existing relation between the dimension of the pixel and the dimension of the corresponding area on the ground. The Ground Sampling Distance (GSD) is the parameter used to describe this relationship (Eq 3.3) (Figure).

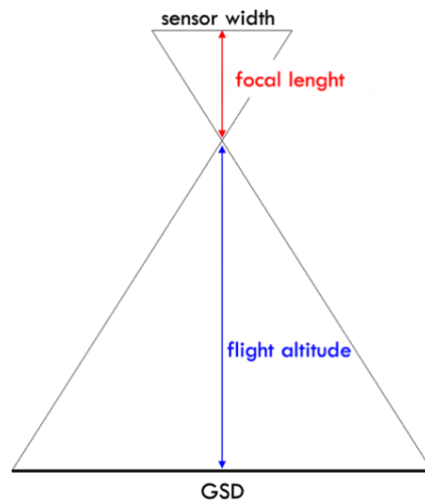


Figure 3.14 – Ground Sampling Distance (GSD).

Thus, the GSD represents the spatial resolution associated with the specific survey, i.e. the actual distance between two neighbouring pixels measured on the ground.

$$GSD = \frac{(H*d)}{p} \quad \text{Eq 3.3}$$

Where: H is the existing distance between the camera and the ground, which corresponds to the flight altitude for nadiral images; d is the dimension of the side of the square pixel of the images, which depends on the employed camera; p is the focal length.

An Unmanned Aerial Vehicle is always equipped with an on-board GNSS receiver, which on the one hand, allows having the vehicle's position and following a defined trajectory during the survey, and on the other hand, gives back the positions usable during the image's alignment. Nevertheless, since these receivers commonly do not provide a sufficient level of accuracy, the acquired positions are usually employed only to ease the SfM process.

The accuracy of a photogrammetric survey can be analyzed from two points of view: relative and absolute. The relative accuracy provides qualitative information about the mutual positioning of the points without considering their position in the real space. Conversely, absolute accuracy refers to the coherence level between the position of points on the reconstructed model and their actual position on the ground. Reasonably, when dealing with monitoring activities or GIS-based analysis, absolute accuracy is required, together with proper data georeferencing and management of the reference systems. The point clouds from the photogrammetric UAV survey need to be aligned to a well-defined reference system, so the vehicle's exact position during each acquisition must be known.

To this aim, a set of Ground Control Points (GCPs) is used. These points on the ground must be easily detectable in the frames during the UAV survey, and their coordinates have to be determined with high associated accuracy by precise techniques. Usually, Total Stations (TS) or double-frequency GNSS receivers working in real-time mode (see Chapter 3.1) are used for the GCPs survey. Note that the overall absolute accuracy of the photogrammetric survey cannot be higher than the one associated with the GCPs measurements. However, this argument is not always true since, currently, UAVs capable of working autonomously by employing on-board double-frequency GNSS receivers are available on the market. Some vehicles are equipped with GNSS instruments able to acquire phase observables to work in RTK or NRTK mode, enabling a real-time positioning of each frame with centimetric accuracy. In some cases, it is also possible to record the GNSS raw data to perform kinematic post-

processing (PPK). This approach would require a master station located within or very close to the surveyed area to send the corrections to the receiver carried by the drone. Please refer to Chapter 3.1 for all the specific requirements related to the RTK technique. In the case of a photogrammetric survey, both these methods can potentially remove the need for GCPs, or at least they can ensure reaching comparable accuracies and a good alignment reducing the number of points, thus saving time for ground measurements [144][53][141]. In particular, the inclusion of a few GCPs ensures the possibility of removing high distortion and helps during the Bundle Adjustment phase [112][142].

In a natural context, some obstacles or other issues can cause signal interruption, leading to lower achievable accuracy than the one declared for the RTK method in ideal conditions. Moreover, when relying on GNSS-RTK, the flight's area is limited by the signal strength, and any possible source of error related to the master station must be corrected in post-processing, reducing the advantages of this approach. About the PPK, this method anyway require a post-processing elaboration of the acquired data for the correction of the vehicle position, even if there are no restrictions tied to the connection between the master and rover receivers. It is essential to underline that this post-processing phase could require a particular amount of time, and specific expertise. In any case, when the drone carries a specific GNSS receiver, the manufacturer has to provide the offset between the antenna's centre and the sensor of the camera.

In order to perform a photogrammetric survey using UAV platforms, some procedures are required before starting with the field operations. It is fundamental to properly plan the survey by identifying the area to be surveyed and planning the flight in detail, choosing the take-off and landing points and checking for any possible obstacles. The working surveyor managing the survey has to be registered to the ENAC (Ente Nazionale per l'Aviazione Civile) society, and sometimes special authorizations could be required. This can happen, for example, when the area of

interest is part of a protected environment or when the vehicle's flight can interfere with an airport area. In this phase, the typology of acquired images is defined. In fact, according to the orientation of the camera with respect to the ground surface during the images acquisition, two kinds of images can be acquired: 1) nadiral, when the camera's plane of acquisition is parallel to the ground; 2) slanted, when there is a certain angle between them.

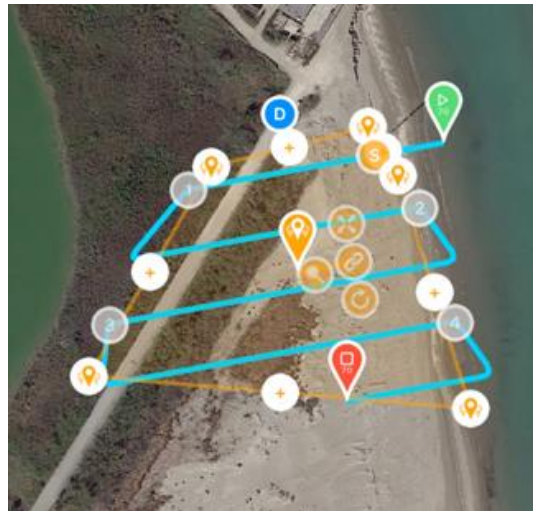


Figure 3.15 – Example of a flight plan for a photogrammetric UAV survey.

Images are collected one after the other according to a regular step, following the so-called strips (Figure). The sequence of several strips results in the final trajectory to be followed by the vehicle. A certain overlapping between neighbouring frames must be ensured when defining the trajectory: commonly, the 80% for adjacent images and the 60% between neighbouring strips (longitudinal covering). The flight plan is therefore completed after these operations, and the vehicle's defined routes can be imported into the navigation program to ensure the complete covering of the surveyed area. Then, the number and the location of the chosen Ground Control Points have to be defined, together with the employed technique for their acquisition. Operatively, GCPs are materialized by artificial targets, being square plastic panels with bright colours (commonly yellow and black), ensuring good visibility and a straightforward definition of their centre to attribute their coordinates accurately (Figure). It is good

practice to have a certain number of GCPs evenly distributed within the surveyed area to avoid possible distortions due to the lack of constraints.



Figure 3.16 – Example of target used as GCP. Source: [176].

Moreover, the final accuracy of the UAV-derived 3D model is dependent on several aspects, mainly related to the practical characteristics of the survey, such as [142][41]:

- flight speed and altitude;
- weather and sun conditions;
- texture of the area;
- configuration and number of GCPs and accuracy of their measurements;
- camera configuration;
- images overlap.

Note that the flight altitude highly impact the reachable accuracy, which can increase (worsen) to one order of magnitude with the same increase in height. Therefore, it is not easy to provide a general assessment of the uncertainty related to the use of this technique. Usually, for precise applications, the final accuracy reached by the measurements can be verified thanks to some additional points, the Quality Control Points (QCPs). These targets are placed on the ground as for the GCPs, using different colours to avoid confusing each other. The QCPs need to be precisely surveyed, but, differently from the GCPs, their coordinates are not used within the photogrammetric process. Having available these independent coordinates, it is possible to compute some error statistics by comparing them with the coordinates obtained from the photogrammetric model after the georeferencing. Reasonably, such an operation

would require proper management of the reference system, which can be ensured by applying the same survey technique for both GCPs and QCPs. Note that as this operation could increase the field time of the survey, it is not always performed.

Regarding coastal applications, to date, many studies have proved the effectiveness of photogrammetric surveys performed employing UAV platforms [127][130][60][31][30][24][40][151][76]. In this context, with an equal area to be surveyed, this technique can considerably reduce the human effort in the field compared to ground surveys. Moreover, UAV photogrammetric surveys take advantage of the high spatial resolutions of the dense point clouds. Therefore, by means of UAV photogrammetry, it is possible to accurately describe complex and uneven surfaces without any significant increase in effort for the field operations. Another significant aspect to be considered is that this kind of measurement does not require physical contact with the observed area. This can be helpful when dealing with areas that are hardly accessible or where some limitations are present. However, UAV surveys need to be approved to ensure that they do not interfere with any other flying vehicles. Through this technique, 3D points can be collected with very high associated spatial resolution on the ground in a relatively limited time. Nevertheless, some considerations must be considered when referring to precise surveys. In fact, the vehicle's flight is only part of the overall survey, as both additional field operations and post-processing phases are always necessary to reach the final dataset. As for the first aspect, a set of GCPs homogeneously placed within the area is required to reach a high overall accuracy without distortions in the model and to align the data to a selected reference system. In particular, this phase cannot be neglected in monitoring activities when subsequent measurements have to be compared to evaluate the morphological variations. These targets are commonly surveyed using GNSS receivers working in real-time mode and have to be properly located to ensure their stability during the survey. As mentioned, recently, UAV platforms equipped with double-frequency GNSS receivers are available on the market. Nevertheless, some issues

related to their application have already been described in the previous chapters, pointing out that they do not entirely solve the need for ground points, at least for precise applications. In addition, considering the second aspect, several processing steps are always necessary, whatever the equipment employed in the survey. In fact, the post-processing of the acquired images is the most time-consuming phase in the photogrammetric process, needing also for a certain computing effort that any processor cannot afford. Dense point clouds result as products of this process, large datasets of 3D coordinates. An interpolation process finally allows for obtaining high-resolution Digital Surface Models (DSMs).

It is inherent in the photogrammetric process that the acquisition concerns the objects' surface, as it is the only feature that can be reconstructed starting from the images. Therefore, where vegetated areas are present, particular attention must be addressed to this aspect. In particular, a semi-automatic data filtering process can be applied to obtain ground-related data using classification algorithms commonly provided by the photogrammetric software. Although, a user-governed phase is required since it is sometimes not easy to discern low and sparse vegetation from the sand itself. This also applies to user-governed filtering, leading to some uncertain situations that may be solved by properly inspecting the surveyed area. Any mistake in this phase can affect not only the results of comparative analysis with other techniques (e.g. DTMs from GNSS surveys) but also the comparison of repeated UAV surveys in the context of a long-term monitoring program (Figure). In such cases, possible changes in the vegetation could be interpreted as morphological variations. In addition, due to distortion effects, the UAV-derived model gradually loses its reliability outside the area where the GCPs are placed.

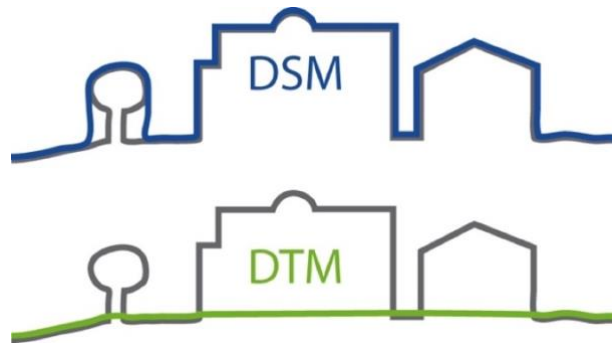


Figure 3.17 – Schematic representation of DSM and DTM. Source: [176].

Other possible sources of error of this technique are related to the presence of water: intertidal zones or areas where saturated sand is present are known to be affected by a loss of accuracy of the SfM reconstruction [24]. Here the rapid changes due to the water's natural movements can reduce the number of identified common points between neighbouring frames. Moreover, surveys performed with different tidal conditions can produce different results along the nearshore strip. This problem must be considered, ensuring to perform the surveys with calm sea conditions.

Another aspect is the shadowing effect that could occur at some hours of the day where high vegetation or structures are present. Finally, it is recommended to perform UAV surveys only under specific wind conditions depending on the employed instrument (specifically on its weight); typically, the wind-speed threshold is fixed at around 5.5 m/s. In general, weather conditions represent a limit for the UAV-photogrammetry technique since it is impossible to work during rainy days, and the presence of fog leading to bad visibility can negatively affect the results [6]. For what concerns coastal waters, UAV photogrammetry cannot be applied as an effective technique due to distortion effects caused by the water column and its natural turbidity [81].

3.4 Light Detection And Ranging (LiDAR)

The birth of the LiDAR technology is related to the study of atmospheric particles, and its development over time is mainly due to the availability of GNSS systems, which allowed the use of such technology mounted on moving platforms. The basic principle

of this technique is that of the LASER (Light Amplification by Stimulated Emission of Radiation). Lasers are active sensors able to transform chemical and electric energy into specific optic electromagnetic radiation which is then sent to the surface with a high energy burden. This way, the existing distance from the system and objects (or surface) can be computed by applying two alternative approaches: measure of the time of flight (t.o.f.) of the radiation (Figure) or measure of the phase shift (Figure). According to the first approach, the light's velocity in vacuum ($c = 299.792.458 \text{ m/s}$) has to be considered together with the refraction index related to the air density in the specific area. Hence, by measuring the time the laser pulse is emitted from the scanner unit (t_1) and the time it returns back (t_2), it is possible to compute the time-of-flight as a difference, thanks to very precise clocks. As a result, the distance (range) from the surface or object can be obtained by (Eq 3.4):

$$D = c \frac{(t_2 - t_1)}{2} \tag{Eq 3.4}$$

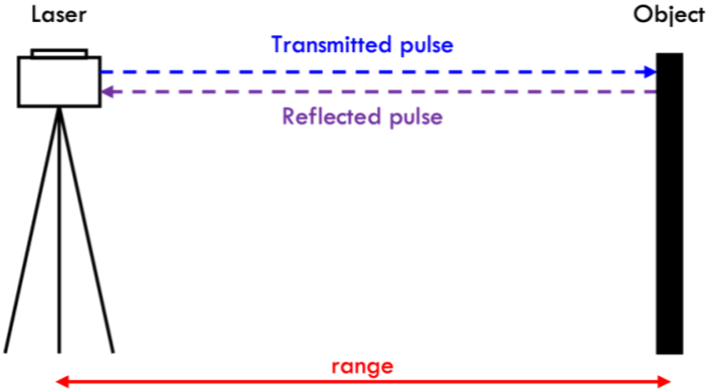


Figure 3.18 – Working principle of the LiDAR - time-of-flight.

The second approach avoids the need for accurate time measurements since it is based on a modulation of the laser ray. The signal is modulated on its amplitude, and, once the signal returns to the scanner unit, the phase shift between the emitted and received waves is computed (as a temporal shift). The distance can be thus obtained by adding the phase-shift ($\Delta\lambda$) to the integer number of wavelengths (M), based on the formula (Eq 3.5):

$$R = \frac{(M\lambda + \Delta\lambda)}{2} \quad \text{Eq 3.5}$$

The phase-based method suffers from some inherent limitations, such as the signal frequency, the accuracy of the shift measurements (depending on the signal power and the noise), the stability of the modulator's oscillator, and the refraction index's variation. The main bound is related to the maximum distance for which it is possible to compute the phase-shift, equal to a maximum of a few hundred meters, meaning that this technique is commonly applied only for terrestrial systems.

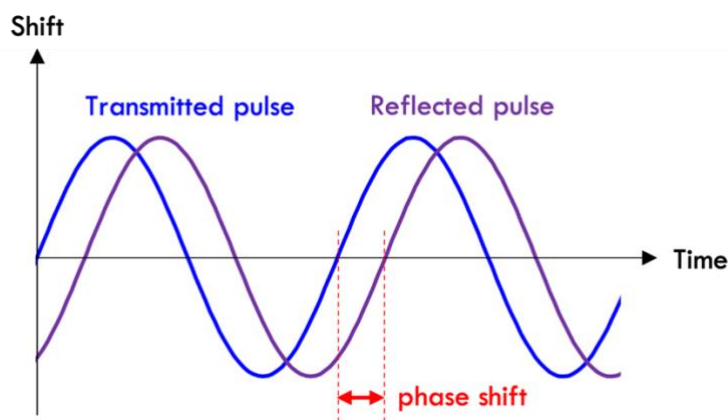


Figure 3.19 - Working principle of the LiDAR – phase shift.

Whatever the employed approach to compute the distance, 3D point clouds representing the acquired surface are obtained, possibly together with the associated value of intensity related to the return pulse. Moreover, LiDAR's working principle is always related to the knowledge of the orientation of the laser's signal. LiDAR systems can be divided into two classes based on the instrument location: Terrestrial Laser Scanner (TLS) or Airborne Laser Scanner (ALS). In the first case, the instrument is static on a tripod within the area to be surveyed. Conversely, ALS can be mounted on vehicles such as aircraft or drones, depending on the application and allow reaching distances of a few km. Reasonably, these working modes have different requirements in terms of additional equipment, practical operations on the field and post-processing, while the working principle of the scanner is the same as explained in the previous paragraphs.

3.4.1 Terrestrial Laser Scanner

Concerning TLS surveys, the instrument to be employed has to be chosen depending on the suitable range for the specific application, considering that medium (60-80 m) and long-range (within 1-2 km) have different associated accuracies of about 10^{-4} m and 15mm/1000mm (depending on the flight altitude), respectively. The main characterizing aspect of TLS is that when multiple scans are required to acquire the broad area, all of them are inherently referred to different scanner-orientated reference systems due to the change of the instrument's position. This means that an operation is required to register all the scans with respect to the same system by orienting each scan to the others. The alignment can be obtained in two ways:

- Directly on the resulting point-clouds using ICP (Iterative Closest Point) algorithms which aim at minimizing the distances between points belonging to different clouds;
- with the support of the so-called *tie points*, i.e. targets which are located within the surveyed area, ensuring their visibility from different scans. This way, having the targets' positions aligned to different scans and considering a roto-translation, the transformation parameter to connect the point-clouds can be deduced and applied to all the points of the clouds.

However, this alignment operation does not ensure an absolute georeferencing of the survey, since all the point-clouds will be referred to a single scan's system related to the instrument itself. When dealing with surveys repeated over time, it is necessary to reach an absolute georeferencing with respect to an external system. In the case of TLS surveys, this can be obtained thanks to the support of the ground-placed targets. As seen for the UAV-photogrammetric survey, their positions need to be acquired by means of other techniques such as Total Station or GNSS [72]. Thus, the transformation from the instrumental to the absolute system can be applied to all the aligned point-clouds. For what concerns the post-processing, this is always required to remove noise effects or possible spike points. Moreover, after the alignment and georeferencing of the point-clouds, commonly, a filtering operation could be required to reduce the

spatial resolution of the points. In general, the TLS technique is more flexible and accurate than the ALS, while it suffers from the limit of a shorter range in the distance. This fact, therefore, leads to the possibility of acquiring smaller areas within a single scan and thus to the possible uneven coverage or shadowing effects when larger areas are surveyed [115][22]. Typically, the average density of point-clouds acquired using TLS surveys is around 10-1000 points per square meter [115].

3.4.2 Airborne Laser Scanner

When the laser is mounted on a moving platform flying over the surveyed area, we refer specifically to Airborne Laser Scanner. In this case, the acquisition is based on three different units: the laser itself, a GNSS receiver, and an IMU platform (Figure 3.20). In particular, the GNSS positioning is commonly obtained in RTK mode (see Chapter 3.1), placing a master station within the surveyed area while the rover moves on the platform.

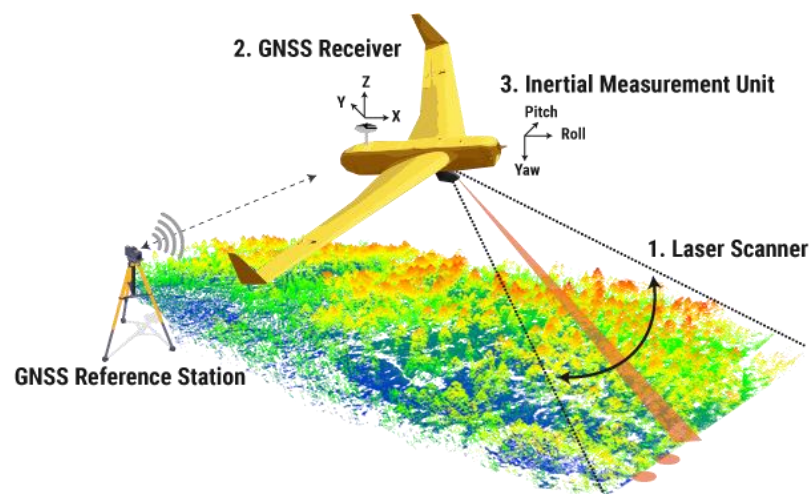


Figure 3.20 – The three sensors of ALS: Laser Scanner, GNSS receiver and IMU. Source: [231]

Thanks to this, the vehicle's position and trajectory are known, allowing not only the alignment of the point-clouds but also the possible overall georeferencing in the chosen reference system. As for the working functioning of the IMU platform, please refer to Chapter 3.2, bearing in mind that it is used to provide the platform's orientation over time. The laser emits the signal perpendicularly to the platform

movement's direction, and the measures from all the sensors can be integrated based on the time tag referred as the GNSS time. Thanks to this synchronization, the computed distance, the position and orientation of the sensor, and the angle between the laser ray and the vehicle are known for each epoch.

Similarly to the photogrammetric UAV survey, the ALS survey comprises different operative steps: the plan of the acquisitions, calibration of the sensors, survey, and post-processing. During the first phase, the flight parameters, such as the flight altitude and the number of scans, must be defined according to the area to be acquired. In particular, the complete coverage of the area must be ensured with different scans having a certain overlapping, considering that the bands' width is related to the flight altitude (H) and the angle of the laser signal (γ) by the relationship in Eq 3.6:

$$L = 2H \tan \gamma \quad \text{Eq 3.6}$$

The calibration phase addresses the alignment of the three employed sensors with respect to a common reference system, thanks to the offsets and orientations between their acquiring units. These parameters are obtained through a specific acquisition involving some scans performed round-trip over a defined area where visible targets are present. It is good practice to perform this procedure before each day of the survey. As for the reference system, the one of the GNSS unit, i.e. the one which is centered in the antenna's phase-centre, is used. After these operations, the survey is performed automatically using a specific navigation software. The post-processing step can be performed by some automatic procedures starting from the 3D point clouds and resulting in the data classification and filtering, noise and outliers' removal (quality check), and the creation of the associated grid.

It should be underlined that the ground footprint of the signal has a diameter ranging from 0.5 m to a few meters, depending on the flight altitude of the aircraft or drone (H), to the laser beam divergence (γ) and the instantaneous field of view (θ_{inst}) (Eq 3.7):

$$F_{p_{inst}} = \frac{H}{\cos(\theta_{inst})^2} \gamma \quad Eq\ 3.7$$

Meaning that the coordinates of the acquired points will be averaged within this range. This fact leads to a loss of accuracy when dealing with steeped slopes when close points with quite different heights are present.

Concerning ALS, the overall accuracy of the technique depends on the ones related to the three components (laser, GNSS, IMU). Furthermore, other factors have to be considered: the process of alignment of the three systems, the surface morphology (slope), the footprint dimension, and possible multipath effects. Some LiDAR systems can acquire multiple echoes, where the first pulse corresponds to the first surface encountered by the signal, commonly trees or vegetation, and so on, since the last pulse will refer to the ground surface. Typically, four echoes can be registered, allowing the user to choose the object of its acquisition. Moreover, multiple echoes must be surely employed to obtain Digital Terrain Models.

Both TLS and ALS have proved to give good results when applied for coastal areas surveying [35][164]. In general, the LiDAR technique has the advantage of providing large amounts of 3D data, ensuring the possibility of creating high-density digital elevation models. The survey's effort for the field operations is lower with respect both to ground surveys and UAV photogrammetry [134]. The laser sensor can work with any weather conditions, even in presence of fog or without the daylight. Since the LiDAR technique directly produces 3D points related to the surface (different from the UAV photogrammetry based on acquired images), the post-processing phase is not that demanding, even if vast amounts of data are recorded, and their management and storage have to be considered. Moreover, this means that .xyz files containing the

coordinates of the points result directly from the acquisition and can be easily used in GIS environments. Specific software allows the planning of LiDAR surveys, which helps identify the proper series of scans. However, the alignment of independent scans remains critical regarding TLS, leading to possible shadowing effects. The main issue occurs when dealing with steep slopes, which cause multiple values of the height associated to a single planimetric position, while areas with slight elevation differences, such as sandy beaches, can be easily detected. Compared to UAV photogrammetry, the associated costs and size of the overall equipment are certainly higher, but the reachable performances in accuracy are superior. About this, using aircraft vehicles has no reasonable costs for limited areas, and drones able to carry LiDAR equipment are commonly costly [35]. The georeferencing of LiDAR data should be addressed with particular care, considering the time required for the GNSS survey of the targets in the case of terrestrial systems. Furthermore, even considering the possibility of registering multiple echoes, the inherent difference between Digital Surface Models and Digital Elevation Models must be considered, especially when dealing with data comparisons over time.

A separate discussion should address the bathymetric application of the LiDAR technique since it can support the mapping of coastal water depth, considering some specific constraints. Theoretically, combining the model between emerged and submerged beaches would be possible by applying a common technique [78]. LiDAR bathymetry follows the same working principle as ALS, with a laser mounted on a vehicle and transmitting pulses across the water surface to the bottom seabed (Figure). In this case, a portion of the signal is reflected back to the system when it hits the air-water interface, while the remaining energy can propagate through the water column. Therefore, the water depth can be computed by measuring the time of flight of the composed signal and knowing the velocity of the light pulse [81]. Moreover, some corrections are needed for the water-level fluctuations and are commonly obtained through gauge measurements. Bathymetric LiDAR sensors are inherently different

from the ones applied for land surveys, as the laser's wavelengths are blue-green and near-infrared (NIR), respectively. This is related to the fact that NIR signals cannot penetrate the water and blue-green ones perform worse in terms of accuracy and spatial resolution when applied to the terrain. For this reason, the combination of topographic and bathymetric LiDAR data cannot ensure a proper continuity since the different specification of the sensors leads to different levels of accuracy, resolution, required post-processing and associated vertical datum [78]. In particular, bathymetric lasers are limited in their precision by the water-column absorption, with about $\pm 15\text{cm}$ of vertical accuracy [80].

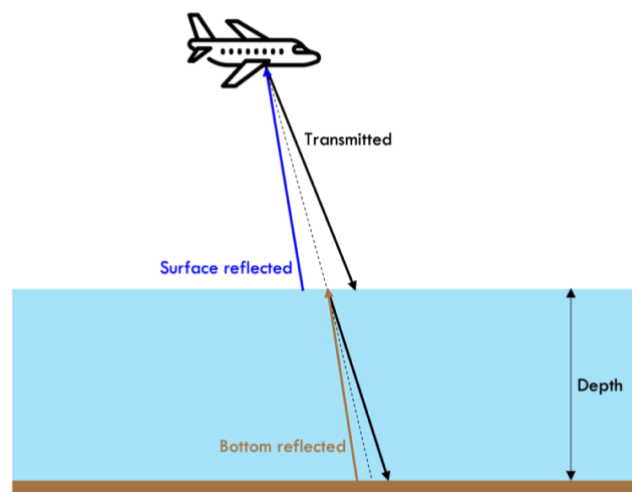


Figure 3.21 – Working principle of the bathymetric LiDAR.

Dual-wavelength LiDAR, equipped with NIR and blue-green lasers, can be a solution to capture seamless topographic and bathymetric surveys in coastal areas. Nevertheless, this is not entirely true since they are unreliable in very shallow depths or over white water in the surf zone because these conditions make it difficult to separate the portion of the signal returning from the water surface and the one reflected at the seabed [81]. Moreover, the maximum detectable depth and the strength of the bottom return are both tied to the water clarity since turbidity situations can limit the technique's overall performance [81]

Chapter 4

4 Case Study: Emilia-Romagna littoral

Emilia-Romagna region is located in the North East of Italy, and it faces the North Adriatic Sea all along its coast. The regional coast is a great naturalistic and economic asset, with considerable tourist attractions, and it is among the most famous sea destinations in all of Italy [129]. This littoral extends for about 130 km of characteristic low and sandy beaches, which follow a particular arch shape. Its boundaries go from the beach of Cattolica in the South to the mouth of the Po River in Volano (Comacchio), including the barrier-lagoon system of the Sacca di Goro, in the North (Figure). The hinterland immediately behind the beach areas is firmly flat and highly urbanised all along the coast. The littoral is a relatively shallow shelf, presenting very slight slopes and shallow tidal variations, while it is particularly vulnerable to intense coastal storms [187]. Moreover, part of this territory is located under the sea level, especially in the province of Ferrara, where reclaimed moist areas belonging to protected zones are present [54].

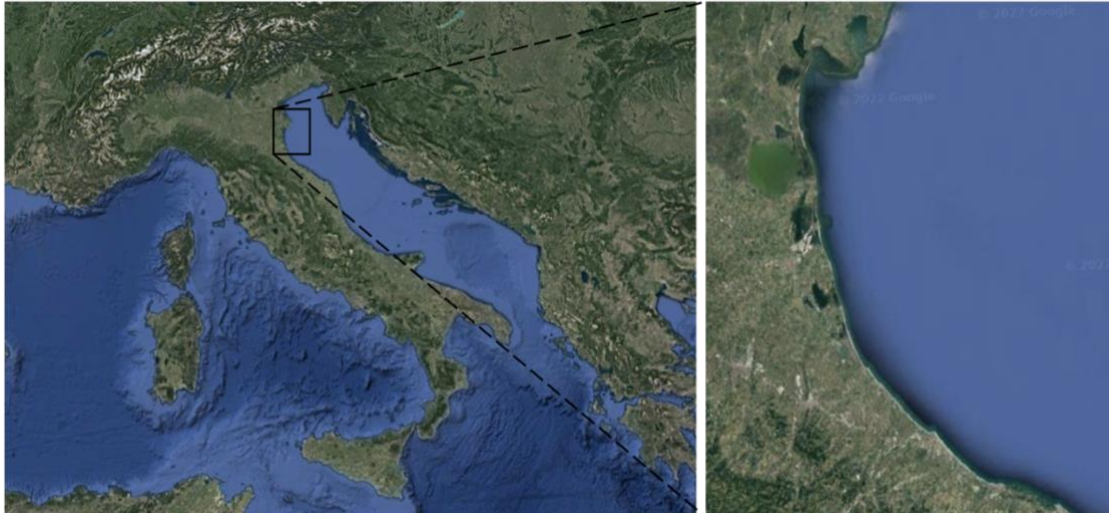


Figure 4.1 – Location of the Emilia-Romagna littoral.

Therefore, in this context, besides the economic and touristic relevance, coastal areas can also represent a natural defence against water ingress. Another characteristic which makes this area particularly exposed to dynamic evolutions is the presence of several river mouths flowing into the sea at a distance of 10-15 km from each other, with their associated material contribution. About this, the behaviour of the Northern area of the littoral is strongly governed by the Po river, the most extended basin in Italy with the greater associated flow rate. However, the trend of the last centuries was characterized by a progressive decrease of the sedimentary supply, leading to an associated redistribution of the material along the littoral, making the regional coast increasingly straighter, especially in the central and Northern sectors [19]. The typical coastal sediment transport has a predominant South-North direction (Figure), which shows asymmetrical shapes with inversion tracts corresponding to river mouths or any significant ports and harbours structures. Due to the reduced solid contribution, the coastal system experienced a gradual reshaping, which caused, in turn, a general growing erosive tendency over time [152].

As already mentioned, the subsidence phenomenon, i.e. the land elevation's lowering over time, inevitably leads to negative impacts worsening the erosion problem. This factor deserves separate considerations since the territory of Emilia-Romagna is

particularly exposed to it due to the low altitude of some areas with respect to the sea level.

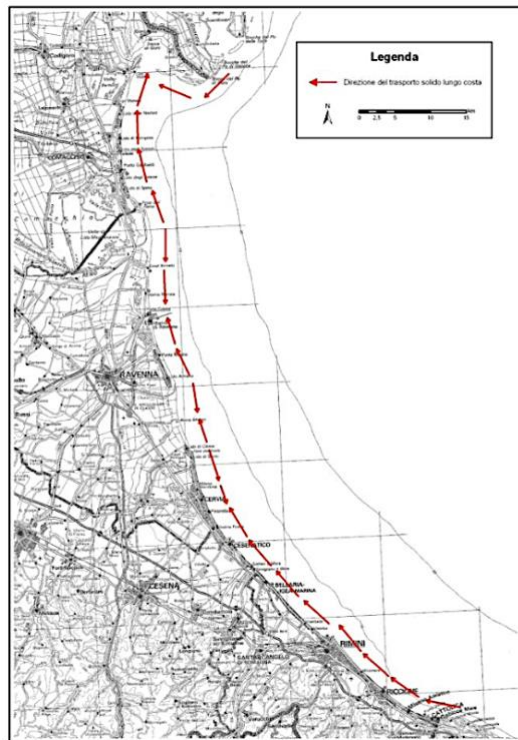


Figure 4.2 – Direction of the sediment transport along the coast of Emilia-Romagna. Source: [74].

In this regard, maps of the subsidence's rates are made available on the website of Arpae [205], with five years of validity. The first approach for their computation was based on spirit levelling measurements supported by the presence of a specific geodetic network, the regional Levelling Network for Subsidence Monitoring. Conversely, starting from 2005, the subsidence rates' assessment takes advantage of the Synthetic Aperture Radar interferometric technique (InSAR), which allows for computing the velocity variations along the vertical component and the associated time series over the considered period. This approach makes it possible to obtain maps representing the vertical movement in all the analysed areas, typically represented through isokinetic curves. In particular, considering the overall processing accuracy stated equal to 2 mm/y, these curves are commonly represented with a spacing of 2.5 mm/y. To date, the last available map of subsidence rates refers to the period between 2011 and 2016 (Figure) since the one related to the current period is under computation. According to the computed values of vertical movement, the overall rate

along the Adriatic coast of Emilia-Romagna presents an average value of about 3mm/y, considering a band of land within 5 km from the coast itself.

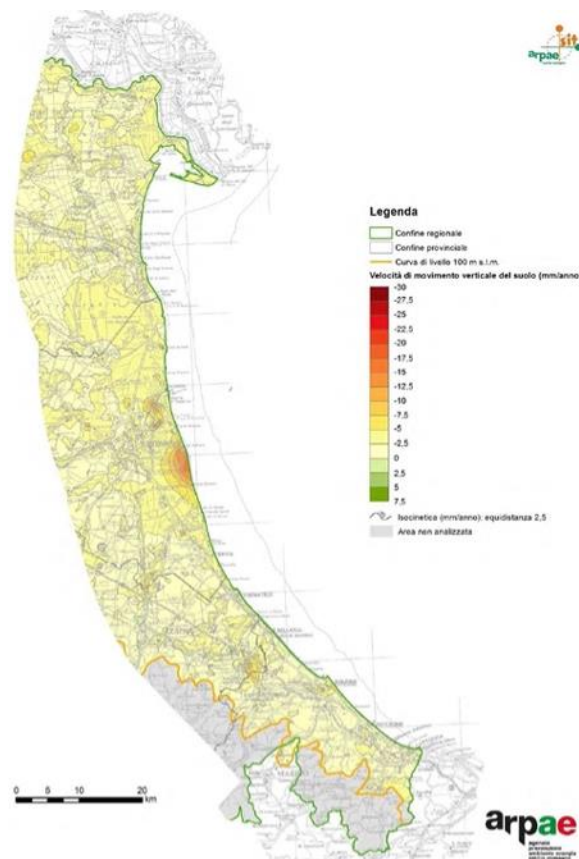


Figure 4.3– Band of territory considered to compute the subsidence rates along the Adriatic coast of Emilia-Romagna and related velocities for 2011-2016. Source: [1].

Furthermore, current values show a slight decreasing trend of the phenomenon over time compared to the previous period (2005-2011). Moreover, it could be attested that the resulting current values are mainly coherent with the natural subsidence rates. Nevertheless, this is not true for the specific area of Lido Adriano-Lido di Dante, characterized by a lowering velocity of about 15 mm/y, even though this rate has decreased from the previous periods. The possible changes in beach sand volume due to the subsidence's land lowering have also been estimated, showing significant amounts only in that area where the rates are much higher than the others. Moreover, after previous considerations it is known that also human activities can significantly affect coastal environments. About this, the intense urbanization due to bathhouses close to the beach areas continues causing the stiffening of the Adriatic coast of Emilia-Romagna, where the tourist impact is evident [113][57][114][122].

The Regional agency for prevention, environment and energy of Emilia-Romagna (Arpae) has defined two different indicators, ASE and ASPE, to describe the current erosive trend of specific beach areas by applying an integrated approach able to represent the complexity of this problem [2]. The ASE indicator describes the actual state of the coast according to three possible situations: Accumulation, Stable, Erosion. The ASPE classification identifies four different categories to consider the hypothetical situation faced by the analyzed area if no defence intervention would have been performed within the observed period: Accumulation, Stable, unstable equilibrium (“Precario”), and Erosion. Both the indicators are based on the same threshold in terms of sand volumes and shoreline changes to discern significant variations, equal to 30 m³/m and 10 m, respectively. According to this second scale, only accumulation and stable situations are considered favourable conditions.

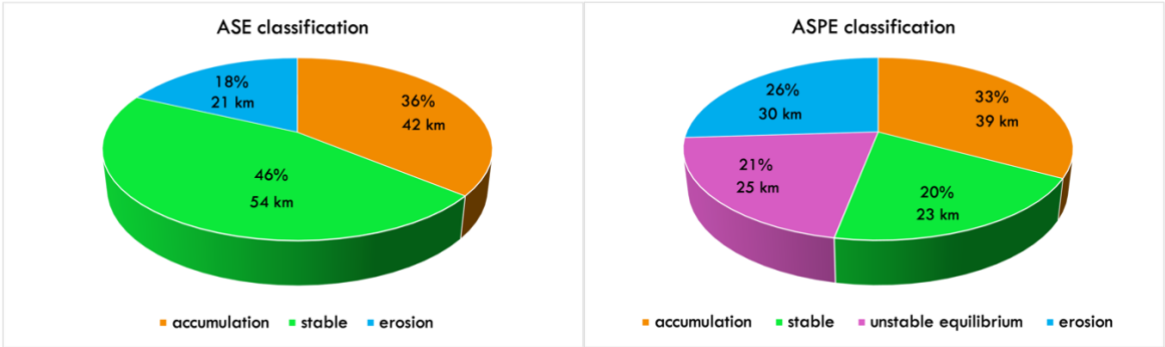


Figure 4.4 - Classification of the Adriatic coast of Emilia-Romagna according to ASE (left) and ASPE (right) indicators, considering the period between 2012 and 2018.

Reasonably, these kinds of classification have to be applied considering a defined range of time, which along the Adriatic coast of Emilia-Romagna is typically equal to 6 years, i.e. the frequency with which topo-bathymetric surveys are realized throughout the coast. Therefore, to date, the last available analysis is related to the period between 2012 and 2018 [1]. Figure shows the classification of the Emilia-Romagna littoral according to ASE and ASPE indicators in that period. Obtained values clearly proved the adopted strategies to be efficient for coastal defence along the regional coast since the overall unfavourable conditions decreased from 47% to 18%. In particular, during the analyzed period, nourishment interventions have been realized throughout the coast, with a total of 3.25 millions m³ of filling material. This

argument deserves a particular dissertation, which will be addressed in Chapter 4.2. All the previous observations highlight the fundamental role of coastal monitoring activities, which have been an essential topic for a long time in the regional littoral. Indeed, all the techniques and approaches described throughout this thesis have been employed for monitoring analysis in this region.

The following paragraphs will address some specific concerns about the Adriatic coast of Emilia-Romagna and its characteristics in supporting geodetic network, defence interventions, surveys performed, and wave-climate.

4.1 Coastal Geodetic Network (RGC)

The requirement for a common and unique reference system has been stressed more than once in the previous chapters when dealing with analysing and comparing multitemporal surveys. Therefore, at this point, it is known that such a system should be adequately defined and adapted according to the desired accuracy and the points realizing the associated frame need to be suitable for the surveying techniques to be used.

In the specific context of Emilia-Romagna, the gained experience in this field led Arpaè and the Region authorities to recognise the need for a geodetical supporting structure. This way, a reference for monitoring activities along the coast could be ensured. This project was also enhanced by the public interest of the regional littoral, meaning that different operating companies could potentially provide different data sources. To this purpose, a supporting infrastructure, the Coastal Geodetic Network (RGC), has been realized with the support of the Department of Civil, Chemical, Environmental and Material Engineering (DICAM) of the University of Bologna (Figure).

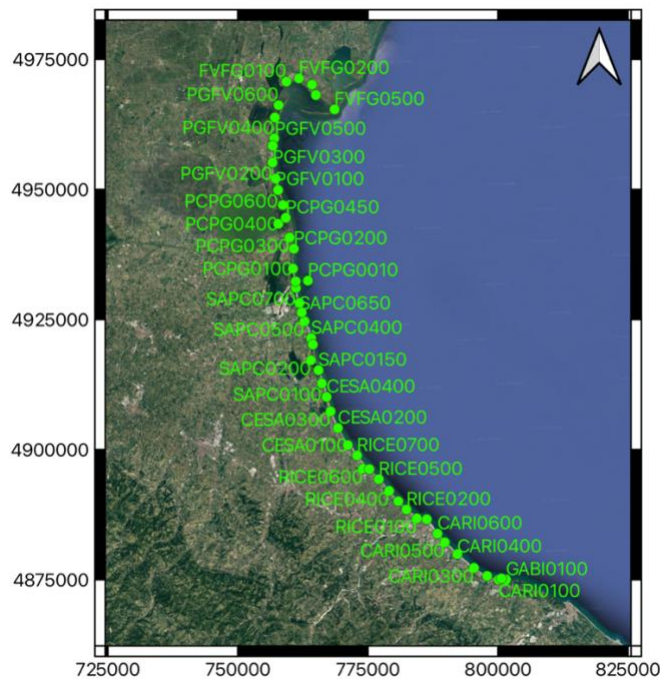


Figure 4.5 – Spatial distribution of the RGC benchmarks along the Adriatic coast of Emilia-Romagna. Coordinates are expressed in ETRS89-ETRF2000 (epoch 2008.0). Base map: Google Satellite.

In order to deeply understand the primary purposes and possible applications related to this network, it is essential to focus on the required characteristics that have been identified during the project’s preliminary phase. These specific requirements are listed below.

- Ensuring proper spatial distribution of the RGC benchmarks along the coast to enable the monitoring operations on the field without implying long distances. Since topo-bathymetric surveys are commonly performed exploiting the GNSS-RTK technique (see Chapter 3.1), a distance of 4-5 km has been chosen as the optimal value.
- Defining the coordinates of each benchmark with a centimetre level accuracy, both for plan and altimetry.
- Choosing points located as close as possible to the coast, behind the bathhouses, and possibly ensuring the long-term durability of the sites over time.
- Ensuring the suitability of all the benchmarks for measurements acquired both with traditional techniques (spirit levelling) and by GNSS positioning. This aspect impacts the site chosen for the installation since good sky visibility must be provided for the GNSS acquisitions, and a suitable position is required to manage the staffs.
- Definition of both the orthometric and ellipsoidal heights for each RGC point.

- Alignment of the points coordinates according to the official national reference system, the ETRS89- ETRF2000 (2008.0 epoch), as established by the Ministerial Decree of the 10th November 2011 [188].
- Avoiding unnecessary duplications and limiting the costs, considering including previously existing points. To this goal, a first inspection was performed to evaluate the possible presence of points belonging to older networks and their potential suitability in terms of associated characteristics.

Following these indications, the already existing networks in Emilia-Romagna have been carefully analyzed. Throughout Italy, in the last decades, many authorities have arranged their monitoring networks for different specific applications, such as the ones managed by the IGM, RER (Emilia-Romagna region), Idroser (Idrorisorse per lo sviluppo dell'Emilia Romagna), Agip and Arpa (today Arpae). Among these, the regional Levelling Network for Subsidence Monitoring [18] was firstly built by Idroser and later handled by Arpae. This network was established in 1984, and the last levelling campaigns were carried out in 1999 and 2005 to monitor the subsidence phenomenon. Thus, some of the existing benchmarks belonging to this network, whose characteristics have been found to be compliant, have been included in the new RGC. However, since the primary purpose of that network was related to levelling measures, the suitability for GNSS surveys was not always provided. Therefore other existing networks or new installations have been considered in these cases. Moreover, during these inspection activities, a “natural” decrease of the benchmarks over time has been observed, reasonably related to possible changes or disposal of the buildings and infrastructures where they were installed.

After that, the reference system used to align the RGC coordinates was chosen to be coherent with the Ministerial Decree of the 10th November 2011. This document states that the ETRS89-ETRF2000 (2008.0 period) is the official national reference system for all the public authorities in Italy [55]. As previously mentioned, in dealing with coastal areas, orthometric heights are fundamental for practical applications, especially considering flat and low-lying land such as the Emilia-Romagna littoral. For this reason, the availability of the orthometric height for each point was selected as a

fundamental requirement to provide proper support for surveying activities performed along the coast. Taking these characteristics into account, once the existing points and the chosen sites for the new installations had been identified, the actual survey campaigns started. The orthometric heights have been estimated by means of spirit levelling measurements starting from existing benchmarks. Since the orthometric heights for those points were referred to the 2005.58 epoch (July 2005), the official subsidence models provided by the Emilia-Romagna Region [205] have been used to update the height values to the current epoch.

For what concerns the plan components, the use of a static differential GNSS positioning has been chosen in order to obtain points' coordinates with high associated accuracies. The GNSS campaigns involved acquisition sessions ranging between 1h and 2h. Therefore, several baselines linking contiguous points have been computed, always considering the shortest possible distance within the 10 km range. Close permanent GNSS stations have been used for the baseline scheme where possible. Thanks to the baseline adjustment procedure, the final coordinates have been obtained for each RGC benchmark.

In 2019, the original RGC network was implemented, aiming at reaching a more homogeneous spatial distribution of the points and solving some issues related to the loss of a few benchmarks due to waterfront renovation works. In these cases, short levelling stretches have been identified for the campaigns, linking the new position with the closest existing benchmark. The GNSS campaigns followed the same approach used for the first RGC installation. Monographs describing each point and the measured coordinates have been published and are available on Arpaè's cartographic portal [178] (Figure).

arpa Regione Emilia-Romagna

Rete Geodetica Costiera per il Monitoraggio Topografico e Batimetrico - Vertici GPS stazionabili -

VERTICE: **RICE0700** Aggiornamento al 02/2018

Comune: Cesenatico Provincia: Forlì - Cesena
 Indirizzo: Viale Giosuè Carducci Località:
 Ubicazione: Presso Istituto Agnelli

Istituto da: Arpa Anno: 2017 Denominazione: RICE0700
 Rete di appartenenza: Rete Geodetica Costiera

Altra rete di appartenenza:
 Denominazione:

Inquadramento geografico

Coordinate geografiche ETRS89-ETRF 2000 (2008.0) EPSG: 6706
 Lat (°): 44,19220344 Long (°): 12,41481162
 Quota ellissoidica h (m): 42,03 Data di acquisizione: 27/04/2017
 Quota ortometrica H (m): 2,56 Data di riferimento: 05/2011

Coordinate plane ETRS89-ETRF 2000-UTM 32N (2008.0) EPSG: 7791
 Est (m): 772898,87 Nord (m): 4898893,04

Descrizione caposaldo

Tipologia: Borchia
 Descrizione: Infissa in cima alla scala che collega l'Istituto Agnelli alla spiaggia

Problematiche d'accesso:
 Data ultimo rilievo GNSS: 27/04/2017
 Data ultimo rilievo livellazione:
 Data ultimo sopralluogo: 27/04/2017 Operatore: Capone, Dovesi - UNIBO

Note: La quota ortometrica è stata ottenuta, tramite livellazione geometrica dal mezzo, a partire da quella del caposaldo 123400 (rilevata da Arpa nel 07/2005) appartenente alla Rete regionale di controllo della subsidenza - La quota Luglio 2005 è stata aggiornata al Maggio 2011 tramite il modello di subsidenza stimato con misure interferometriche. Borchia posizionata sul retro dell'Istituto Agnelli, nelle vicinanze di Piazza Marconi nota per il monumento a Marco Pantani.

Figure 4.6– Example of a monograph of an RGC benchmark.

The RGC geodetic network realises fundamental support for any monitoring activity performed along the Adriatic coast of Emilia-Romagna. It ensures the possibility of performing surveys both using classical topographic techniques and GNSS measurements, having available precise coordinates of reference points aligned to the official Italian reference system. This fact, in turn, allows proper management and reliable comparisons of repeated surveys performed over time, which are essential aspects of coastal dynamics studies. Moreover, it should be stressed that all the project has been carried out following an approach of reuse and economic saving, trying to include already existing benchmarks [55].

4.2 Nourishment interventions

The maintenance of the current status of a coastal stretch or the reduction of coastal erosion problems can be obtained through the realization of coastal defences interventions. These are commonly included in management projects and strategies,

aiming at the prevention and maintenance from a short or long-term point of view. Structural interventions include the so-called "hard structures", with specific layouts which imply different interactions with the beach's morphology, depending on the natural trend of the coastal stretch of interest. Hard structures include for example: detached breakwaters, low-crested structures, field of wood and rock groynes and submerged sandbag barriers (Figure). However, in general, the construction of hard defence structures can lead to collateral impacts due to the modification of the beach's profile and sediment dynamics, with possible increased erosion seaward of the structure itself [132][95]. On the other hand, they naturally induce visual and environmental effects and require continuous maintenance, even if they are properly designed to adapt to extreme events [156].



Figure 4.7 – Detached breakwaters at Rimini beach.

The current trend of coastal policies is going towards decreasing effects on the environment and the population, also considering the increasing issues related to climate change. In this context, “soft” techniques such as beach nourishment could represent a suitable alternative [116][133]. Beach nourishment is a non-structural defence intervention, which consists of replacing sand on eroded beaches, where the material can be later rearranged by natural processes (Figure). In fact, thanks to the natural coastal drift, the benefits of such interventions are not limited to the original area where the material is filled but can also involve the downdrift beaches. These

interventions balance the natural sediment contribution's lacks, thus generating a more robust beach system, thanks to the height increase and the sandy shore enlargement [133]. The sandy material can be extracted from different areas, such as land quarries, river beds, coastal areas or under-water borrow areas. In order to choose the proper source of the material, it is necessary to carry out sampling campaigns to evaluate the grain size and the composition of the sediments, ensuring that it is consistent with the in-situ sand. Then, the selected material can be transported both by land, using trucks or pipelines, or by sea. In the second case, material from submarine borrow areas can be transported by dredging-equipped vessels through floating ducts directly connecting them with the beach. Therefore, nourishment interventions which imply the exploitation of underwater material and sea transportation, allow for minimizing the environmental effects on the coast, the surrounding areas and the transports, i.e. all the factors that can also burden touristic activities [157].



Figure 4.8 – Work in progress during the third beach nourishment intervention along the Adriatic coast of Emilia-Romagna.

The scaling of these interventions is not a simple matter, as several factors must be considered, such as the sediment granulometry, the characteristic wave climate and sediment transport, and the interaction with any hard structures present in the area. Within the framework of a nourishment project, it is necessary to determine the precise area interested in the filling, the total sand amount (m^3/m), the material characteristics in terms of required granulometry and extraction source used, the volume

configuration and the possibility to combine the intervention with any hard defence structures (“protected nourishment”). The durability of the desired effects is connected with the extension of the beach where the material is filled since the wave action is more intense for smaller areas; therefore, a good option could be to extend the interventions in width and length. Unlike hard defence structures, these interventions imply a meager visual impact, only concerning the days of material transportation and do not require any maintenance works [157].

On the other hand, beach nourishments, like any other defence intervention, need to be related to monitoring plans to analyse the state and the evolution of each involved beach and the effectiveness of the intervention itself. In this context, monitoring activities are realized by performing multitemporal surveys at different times on the emerged and submerged beach: before the nourishment intervention (*first plant survey*), immediately after the nourishment intervention (*second plant survey*), and about one year or more after the activities. Thus, the amount of material, the shoreline changes, and the height variations can be evaluated by comparing surveys related to different times in the same area [58].

Since the last century, the Emilia-Romagna Region has addressed the problem of coastal erosion with specific coastal plans consisting of several defence interventions. In the beginning, the used approach involved the construction of different types of hard structures, which resulted in a total of about 75 km of regional beaches protected in this way [4]. Among these, the most common are the emerged detached breakwaters that defend about 40 km of coastline [152]. However, the regional shoreline has stiffened over time with the presence of these structures, thus inducing public authorities to change the employed approach [114]. The Project for the protection of the Adriatic shoreline in Emilia-Romagna - “Piano Costa 1981”, adopted by the Region at the beginning of the ‘80s, suggested nourishment interventions as an alternative to the hard defence structures. One of the first nourishment techniques consisted of taking sand from inland borrow areas and transporting it with trucks to the beach. In

2002, the Emilia-Romagna Region carried out the first beach nourishment intervention on a regional scale, using material from a submarine borrow area located offshore the regional coast. Specific surveys have been performed to constantly monitor the environmental effects, confirming the obtained decrease in erosion effects. In 2007, the Region Authority decided to carry out a second intervention on a regional scale [121] and thanks to the good results obtained from previous interventions [4], lastly, in 2016, the third intervention of “Security projects through submarine sand nourishment for critical areas of the regional coastline” was completed [126][157] (Figure). Currently, this is the most crucial intervention ever realized along the Adriatic coast of Emilia-Romagna regarding technical and economic resources and sand volumes involved. The material filling involved eight beach areas in a critical state, with a total extension of more than 12 km. For the withdrawal, an underwater sandy deposit located about 57 km offshore of Porto Garibaldi at a depth of about 40 m was chosen (Figure). Actually, since the beginning of 2022, a fourth nourishment intervention has been launched, involving about 11 km of beaches. The first part of this project concluded in May 2022, while the activities will continue on other coastal stretches starting the next year.

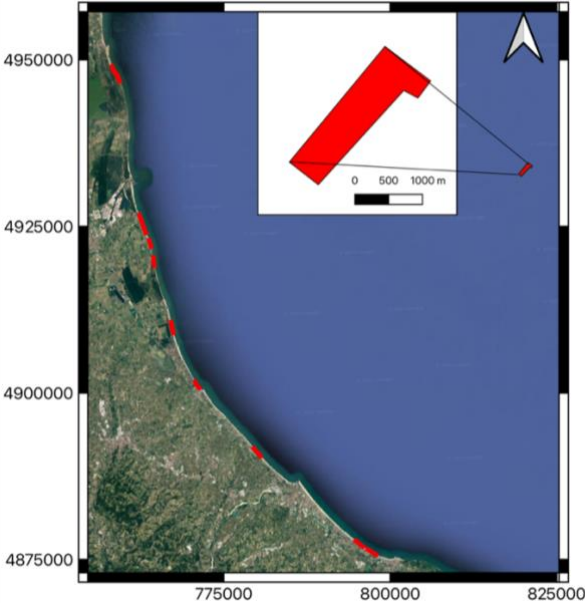


Figure 4.9 – Coastal stretches involved in the third beach nourishment of 2016 and submarine borrow area offshore Porto Garibaldi.

The nourishment intervention of 2016 required a monitoring plan for the years 2017 and 2018: the surveys concerned a wider area than the one involved in the sand nourishment, allowing the evaluation of the dynamics of the sediment transport, as well. Moreover, surveys in areas where changes are not expected could guarantee a further possibility to verify the obtained results. The monitoring, designed by Arpaè - Coastal Monitoring Unit, involved the survey of over 200 km of topo-bathymetric profiles on about 20 km of emerged and submerged beach and the bathymetry of the withdrawal area [3]. The extension of the surveyed submerged beach was limited at the bathymetry of 5 m. Transects were about 500-1000m long, with 100-200m inter-transect spacing. The monitoring sections defined within the project mainly included cross-shore transects (i.e. orthogonal with respect to the coast) and a certain number of along-shore transects (i.e. parallel to the shoreline), especially over the emerged beach or in other areas close to hard defence structures.

4.3 Marine dynamics

The analysis of the littoral dynamics and the morphological variations requires knowledge of the wave climate conditions experienced by the observed coastal area. Commonly, the wave climate over a particular zone can be identified by four main parameters: the significant wave height (H_s), the mean origin's direction of the waves (D), the relative mean period (T_m), and peak period (T_p). In particular, the significant wave height represents the mean value of the highest third of the occurred waves, the peak period is defined as the time associated with the most intense waves, and the mean period is the mean of all waves-associated periods over a certain time span.

The Italian Rete Ondametrica Nazionale (RON) consists of 15 measuring stations located at specific sites all along the coasts of the Italian peninsula and around the main islands [167]. All the buoys belonging to the network continuously acquire wave climate-related data able to describe the state of the sea of a specific neighbouring area.

However, along the Adriatic coast of Emilia-Romagna, the wave parameters are currently measured, taking advantage of a buoy located 8 km offshore of Cesenatico at a depth of about 10 m. This buoy, named Nausicaa, has been managed by Arpae since May 2007. In particular, the Nausicaa buoy is the closest station with respect to the Emilia-Romagna littoral, located in a central position considering the shape of the regional coast (Figure).

The onboard system acquires wave climate data at semi-hourly frequency, together with the local temperature of the water. The wave parameters acquired by this buoy are publicly available thanks to the Dext3r web service of Arpae [206], which also archive the complete time series.

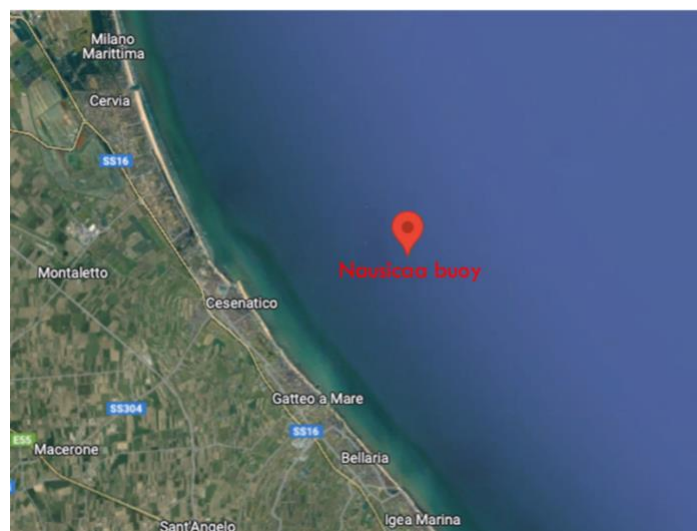


Figure 4.10 – Localization of the Nausicaa buoy offshore the beach of Cesenatico.
Coordinates (WGS84): Lat 44°12'55.8'' N, Lon 12°28'35.8'' E.

Typically, the wave climate is represented by pie charts linking the significant wave heights to the wave origin's directions, classifying the waves' distribution based on heights and directions classes. Both for height and direction, the ranges can be arbitrarily defined according to any specific requirement. However, a common approach is usually adopted: the Douglas Scale classification is used for the H_s , and the nautical sectors are used to classify the wave directions, using centred classes with 22.5 degrees of width (Table).

Table 4.1 – Classification of wave directions according to the nautical sectors (N: North, E: East, S: South, W: West).

| | | | | | | | | | | | | | | | |
|----|-------|-----|-------|-----|--------|-------|--------|------|--------|------|--------|------|--------|------|--------|
| 0° | 22,5° | 45° | 67,5° | 90° | 112,5° | 135°N | 157,5° | 180° | 202,5° | 225° | 247,5° | 270° | 292,5° | 315° | 337,5° |
| N | NNE | NE | ENE | E | ESE | SE | SSE | S | SSW | SW | WSW | W | WNW | NW | NNW |

The present analysis defined four classes adapting the Douglas sea scale to the experienced values in the considered area, thus excluding the more intense conditions (Table).

Table 4.2 - Used classification for the significant wave height.

| | | | | | |
|-----------|-----------|-----------|-----------|-----------|-------|
| H_s (m) | 0.20–0.50 | 0.50–1.25 | 1.25–2.50 | 2.50–4.00 | >4.00 |
|-----------|-----------|-----------|-----------|-----------|-------|

Considering the period between 2012 and 2018, calm conditions occurred for about one-third of the total acquisitions. Observing the waves' direction, the East sector (90° N - Levanter) is experiencing the higher number of waves, equal to about 20% of the total incoming ones. The occurring percentage gradually decreases from ESE (112,5° N) to ENE (67,5° N), with 13% and 12%, respectively, while other sectors have lower associated values.

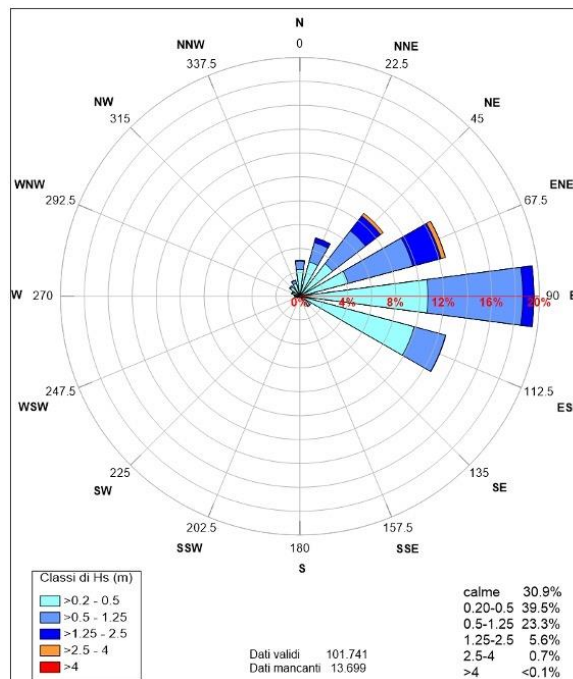


Figure 4.11 – Pie chart of the wave climate measured by the Nausicaa buoy between April 2012 and October 2018.

Source: [1].

Looking at the significant wave heights, low waves (0.20-0.50 m) are the most frequent in the whole period, equal to about 40% of the total. Medium-high waves (>1.25 m) are mainly generated from the ENE sector, with a rate of occurrence of about 6%. The sector associated to Bora (NE – 45°) also presents a certain occurrence of moderate waves, equal to 1.8% of the total [1] (Figure). The same analysis was performed on a seasonal scale, thanks to the high data coverage (about 88%) in the analyzed period. The observed trends can be summarized in the following points [1]:

- Calm conditions are more frequent during winter and summer seasons than during autumn and spring, with associated rates of 33%-36% and 26%-27%, respectively;
- the more frequent wave direction is East for spring, autumn and winter, with similar associated rates (21-26%), while ESE has the higher rate in summer (about the 18%);
- low waves (0.20-0.50 m) occur with the highest frequencies for all the seasons, with values of about 30-37% in autumn and winter, and 42-47% during summer and spring;
- medium-high waves (>1.25 m) are mainly generated from ENE sector, apart from the summer period when they present very low rates;
- higher waves (2.00-4.00 m) come from ENE both in autumn and winter, which presents higher rates of occurring.

The acquired surge's conditions between 2012 and 2018 are generated from a minimal sector of directions. Higher waves ($H_{max} > 3.5 \text{ m}$) are related to the directions from Bora to Levanter (45°-67.5°), also with the associated longer durations.

Wave-climate parameters also allow computing the closure depth, whose relevance was already mentioned in Chapter 1, as the value representing the seaward limit of the active area of a beach [10][135][104]. A study by [135] estimated the closure depth along the regional littoral, considering the period between May 2007 and December 2014, amounting to about seven years and a half. Four different approaches have been adopted for the computation, i.e. the medium and maximum values within the whole distribution, the depth corresponding to the 95% cumulative frequency, and the value

according to Hallermeier [65][66] which uses H_s values exceeding 12h/y. Obtained values are listed in Table .

Table 4.3 – Values of closure depth according to four different approaches, as estimated by [135]. Mean and maximum values of the total distribution, depth corresponding to the 95% of cumulative frequency, and value according to Hallermeier formula.

| Approach | D_c (m) | H_s (m) | T_p (s) |
|--------------------|-----------------------------|-----------------------------|-----------------------------|
| mean | -0.9 | -0.4 | 4.3 |
| max | -7.6 | 3.9 | 9.1 |
| 95% | -2.7 | 1.3 | 6.6 |
| Hallermeier | -4.4 | 2.2 | 7.2 |

Therefore, for about eight years, the active submerged beach extends until the bathymetric of 4.4 meters, where waves of 2.2 meters operate. Another sector of the beach can be identified beyond the closure depth, the lower shoreface, which represents the area which could be potentially affected by morphological changes only in case of intense events occurring [170]. This limit, reasonably related to less common events, could be estimated by considering the higher wave conditions in the selected period, equal to 3.9 meters, resulting in a depth value of about 8 meters [135].

Chapter 5

5 Processing and Products

Whatever the employed technique, coastal analysis usually relies on several parameters, which are required to extract useful information for the sake of the following evaluations. Therefore, depending on the final goal of the monitoring surveys, different elaborations can be performed starting from the data collected on the field. In some cases, specific monitoring activities can be based on particular parameters, while, in general, the same products have to be extracted. The primary products required to carry out coastal studies include topo-bathymetric maps (DEMs), profile sections, maps of height-variation and shorelines. Reasonably, considering the existing differences between the employed geomatic techniques, especially in terms of the nature of the acquired raw data, the same product can be obtained by applying different elaborations, using different software, with different processing time and computing efforts, and with different associated accuracy and reliability [30][24][118][143][101][37][163]. Employing the mentioned products, most studies on coastal zones need to extrapolate some parameters to understand and describe the observed trend affecting the selected areas. Among these, we can refer to topo-bathymetric profile changes along defined sections, sand volume variations, accumulating/eroding beach sectors, and shoreline trends over time.

Figure shows the typical workflow of coastal monitoring analysis, aiming at producing 3D maps as a starting point for all the following analyses. This Chapter provides a description of the standard approaches employed to produce the primary products and some additional considerations to optimise the processing as much as possible.

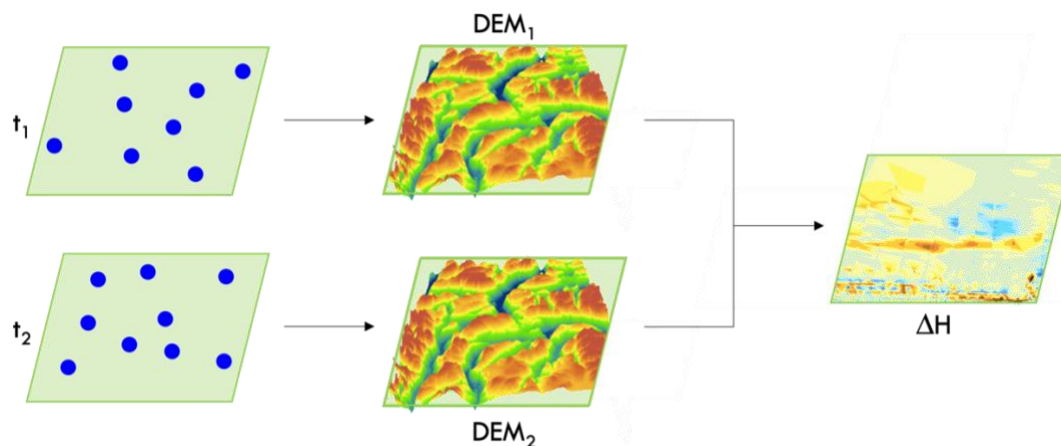


Figure 5.1– General workflow of coastal monitoring, independently from the employed technique. 3D maps (DEMs) are produced starting from the measured points and compared at different epochs.

To perform the elaborations, the support of Geographic Information Systems (GIS) can be very useful, as they allow managing geographic data, together with the associated databases, enabling several different analysis and visualizations. Another benefit of using GIS-based software is the possibility to couple different data sources with proper management of the associated reference systems, which is known to be a significant issue when dealing with different data sources. In fact, in a GIS environment, data are organised into overlapping layers, that can be combined exploiting different kinds of processing and tools. Moreover, many public data sources are currently available, in different file formats, and can be coupled with the data collected by the user to have additional information or general overviews of the analysed areas. Another advantage of using GIS is related to the Open Geospatial Consortium (OGC) Web Services (OWS), which allow many different geospatial functionalities, including access to several data sources and their processing [224].

This public availability is mainly due to the development of policies which led to simplifications in the administration of geographic and spatial data. About this, the INSPIRE Directive 2007/2/EC took effect on the 15th May 2007, to establish an infrastructure of spatial information in the European Community, to enhance the sharing of spatial data among public administrations, simplify the public access to environmental data throughout Europe, and assist decision-making processes concerning the environment and land [174]. In this context, particular attention is given to the metadata which is fundamental when managing products from different sources. Therefore, this infrastructure is strongly supported by policies, legislation, and technical guidelines, concerning both the applied processing, the associated metadata and web services [214].

According to this shared approach, many public authorities started making many available sources of data, such as the National Geoportal [174], the regional Geoportals (e.g. <https://geoportale.regione.emilia-romagna.it> in Emilia-Romagna) and the Regional agency for prevention, environment and energy (e.g. <https://www.arpae.it/it> - Arpae in Emilia-Romagna), in Italy.

Indeed, other software packages can be used to perform the required elaborations, sometimes with advantages related to an amplitude of processing possibilities, more customizable options or even more choices for the data representation. On the one hand, of course, using a specific software can ensure obtaining the products with greater confidence, at least for certain kinds of elaboration. On the other hand, however, due to the continuously increasing availability of software and tools, the choice of the most suitable one may be complicated and influenced by the study to be performed [99]. For this reason, sometimes it could be better to address the choice toward open-source and free software, which can lose some benefits in terms of processing possibilities, at least for the default options, requiring more customization by the user, but at the same time can entail several advantages. These include, for example, the possibility to find public repositories, tools and scripts which can speed

up and improve the elaboration phases. For example, QGIS software [228] is related to wide dissemination of publicly available tools created by common users, and thanks to the relying on the python console, lots of the processing can be managed by generating automated workflows more efficiently.

Another significant available option in recent years is the Google Engine platform, that is free for academic and research use [183]. This application, launched in November 2011, provides the possibility to develop and host data processing in Google-managed data centres, allowing all users to rapidly and accurately perform elaborations on vast amounts of data even without having powerful workstations. In fact, the availability of computation facilities combined on the server side of the platform can enormously reduce the processing time for several possible applications [89]. Earth Engine Explorer (EE Explorer) is a data viewer for geospatial imagery with a simplified graphic user interface (GUI). This is related to the access to a large set of regional and global datasets, containing a continuously updated satellite image archive and geospatial datasets with planetary-scale analysis capabilities, the Earth Engine Data Catalog [89]. The EE Explorer has an integrated Data Catalog page and a Workspace [217]. Moreover, thanks to the EE Code Editor, all the operations can also be managed using different programming languages, making the workflow of complex geospatial analysis speedy and straightforward.

5.1 Topo-bathymetric maps

Topo-bathymetric maps are obtained starting from the data acquired on the field, by processing them to realize a surface describing the height trend in all the analysed areas, including both the emerged and the submerged beach. In fact, as surveys are typically carried out on a discrete level, and collected points can be unevenly distributed, it is necessary to have information able to describe an overall picture of the entire area of interest. Note that referring to the acquired points, a set of 3D

coordinates, two for the plan and one for the altimetry, is meant (Chapter 3). The positions of the points collected on the field are organized in tables containing the three coordinates values, usually converted into *shapefile* format for more effective use in the GIS environment [215]. The first operation consists of analysing the detected points to visually check for the possible presence of any outliers or other points that could produce misinterpretations (e.g. points acquired on defence structures), improving the reliability of the final maps. Such maps can easily give a general overview of the area with respect to a set of acquired points, even though they are densely distributed. Topo-bathymetric maps, called Bathymetries for sick of simplicity or if they only concern the submerged beach, are full-fledged Digital Elevation Models (DEMs) (Figure). Moreover, they represent the most conspicuous variable to be considered in any study involving marine environments and the starting point for most of the following elaborations [17].

Bathymetries are commonly obtained through spatial interpolation processes, which basically require four parameters to be selected: the interpolation algorithm, the variable interested in the interpolation, the extension of the newly created map, and the spacing.

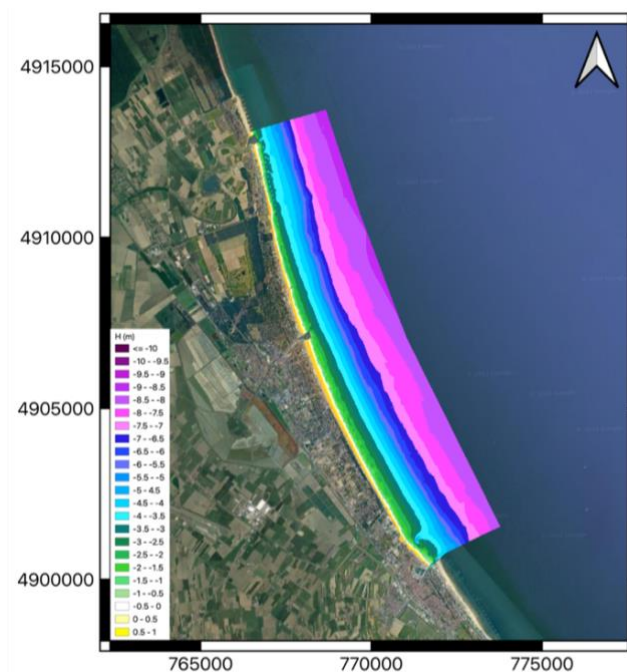


Figure 5.2 – Example of a topo-bathymetric map in the area of Cesenatico in Emilia-Romagna.

The chosen interpolation method directly impacts the final DEM product since it is the algorithm used to estimate the values at the centre of each pixel of the newly produced grid. In general, interpolation is the process of mapping a variable at unsampled locations using a set of samples of known location and value, which in this case come from a survey campaign carried out on the field [210] (Figure).

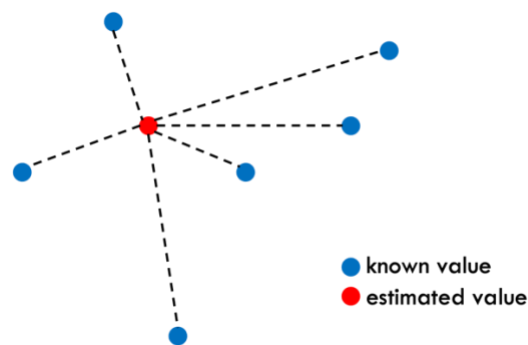


Figure 5.3 - Basic principle of the interpolation process.

In general, dealing with interpolation processes, it is crucial to be aware of the real meaning of the created map, as a final product can be obtained in several ways [108]. Spatial interpolation methods can be classified into two main categories: deterministic and geostatistical techniques. The first class of approaches is based on mathematical equations that allow predicting values at unsampled locations, while they do not consider the spatial structure of the data. Depending on the particular algorithm, clearly, the estimated values will depend on different known samples in terms of number, location, geometry, and weights associated to the considered points. For what concerns geostatistical algorithms, they must fit a spatial model to the input data, thus obtaining not only the predicted value at the unsampled location but also the estimated uncertainty of each prediction [17]. Among the deterministic approaches, the Triangulated Irregular Network (TIN) is one of the most commonly used algorithms for its inherent simplicity and its characteristic smoothing effect, which leads to easily readable maps. This method is based on constructing a triangular network, or tessellation, which depends on the input samples' location. Commonly, the Delaunay's triangulation method is applied, having the following main characteristics: a) triangles are as equilateral as possible, b) triangles never overlap

each other, c) each circumscribed circle contains only the three triangle's vertexes and no other sample points are present inside it [150] (Figure).

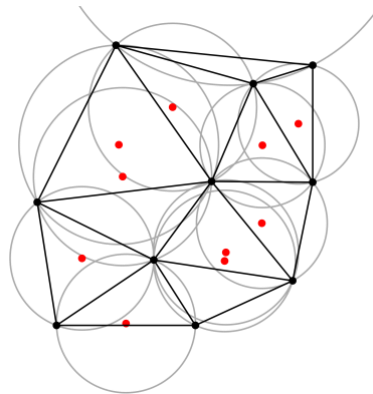


Figure 5.4 – Delaunay triangulation: triangles, circumcircles and centres (red dots). Source: [185].

The positions of the new estimates inside the triangles are then obtained by weighing the values of the three vertexes. Thanks to its simplicity and low computing effort, the TIN method can be applied by means of many different software. In fact, contrary to other interpolation approaches, it can be easily applied with lots of input samples without leading to high computational efforts. For this reason, it is commonly used to interpolate 3D points from topo-bathymetric surveys. The main drawback of this approach results when isolated samples are present, as the triangles become larger making the estimation more imprecise and less reliable. In such cases, unrealistic discontinuities or slope effects can appear due to very abrupt height variations in the considered triangle's vertexes.

A preliminary analysis of the effects of interpolation methods on coastal-related products has been performed in the context of a master thesis which I followed as co-supervisor during the PhD period [177]. Here, starting from the same set of points collected by means of GNSS-RTK coupled with a multibeam echo sounder (Chapters 3.1 and 3.2), some elaborations have been performed by changing the interpolation method and the spacing in order to evaluate any qualitative and quantitative differences. The considerations obtained within that study can be meant as preliminary results, primarily since they are related only to one selected study area.

Indeed, to obtain more significant results, which could be extended and applied for any case study, it would be necessary to have a ground truth reference, such as a high-density digital elevation model. Anyway, the performed analysis showed that, at equal spacing, the interpolation method results more impactful for higher spatial resolutions, while the differences strongly decrease when lower resolution maps are considered due to a general smoothing effect. Moreover, the geometric distribution of the samples is commonly the main impacting factor in such analysis.

Going back to the parameters used in the interpolation processes, the variable to be estimated for each future pixel of the DEM is the height. Depending on the data source and thus on the adopted surveying technique, one will deal with orthometric or ellipsoidal heights (Chapter 2.1). The extension evidently represents the area that is described by the map; therefore it is directly connected to the survey's extension and to the area of interest for the specific purpose. It is necessary to note that interpolation algorithms commonly fail close to the boundaries for the so-called "boundary effect" which leads to errors in the prediction due to the lack of enough data for the computation. For this reason, it is often necessary to proceed in clipping the maps by visually analysing where these effects are present. The spacing parameter is the most significant because it impacts the accuracy and reliability of the obtained product in the whole area. It represents the dimension of each pixel of the grid, i.e. the detail scale that we will be able to observe from the map. The chosen spacing is directly connected with the effective spatial structure of the points collected on the field to avoid possible mismatches and interpolation errors, which are mainly tricky for low spatially distributed data [101][92]. An over-estimated value of the spacing leads to an unjustified smoothness in the map and a loss of important data because from the bathymetry we will be able to observe information only at pixel scale. On the other hand, if the spacing is under-estimated, the interpolation process can produce fiction effects in the map, because there are no actual data to be used for the interpolation at the chosen detail level.

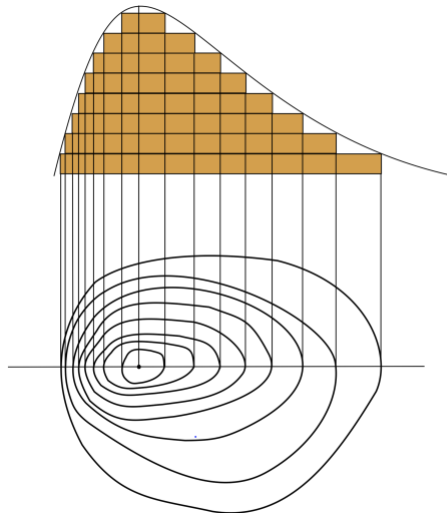


Figure 5.5 – Basic principle of contour lines jointing points at the same height. Source: [184].

It is inherent in their definition that matrices of pixels represent topo-bathymetric maps. This means that data are organized into columns containing the pixels' coordinates and the estimated value (height) obtained from the interpolation process. Such tables can be saved and shared through different text file formats, such as .csv, .txt, and .xyz. When working in a GIS environment, bathymetries have to be converted into raster files, typically using the .tif format (Figure). A raster file can be easily obtained by means of GIS-based software, using other particular software, or by converting the .xyz file into .tif using specific python packages. The obtained product can finally be managed using different visualizations, such as the contour lines, i.e. curves which joint points at the same height (Figure 5.5). Using this kind of visualization, it is good practice to choose the spacing among the contour lines related to the spatial resolution of the bathymetric map.

As discussed in the previous paragraphs, topo-bathymetric maps are obtained starting from available topo-bathymetric surveys, which always require significant time and efforts, whatever the employed technique. It is not difficult to deduce that these bathymetric maps are usually available only for specific and limited areas where dedicated surveys are performed.

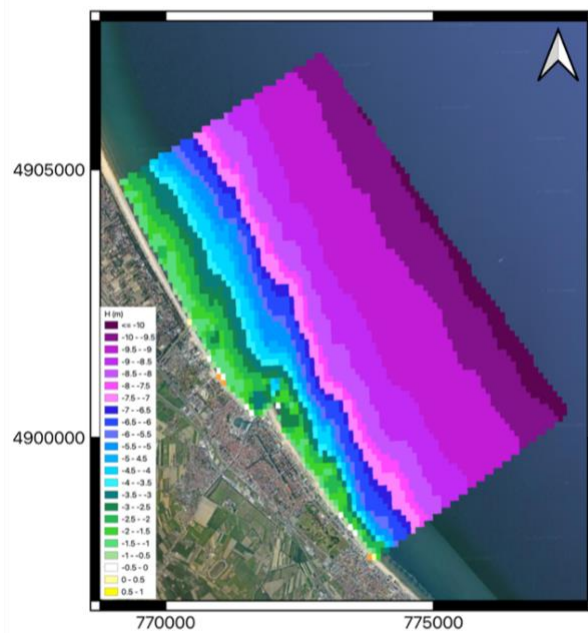


Figure 5.6 – EMODnet Bathymetry for a selected area in QGIS software.

Nevertheless, at higher spatial scales, other data sources can be considered, including, for example, the EMODnet Bathymetries which are freely available for browsing and downloading through the Bathymetry Viewing and Download service [214]. EMODnet DTM has been generated for European sea regions (36W,15N; 43E,90N) exploiting and integrating different data sources, such as composite DTMs and Satellite Derived Bathymetry (SDB, produced from Landsat 8 and Sentinel images) data products. Therefore, thanks to the availability of bathymetric surveys and DTMs datasets from public and research organizations, these final products have been processed for different maritime regions in Europe. Moreover, any possible gaps with no data coverage have been filled by using the global GEBCO Digital Bathymetry [216]. EMODnet bathymetric grids are aligned to the WGS84 geodetic system, and the water depth values are in meters with reference to the LAT. Reasonably, due to the integration of different sources, the accuracy and precision of the final products are variable within each area, although the processing involves different steps to check for possible anomalies or datasets not satisfying the chosen criteria. The DTM products can be freely downloaded in several output formats (ex. GIS layers) or managed as OGC web services (WMS, WFS, WMTS, WCS) (Figure).

5.2 Profile sections

Another significant product that can be helpful in understanding and describing the trend of a coastal area is the so-called beach profile. In particular, a profile section is a curve representing the height values with the increasing distance. These trends are commonly analysed in the cross-shore direction, where the zero-distance coincides with the first acquired point on the backshore [88][80].

Depending on the surveying technique used, these profiles can relate to both emerged and submerged beach, allowing, in this second case, also to evaluate the shape of the seabed in the area. As mentioned in Chapter 1, when dealing with coastal monitoring activities, it is necessary to define a Monitoring Plan which includes the definition of some sections, both along and cross-shore (Figure). This means that data will be acquired approximately on the same positions when repeating multi-temporal surveys, even if realized by different surveyors or companies. Obviously, it is impossible to have the confidence to say that the exact point will be surveyed after a while, due to the fact that the analyzed techniques deal with the collection of points spaced out of a certain distance. On the other hand, the exact point-wise information has no meaning in itself, since the trend of several points is observed, and, certainly, the existing spacing among them is coherent with the overall profile analysis.

Unlike the topo-bathymetric maps, which provide a global description of the area and reasonably do not allow inferring small-scale information, profile sections allow observing local trends and variations in the study area. In particular, profile sections related to multitemporal surveys are commonly compared to acquire different information about the beach trend over time. At a short time scale, these comparisons are performed in the context of defence interventions, such as the realization of beach nourishments or the construction of new structures, to observe their effects on the neighbouring areas. These effects can include, for example, the generation of bars and dunes, or other local patterns close to any defence structures.



Figure 5.7 – Monitoring sections along the Emilia-Romagna littoral. (Arpae).

At longer time-scales, the comparison between repeated profiles allows the evaluation of the shoreline’s advancement or retreat and the raising or lowering of the beach height over time (Figure). All these parameters are fundamental for coastal management, as they can indicate the overall condition of each area.

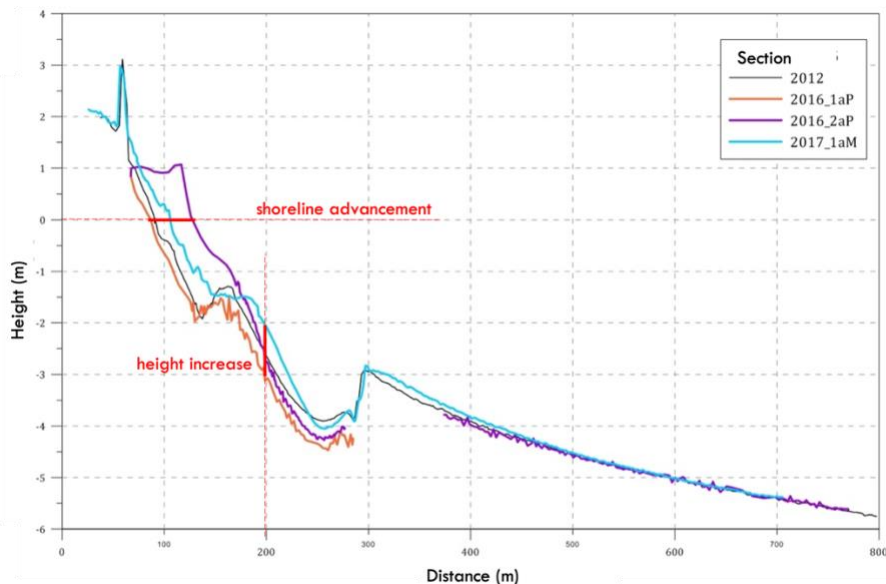


Figure 5.8 – Example of a beach profile and significant derived parameters.

The method used to extract this kind of product is related both to the survey technique, thus to the acquired points’ configuration, and to the computing approach. Available

approaches can be mainly divided into those based directly on the acquired points and those relating to the already interpolated data. As it often happens, it is not generally possible to determine whether one method is better than the other or vice versa in absolute terms. The obtained products' reliability is primarily related to the survey's nature, meaning that the spatial resolution of the acquired points determines how to deal with the profiles' extraction. In these terms, some general considerations can be done. The computing of beach profiles starting from the acquired 3D points is more time-consuming, as it involves different steps commonly performed using different software, even if some of these can be done within automated workflows. Differently, when profile sections are extrapolated starting from topo-bathymetric maps, the computing's effort can be very low, involving even only one processing phase. In the paragraphs below, the two methods will be more deeply described.

From the previous paragraphs, we are now aware that the positions of the collected points are managed through tables which contain the three coordinates in the selected reference system and that they are usually handled in the form of shapefiles for use in the GIS environment. Indeed, GIS-based software are used for most of the required operations to obtain the profile products. Having available the sections defined within the monitoring plan, which hopefully have been followed during the survey on the field, the first operative phase consists of creating a neighbourhood of each of these lines. This is required since lines' geometries, like the ones of the monitoring sections, have no associated thickness, which is needed to differentiate points placed along them from those not. Commonly, the Buffer operation is employed for this phase, computing a neighbourhood of the selected geometry with an associated distance chosen by the user. The distance's value is therefore arbitrary determined, with the priority of being coherent with the data source. This means that it should be chosen depending on the spatial resolution of the acquired points, following the right trade-off between containing enough points for each section and having lots of them. In both

cases, having a few points or too many contained within a section's neighbourhood will require a following manual post-processing phase.

Figure graphically shows the problems related to the two mentioned situations. The first case (Figure a) would lead to a loss of information, which can also be related to particular or local trends, because the obtained curve will be generated by interpolating between points too far apart. On the other hand, the second case (Figure b) would result in too scattered curves, making the visual analysis tricky and sometimes even erroneous, also bearing in mind that, since these kinds of products are commonly used for data dissemination, they should be easily understandable. For this reason, there is no better method in absolute terms, but this conceptual approach should be applied to avoid long manual processing and primarily to ensure reliable results. This is even more important for the submerged beach, where it is more difficult for the surveying vessels to follow exactly the monitoring sections (see Chapter 3.2).

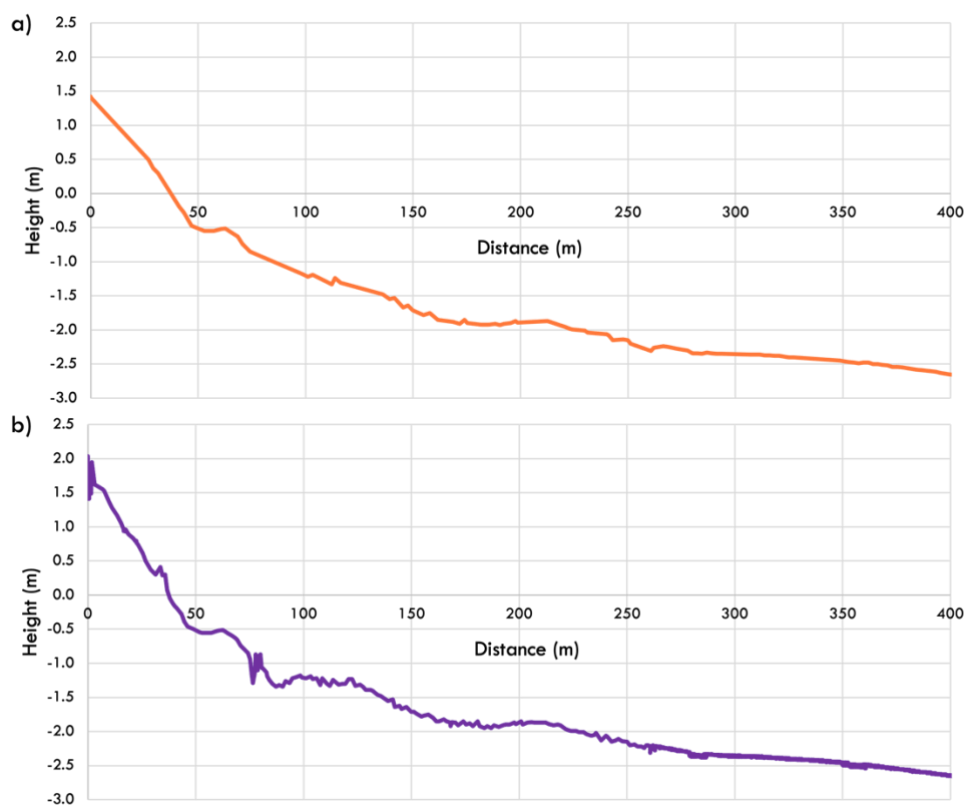


Figure 5.9 – Examples of the same profile extracted using few points (a) and too many points (b). In the first case, the loss of information, especially at smaller distances, is shown, whereas the second approach leads to confusing patterns.

After creating the neighbourhood, a selection is made to highlight the inside points, i.e. the ones belonging to the selected profile section. After that, it is possible to proceed differently depending on the final goal. If only the profiles for the specific survey are required, many tools to extract them from the previously selected points are available and can quickly generate the desired results. However, monitoring activities usually deal with multi-temporal surveys; thus acquired profiles along the defined sections are always compared with previous results, also years later. Figure 5.10 shows the typical procedure to compute beach profiles starting from the acquired 3D points.

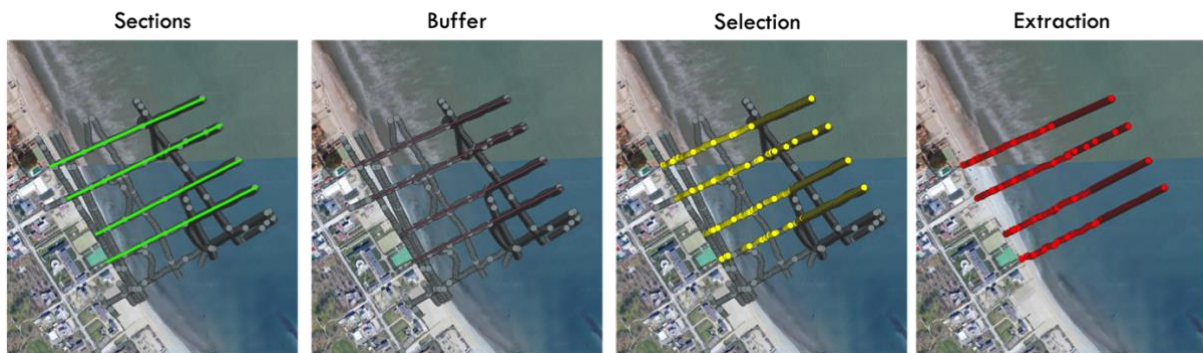


Figure 5.10 – Required steps to extract points along the monitoring sections through Buffer and Selection operations.

Therefore, extracting the profile data in a way that can be easily managed and repeated for different surveys could be useful, maybe also using automatic workflows. To do this, the coordinates of the selected points are extracted and handled in Excel sheets or similar environments (Figure). Here, the points' planimetric coordinates, being them cartographic (E, N) or geographic (lat, lon), are transformed in order to obtain the increasing distance (D) from the first point in the backshore (P_0) by using the mathematical equation of the straight line joining the first and last section's points. The distance value (D) for each profile point is obtained through the formula expressed in Eq 5.1, in the case of cartographic coordinates.

$$D = \sqrt{(E_{p_i} - E_{p_0})^2 + (N_{p_i} - N_{p_0})^2} \quad \text{Eq 5.1}$$

Where D is the obtained distance from the reference point in the backshore; E_{p_i}, N_{p_i} are the coordinates of the i -th point; E_{p_0}, N_{p_0} are the coordinates of the reference point P_0 .

Having available for each point along the section the computed distance D and the measured height (H), these can be easily used to create 2D profile graphs using any graphics software (Figure). If data related to different multi-temporal surveys are managed using the same method, it is possible to obtain a single graph containing profiles related to different epochs. This allows valuable comparison if the starting points are aligned to a common reference system. Moreover, by graphically analysing the obtained curves, it is possible to detect any possible outlier which got away from the previous analysis.

| | A | B | C | D | E | F | G | H | |
|----|---|--------------|---------------|-----------|---------------|-----------|------------|-------|--|
| 1 | EPSG 7791: ETRS89 - ETRF2000 UTM32 | | | | | | | | |
| 2 | Reference point landward | | Seaward point | | | | | | |
| 3 | EO | No | Em | Nm | | | | | |
| 4 | 771658.82 | 4900413.1 | 772450.5 | 4901124.5 | Acquired data | | | | |
| 5 | | | | | Computed data | | | | |
| 6 | Section coefficients | | | | | | | | |
| 7 | m_n | 0.898595392 | | | | | | | |
| 8 | q_n | 4207004.04 | | | | | | | |
| 9 | | | | | | | | | |
| 10 | Coefficients of the straight line from the point perpendicular to the section | | | | | | | | |
| 11 | m_n | -1.112847906 | | | | | | | |
| 12 | q_n | | | | | | | | |
| 13 | X_E32 | Y_E32 | Z_2005 | D | q_n | Ep | Np | Dp | |
| 14 | 771659.5 | 4900413.5 | 1.51 | 0.79 | 5759153.16 | 771659.40 | 4900413.62 | 0.77 | |
| 15 | 771657.5 | 4900412.5 | 1.53 | 1.45 | 5759149.93 | 771657.79 | 4900412.18 | 1.38 | |
| 16 | 771656.5 | 4900411.5 | 1.55 | 2.82 | 5759147.82 | 771656.74 | 4900411.23 | 2.80 | |
| 17 | 771660.5 | 4900415.5 | 1.48 | 2.93 | 5759156.27 | 771660.94 | 4900415.01 | 2.85 | |
| 18 | 771662.5 | 4900416.5 | 1.44 | 5.01 | 5759159.50 | 771662.55 | 4900416.45 | 5.01 | |
| 19 | 771654.5 | 4900409.5 | 1.57 | 5.62 | 5759143.59 | 771654.64 | 4900409.34 | 5.62 | |
| 20 | 771653.5 | 4900408.5 | 1.59 | 7.03 | 5759141.48 | 771653.59 | 4900408.40 | 7.03 | |
| 21 | 771663.5 | 4900418.5 | 1.39 | 7.15 | 5759162.61 | 771664.09 | 4900417.84 | 7.09 | |
| 22 | 771651.5 | 4900407.5 | 1.6 | 9.22 | 5759138.28 | 771651.99 | 4900406.96 | 9.19 | |
| 23 | 771665.5 | 4900419.5 | 1.34 | 9.25 | 5759165.84 | 771665.70 | 4900419.28 | 9.25 | |
| 24 | 771666.5 | 4900420.5 | 1.29 | 10.67 | 5759167.95 | 771666.75 | 4900420.22 | 10.66 | |
| 25 | 771667.5 | 4900421.5 | 1.29 | 12.08 | 5759170.06 | 771667.80 | 4900421.17 | 12.07 | |
| 26 | 771667.5 | 4900422.5 | 1.62 | 12.79 | 5759171.06 | 771668.30 | 4900421.61 | 12.74 | |

Figure 5.11 – Example of Excel sheet employed to compute the increasing value of distance required to obtain the profile sections.

As previously mentioned, the extraction of profiles from interpolated maps requires a much lower computing effort. In particular, concerning QGIS software, a specific tool is available named *Terrain Profile Tool*. Using this method, it is possible to obtain the 2D graphs only by selecting the base map and the chosen section (Figure).

From a computational point of view, it is clearly worthwhile to apply this second method with respect to the one based directly on the acquired points. However, this approach suffers from the interpolation process applied to compute the topographic maps, which sometimes can lead to smoothed profiles with missing local patterns. On the other hand, this is not entirely true when dealing with point clouds where the spatial resolution is very high since the computed bathymetry could also

reflect small-scale variations. Nevertheless, it is always necessary to consider the method used to process the previous data to perform reliable comparisons.

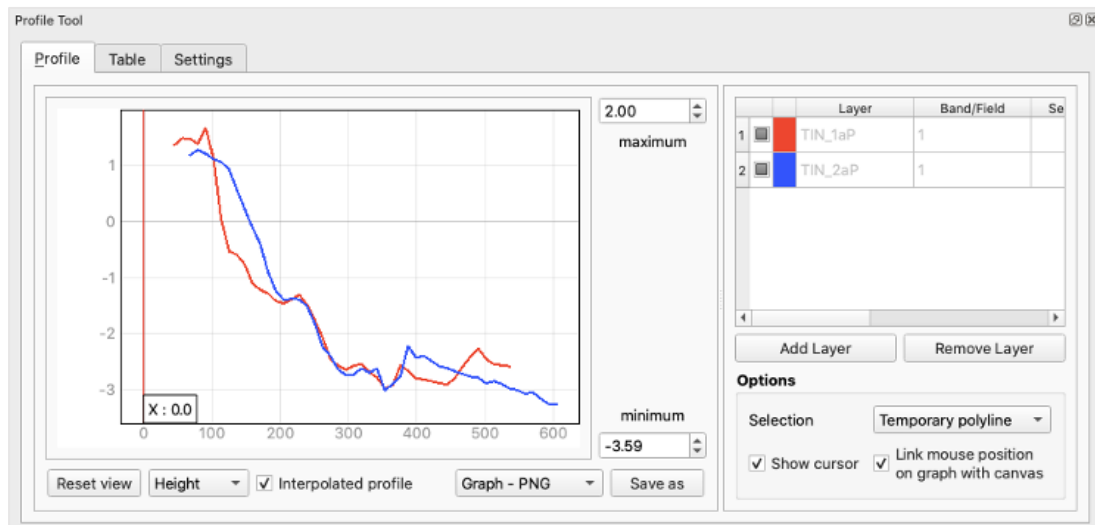


Figure 5.12 – Screenshot of the Terrain Profile Tool in QGIS software.

5.3 Maps of height variation

In Chapter 5.1, we saw that topo-bathymetric maps are the instrument used to acquire a “picture” of the overall situation of a beach area in terms of height and depth patterns. However, the final goal of monitoring activities is that of analysing an evolution over time, which means that it is necessary to assess how the area is changing. This can be done by computing the maps of height variation, i.e. the difference between bathymetries related to the same beach area at different times. Even in this case, the comparison can be performed at a short time-scale, related to specific activities or interventions on the beach or at longer time-scale, to provide important information about the natural evolution of the area. In the common approach for coastal studies, the DEMtoDEM comparison gives information about the evolution of the beach in terms of accretion or erosion, and usually extended datasets of height variation maps related to yearly time-scales are employed.

Operationally, the processing of this kind of product is straightforward, being a mathematical difference between two maps, and can be performed by means of any

GIS-based software. Nevertheless, some significant aspects have to be considered. The difference operation is only possible if the grid spacing is the same for all the grids to be compared (those related to the same beach). This does not mean that surveys have to be necessarily performed using the same geomatic technique, but, at least in the context of this computation, the same pixel dimension must be selected when producing the related topo-bathymetric maps. If the bathymetries to be compared have different associated spacings, a good standard can be to choose the bigger pixel dimension for both. On the contrary, if the higher spatial resolution (i.e. the smaller grid spacing) is chosen, the final product will compute values even where no actual information is present.

Maps of height variation are commonly displayed according to colour classes related to different ranges of height difference. Here it is crucial to determine the range of values which consider the equilibrium situation, also taking into account variations that could be due to the surveying methods' accuracy (Figu).

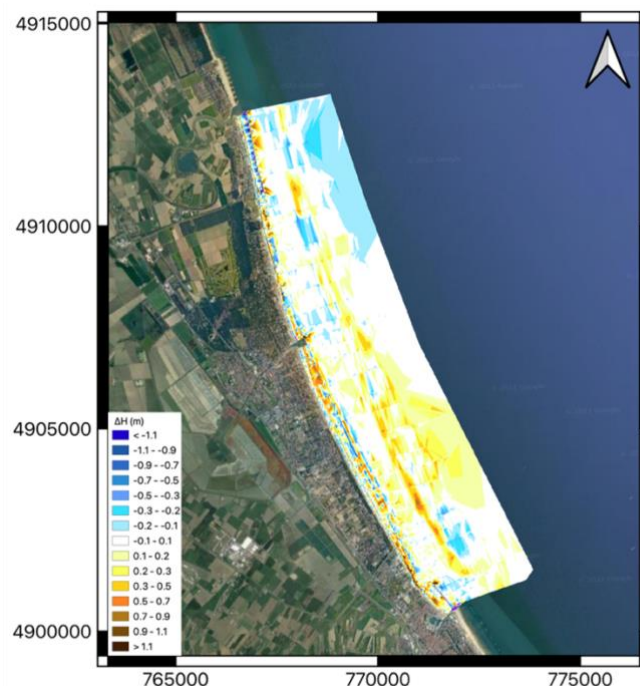


Figure 5.13 – Example of map of height variation in the beach area of Cesenatico in Emilia-Romagna. $\Delta H < \pm 10$ cm are represented in white to indicate equilibrium situations.

The main parameter that can be extracted starting from the maps of height variation is the volume, particularly the volume of accumulated or lost sand in the period between the two analysed surveys. Different tools are available depending on the chosen software, requiring selecting the comparison map and the reference plane to distinguish between positive and negative values. Reasonably, in the considered case, this lower surface corresponds to the $H = 0$ plane, i.e. to the zero of the altimetric reference used. It is also possible to define an arbitrary area for the computation, thus allowing to evaluate variations due to sand migrations in nearby areas.

The computed results are commonly given in terms of the following:

- positive volume: above the reference surface $z = 0$, i.e. volume of accumulated sand;
- negative volume: below the reference surface $z = 0$, i.e. volume of eroded sand;
- net volume: given by the combination of previous ones [157].

In the context of the paper published in 2020, of which I am the first author, *Third beach nourishment project with submarine sands along Emilia-Romagna coast: Geomatic methods and first monitoring results* [157], the mathematical formula for the uncertainty related to the computed volume has been given, together with the associated values in particular surveying conditions. The main finding of this research will be summarized below.

Considering a general map of height variation, this can be seen as a grid of cells with side p in the case of square cells, i.e. same spacing in both directions. Therefore, the computed volume V will be the total sum of each cell's volume, obtained by considering the product of the single cell's area (common for all the cells) and the associated height value, h_i (Eq 5.2):

$$V = \sum_{i=1}^n h_i * p^2 \quad \text{Eq 5.2}$$

Where n is the total number of cells.

Due to the law of uncertainty's propagation, starting from the variance of the height estimation for each i-th cell ($\sigma_{h_i}^2$), the variance associated with the Volume (σ_V^2) can be estimated through the Eq 5.3:

$$\sigma_V^2 = \sum_{i=1}^n \sigma_{h_i}^2 * p^4 \quad Eq 5.3$$

Which turns into Eq 5.4 in the case of height measurements performed using the same geomatic technique (thus with the same associated value of $\sigma_{h_i}^2$):

$$\sigma_V^2 = n * p^4 * \sigma_{h_i}^2 \quad Eq 5.4$$

As a result, the uncertainty related to the total volume (at 68% confidence level) and the one related to the volume variation are obtained by Eq 5.5 and 5.6, respectively:

$$\sigma_V = \sqrt{n} * p^2 * \sigma_h \quad Eq 5.5$$

$$\sigma_{\Delta V} = \sqrt{2n} * p^2 * \sigma_h + bias_{RTK} * A \quad Eq 5.6$$

Where the second term in Eq 5.6 considers the potential bias that might occur during field operations in the case of GNSS-RTK surveys (master station set-up, antenna height measurement – see Chapter 3.1) and which could induce a systematic shift in the coordinates.

The following values have been used in Eq 5.6 to give a possible estimation of $\sigma_{\Delta V}$ in the case of applying the GNSS-RTK technique and an echo sounder for the emerged and submerged beach, respectively:

- $\sigma_h = 5$ cm, combining the uncertainty related both to the GNSS and to the echo sounder's measurements;
- $bias_{RTK} = 1$ cm, having considered some tests performed on the field;
- 95% confidence level obtained considering double the $\sigma_{\Delta V}$ value;

obtaining final values ranging from 1.1% to 1.5% in terms of volume uncertainty per square meter (m^3/m^2).

5.4 Shoreline

The final product analysed is the shoreline, i.e. the ultimate boundary between land and sea. Although this definition could seem very simple, it implies significant issues. In fact, the location of the shoreline is subject to continuous variations, which condition the actual position where the water meets the land. It should be highlighted that different shoreline definitions exist, depending on the specific context and application; thus, the need to cautiously manage this product arises.



Figure 5.14 – Shoreline extraction from the bathymetric map (zero-contour line).

From a more analytical point of view, the shoreline coincides with the bathymetry of 0 m; therefore, it can be easily extracted from the computed topo-bathymetric maps as a contour line (Figure). Such a definition is bounded to proper management of the altimetric reference system, leading to unavoidable mistakes if this is not ensured. In particular, a reliable connection with the geoid surface must be provided when defining the orthometric height of the reference point. According to this, please refer to Chapter 4.1, where the relevance of a reliable geodetic infrastructure as a support for technical applications has been deeply explained.

However, it is necessary to consider that usually what is significant within coastal monitoring studies is shoreline variation over time, since the “picture” of the instantaneous position could vary even at very short time-scales due to several factors. In particular, the primary key drivers affecting the shoreline behaviour are climate-driven responses, such as tides and waves [13], effects of the sea levels changes [23], storminess [52], and natural inter-annual variability [117] [140].

Concerning long-term monitoring, typically shoreline variations at yearly time-scales are considered. In these cases, the comparison between shoreline positions related to subsequent surveys is a fundamental tool to determine the state of health of a beach area in terms of erosion trends and rates [95]. About this, monitoring plans can rely on maintaining a particular beach extent, both from an environmental and economic point of view. In this context, the distance between the shoreline and the landward baseline is considered as emerged beach extent. The baseline can be arbitrarily identified as the foot of the natural beach dunes or as the first non-erodible point, usually corresponding to a low wall or sidewalk located backwards from the beach establishments [1]. Moreover, shoreline variations due to nourishment interventions can be analyzed to evaluate their impact and effectiveness on the area. In such cases, reasonably, it is necessary to acquire shoreline measurements with high associated spatial resolution, like the one ensured by GNSS-derived data.

During monitoring activities, when repeated surveys are performed, the average and the maximum values of the shoreline’s variation are computed for each coastal stretch [157]. When dealing with several collected surveys and, therefore, a certain number of extracted shoreline measurements, it could be helpful to define some transects to be used for this purpose. This approach allows for reliable measurements since the intersection between the transects and each available shoreline can be computed automatically (Figure). “Baseline and transects” methods require the arbitrary definition of a baseline, which should be as oriented as the coast in the study area, and transect lines perpendicular to it (i.e. cross-sections) [59]. These attributes can be

realized in a GIS environment, providing they respect a defined format with associated attributes. This is the case of Digital Shoreline Analysis Systems tool (named DSAS) available within ArcGIS software [149], which now has the corresponding one for the open-source [59].

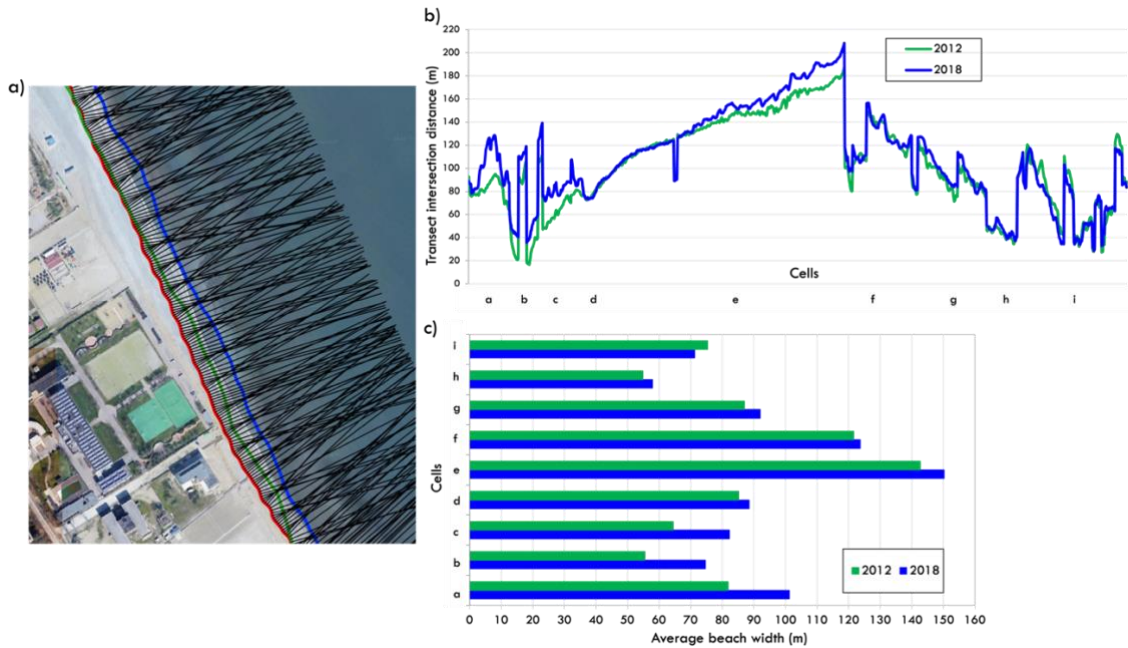


Figure 5.15 – Baseline and transect method: a) transects orthogonal to the baseline, b) time series of intersection distances, c) average beach width of defined beach cells.

Therefore, this kind of tool provides a comparison between a defined set of shorelines related to subsequent epochs, which is given in the distance at which each shoreline intercepts a defined transect. Besides the rates computed for the different shorelines, it is possible to extract some related indexes. These include the End Point Rate (EPR), which is commonly calculated by dividing the distance of the shoreline’s movement by the time elapsed between the oldest and the most recent shoreline [137]. Eq 5.7 shows the formula used to compute the EPR index. Reasonably, negative values of the EPR index occur when landward erosion of the shoreline is present.

$$EPR = \frac{d_{t_n} - d_{t_0}}{n} \left(\frac{m}{y} \right) \quad Eq\ 5.7$$

Where d_{t_n} is the interception between the most recent shoreline and the selected transect, given in meters; d_{t_0} is the interception between the oldest shoreline and the

selected transect, given in meters; n is the time between the two considered surveys, given in years.

Although its calculus is elementary, the EPR index can only compare two survey epochs, commonly the oldest and most recent ones. This value is not assumed to be linear within the considered period, since the computed rate only represents the net change occurred between the two shorelines, annualized to facilitate comparisons with long-term rates found through linear regression [201]. Furthermore, associated statistics are given by these “Baseline and transects” methods in the form of standard errors, correlation coefficients and confidence intervals. Note that the computed rate of shoreline trends can be used to obtain predictions about future shoreline changes employing numerical models [95].

In some contexts, it could be helpful to have several repeated shoreline positions, available at short time-scale (such as weekly level), to deduce how tides and wave action can impact the surveyed area. Otherwise, some studies could deal with regional or global scale assessments, meaning they would require products with a broad spatial coverage. Both the listed cases represent entirely different applications from the one described before since, reasonably, it would be impossible to perform ad hoc in-situ surveys with regional/global spatial coverage or weekly repetition on a limited area. For this reason, obviously, these kinds of studies rely on completely different levels of accuracy with respect to the one associated with GNSS-derived data (i.e. those considered for the previous considerations about shoreline analysis).

This is the case of the Satellite Derived Shorelines (SDS), whose temporal scale and availability are related to the satellite revisit time (in case of absence of cloud cover) [56][64]. The use of shoreline observations acquired from satellite images can provide new opportunities for large-scale coastal change studies, which would be unfeasible in exploiting other geomatic techniques [140][89]. Moreover, the reliance on satellite

images allows for evaluating trends over long time-scales, provided that an archive of older acquired images is available.

In this context, the previously mentioned GEE platform represents a considerable tool allowing to perform several processing without leading to high computing efforts [89][183]. Besides, thanks to the development of such an instrument, other processing possibilities are increasingly available at the time. Among these, a recently launched open-source toolbox named CoastSat has to be mentioned [159]. This tool enables the extraction of shoreline products on sandy beaches with a declared resolution of about 10 m. As previously mentioned, SDS method is not commonly applied for the type of coastal monitoring analysis addressed by this study, i.e. the ones relating to limited spatial coverage and with a yearly frequency of the surveys. This is primarily due to the associated resolution, which is definitely not coherent with the expected tolerance.

Some preliminary analyses have been performed by means of the CoastSat platform in the context of the Emilia-Romagna littoral and considering the typical requirements for the monitoring activities considered throughout this study (Figure). The main goal was finding a way to exploit the high frequency of SDS (as we said, weekly) to compute an average shoreline, at yearly level, with higher associated reliability. In this case, reliable ground truth datasets of shorelines over common years could represent a helpful source for validation. Please note that this study is not completed yet, but some interesting considerations can already be reported.

When dealing with Satellite Derived Shorelines, it is always necessary to apply tidal corrections since the separation between land and sea, i.e. the shoreline itself, is extracted by single images related to certain tidal conditions. Therefore, there is a need to extract the exact time of acquisition of each used image and to obtain the associated data from a close tide gauge. Commonly, for the sake of simplicity, global tide models can be employed, inevitably leading to a loss of reliability of the final products. In fact,

the accuracy of the used model has to be considered when computing the final overall accuracy related to the obtained shorelines.

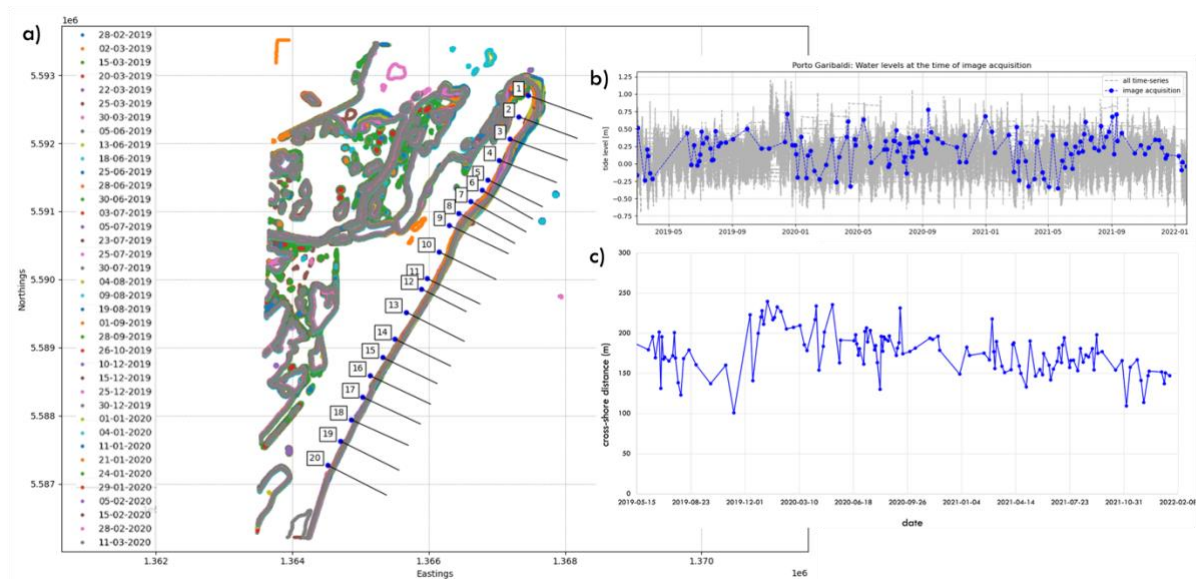


Figure 5.16 – Preliminary analysis performed using CoastSat tool. a) SDS and transects, b) water levels of Porto Garibaldi's tide-gauge used for the shoreline's correction, c) an example of time-series of shoreline's interception for a specific transect.

For two main reasons, even applying local tidal acquisition is not straightforward. Firstly, the tide-gauge measurements must be properly aligned to the altimetric reference of the other data sources. Secondly, measured values represent a particular area, which should be considered according to the extension of the whole area addressed by the analysis. Moreover, the sea level reference is another significant issue regarding SDSs since they are not bounded to a reference geoid.

Another aspect to be considered is the local value of the beach slope. In fact, the extracted boundary between land and sea under certain tidal conditions is reasonably dependent on the local value of the beach slope. Therefore, it is not sufficient to correct the shorelines according to the tidal conditions, but the wave run-up effect should also be considered. In this regard, no significant problems are present with calm sea conditions, while particular issues can arise if intense waves are present, especially when dealing with slightly sloped beaches where the boundary between wet and dry sand can change up to tens of meters. This problem could be theoretically solved by

excluding images acquired during particularly stormy seasons. With the availability of a ground truth dataset, the beach's slope can be computed considering profile sections both on the emerged and submerged beach, bearing in mind that also this computation is affected by uncertainty, and there is not a defined standard method suitable for any possible profile shape.

Hypothetically, considering the SDS after the tidal correction with the “exact” value of the related beach slope and the corresponding shoreline from ground-based surveys (acquired at very close epochs), the two products should be superimposable. Reasonably, this situation is not achieved due to other impacting factors. Among these, as mentioned, there is the beach slope’s computation itself and the chosen tidal model. It could also be interesting to understand how the tool responds to different input values, i.e. at what level the extracted products result in different depending on the slope. Indeed, another exciting analysis concerns the sensitivity of the shoreline's extraction independently from the other factors. It is known that the general separation between land and water can be obtained by applying the Normalized Difference Vegetation Index (NDVI) index [43][83]. In optic remote-sensing, this differentiation is obtained by analysing the response in the near infrared since water has shallow reflection levels in this field. In this regard, the slope of the beach can also affect the ability of the parameter to operate the sea-land separation, meaning that with higher slopes, the boundary appears very marked, while flat areas can lead to possible misinterpretations. Moreover, the NDVI value also depends on the water’s clearness, leading to a possible variability of this index in turbidity situations. Finally, depending on the employed images, the processing would lead to different resolutions, i.e. different pixel dimensions, which directly impact the maximum possible accuracy associated with the SDS.

Considering the primary purpose of the present analysis, which is to compute an averaged shoreline over a specific period starting from a set of SDS, even the method to compute this mean would affect the resulting product and its accuracy. In order to

obtain data representative of a defined range of time, a possible approach could be to extract all the available SDS in that period and then apply the Baseline and transects method (i.e. the one commonly used to evaluate the variations occurred in the range between two surveys). This way, the mean distance along each transect can be computed by having the distances of interception of the considered SDS along a highly dense series of cross-shore transects covering the whole area. Then, based on these averaged interception distances, an average shoreline could be recreated by linking the interception's points. As mentioned, ground truth datasets represent the fundamental instrument to validate the obtained averaged shoreline, always considering the levels of uncertainties related to both. Furthermore, this source of data can find its application in a reverse analysis, trying to assess the parameters' influence on the extraction processing and possibly calibrate the tool for a specific context.

If the result is satisfactory, another field of application for these data sources could be easily found, at least regarding possible calibration of SDS tools according to particular conditions. Interesting considerations could also address the variability of these shorelines considering different time-scale, thus evaluating the short-term patterns in specific areas.

5.5 GNSS and photogrammetric UAV-derived products

Concerning the analysis of products obtained to different geomatic techniques, a paper has been published regarding comparing between data from photogrammetric UAV and GNSS-RTK surveys over a common area located in Lido di Spina, a coastal stretch in the Emilia-Romagna region, Italy (Figure). The considered dataset, the methods and the obtained results of this study will be summarily reported in the following paragraphs.

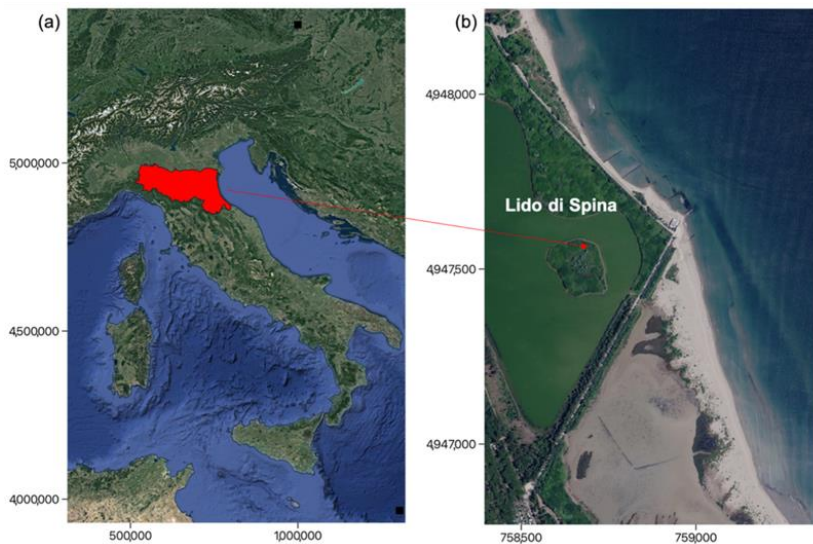


Figure 5.17 - Lido di Spina beach (b) located between Porto Corsini and Porto Garibaldi, on the Northern Adriatic coast of Emilia-Romagna (a). Base map from Agea orthophoto 2018 (<https://geoportale.regione.emilia-romagna.it/servizi/servizi-ogc/elenco-capabilities-dei-servizi-wms#b>) and Google satellite.

The considered dataset includes two multitemporal surveys (2019 and 2020) acquired on the emerged beach in the area of Lido di Spina, both using GNSS-RTK technique and UAV photogrammetry a few days apart at most (Figure 5.17). The proper alignment in the official national reference system ETRS89-ETRF2000 (2008.0) has been ensured by a supporting benchmark belonging to the Coastal Geodetic Network of Arpa, PCPG0500 (Chapter 4.1). Moreover, the geoid height related to the same benchmark was used to transform ellipsoidal heights into orthometric heights for all the considered datasets. This approach ensured internal consistency between data collected from different operating companies, allowing intercomparisons and proper DEMtoDEM differencing. Both the GNSS survey campaigns have been performed employing the RTK mode, placing the master station on the RGC benchmark (Chapter 4.1). A low-cost DJI Phantom 4 RTK has been used for the UAV surveys, with the support of six and one GCPs, for the two campaigns, respectively. Both the flight plan have been set to have an 80% overlapping between the photograms in both directions. The main technical specifications of the two UAV datasets are listed in Table 5.1.

Since the operating companies have carried out the elaboration process of the UAV-acquired data, we considered the residuals obtained on the GCPs positions to evaluate

the photogrammetric model accuracy. For the 2019 and 2020 surveys, these values are 4.77 and 0.31 cm, respectively, for the horizontal component, whereas 4.10 and 2.67 cm in height.

Table 5.1 - Summary of the key parameters of the available UAV photogrammetric surveys.

| Survey data | 2019 | 2020 |
|----------------------------|-------------|-------------|
| Camera model | FC6310R | FC6310R |
| Resolution (px) | 5472 x 3648 | 5472 x 3648 |
| Focal length (mm) | 8 | 8 |
| Pixel size (µm) | 2.41x2.41 | 2.41x2.41 |
| N° frames | 563 | 638 |
| Flight altitude (m) | 104 | 108 |
| GSD (cm/px) | 2.87 | 2.64 |

The comparisons have been performed considering three aspects: the point-wise values of the height differences, the shape of height profiles on cross-shore and along-shore sections, and the volume change over time. Firstly, point-by-point comparison of the height values on the GNSS points positions has been performed using a processing tool included in the QGIS software package [228], named “Point sampling tool”. Considering the high spatial resolution of the photogrammetric UAV surveys, this approach allowed to directly compare independent GNSS points with the UAV corresponding ones, thus minimizing the influence of inherent interpolation errors on the GNSS data. How the calculus has been set up relates to negative values for photogram-metric UAV heights higher than the GNSS ones and vice versa.

The spatial distribution of the height differences over all the common points for the GNSS and UAV datasets is shown in Figure and Figure , for the 2019 and 2020 campaigns, respectively. Figure a and Figure a show all the values focusing on higher residuals, while Figure b and Figure b emphasize only residual values up to 10 cm. Looking at the distribution, we can observe that most of the differences are related to the ± 10 cm interval, with higher variability located only in areas very close to the shore or where the data filtering was probably insufficient. Differences in the intertidal area are more evident in the comparison between the 2020 surveys, which have been

performed with few days of delay. Hence, in this specific case, tides and waves may have changed the surface's shape near the shore, leading to different measured heights. On the other hand, it is known that the SfM process can lose accuracy in the intertidal zones (Chapter 3.3). Focusing on the residual values within the range of 10 cm, a relatively homogeneous spatial distribution of the different ranges of values is observed in the whole analyzed area.

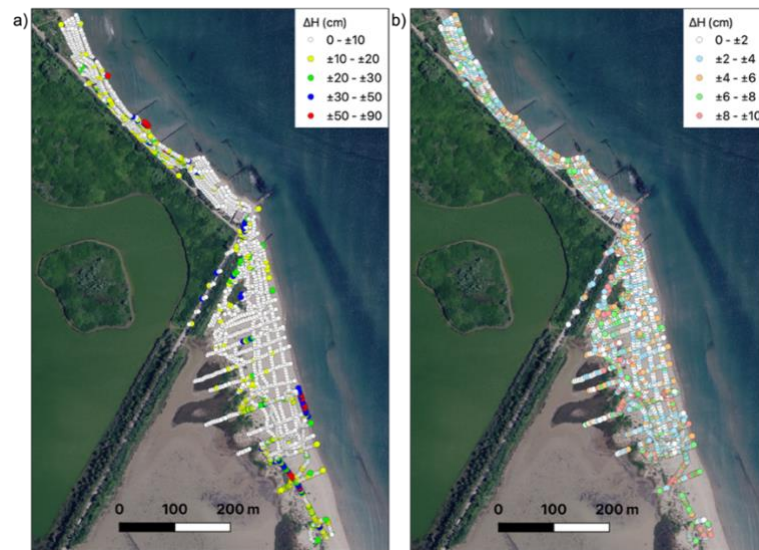


Figure 5.18 - GNSS-acquired points and related height differences between RTK and photogrammetric UAV surveys for the 2019 campaign. a) relates to all the values emphasizing the higher discrepancies; b) relates to differences within 10 cm.

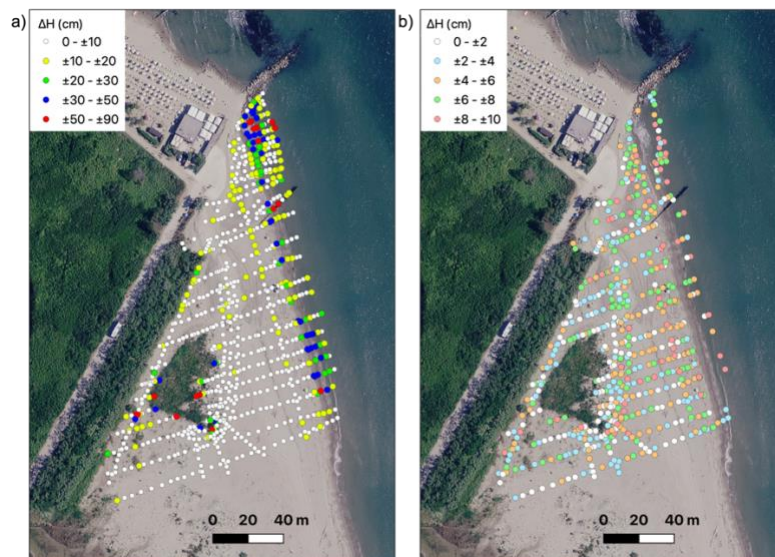


Figure 5.19 - GNSS-acquired points and related height differences between RTK and photogrammetric UAV surveys for the 2020 campaign. a) relates to all the values emphasizing the higher discrepancies; b) relates to differences within 10 cm.

Obtained results have also been reported in terms of mean values and standard deviations of the height differences, supported by the related frequency histograms. Due to possible tidal effects, which can affect also surveys realized after a few hours, the nearshore zone is excluded from the histograms and the related statistical analysis. Figure shows the statistical distribution of the height differences between the GNSS and UAV datasets for 2019 (a) and 2020 (b) survey campaigns. An almost symmetric distribution is observed for the 2019 survey (Figure a), with a mean value of -3 cm and an STD of 9 cm. Differently, the mean is about 1 cm, and the STD is 8 cm for the 2020 survey (Figure b).

The observed mean biases can be addressed mainly to three different issues:

1. errors in the stationing operations on the master station (RGC benchmark);
2. unsuitable managing of the pole during GNSS surveys;
3. errors in the GCPs measurements used to align UAV photogrammetric models.

Overall, the two techniques have proved consistent and comparable: 50% of the height differences range within 7-8 cm and 90% within 25/18 cm, for the 2019 and 2020 surveys respectively. Moreover, the obtained values have been compared with those that resulted from other similar studies. Our computed standard deviations are very similar to what was found in [92], even though a higher class UAV instrument at a much lower flying altitude was used in that work. Another similar analysis has been carried out by [165] employing a low-cost drone flying at a very low altitude of about 53 m, resulting in a final STD of 3 cm. Taddia et al [144] applied the same model of drone (Phantom 4 RTK) used in our analysis, acquiring only nadiral images, resulting in a standard deviation of about 7.5 cm without any GCP and 3.4 cm considering a sufficient number of GCPs.

The main reason for the difference between our values and these results can be differences in the flying altitude (80 m instead of about 110 m).

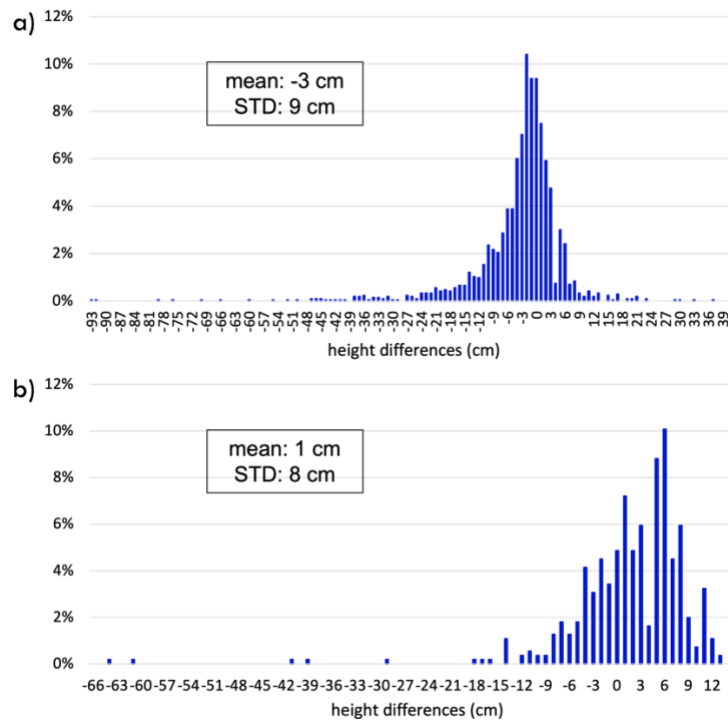


Figure 5.20 - Histogram distribution of the height differences (GNSS-UAV) expressed in cm for 2019 (a) and 2020 (b) surveys. (a) 2165 points, (b) 556 points.

The second comparison considered the differences between beach profiles extracted from the two data sources along some of the GNSS-acquired sections (along-shore and cross-shore). Four height profiles defined using both GNSS and UAV are shown in Figure and Figure for the two campaigns. Results are generally consistent at a few cm level, and the same profile shape is described by both techniques. Moreover, since the data scattering is very small with respect to height variations along the profiles, it could be deduced that both methods allowed capturing profile variations with high precision. We found mean biases at the cm level for quite all the analysed sections, while differences rising up to 10-30 cm are present when the profiles cross bushed areas (Figure a, Figure d). In the alongshore profile of the 2020 survey (Figure c), which lies close to the shoreline, the observed quite regular bias in the dm order can be addressed to the fact that the two campaigns (GNSS and UAV) have been realized a few days apart. This leads to considering the mentioned issue due to tidal effects that can affect the comparison results.

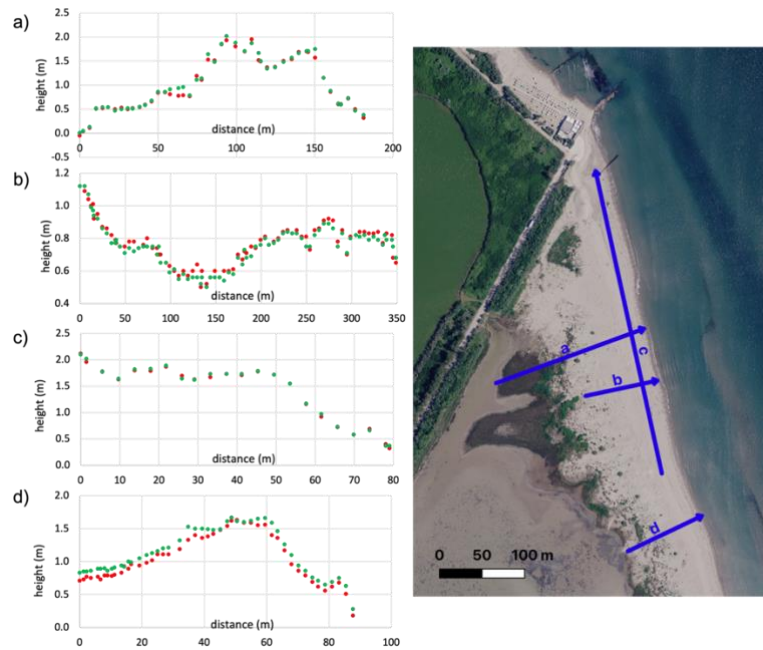


Figure 5.21 - Examples of cross-shore (a; b; d) and along-shore (c) profiles of the 2019 survey for GNSS (red) and UAV-derived (green) data.

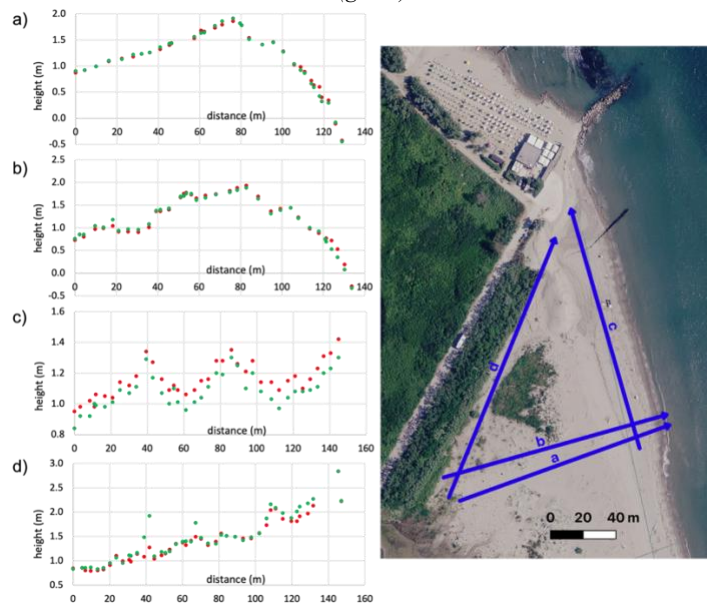


Figure 5.22 - Examples of cross-shore (a; b; d) and along-shore (c) profiles of the 2020 survey for GNSS (red) and UAV-derived (green) data.

Finally, the maps of height variation (2020-2019) in the case of monitoring using GNSS-RTK or UAV photogrammetry techniques have been compared. For this purpose, the GNSS-acquired points and the UAV-derived point clouds have been interpolated for both the 2019 and 2020 campaigns by applying a TIN algorithm. In this phase, the DEMs spacings have been chosen according to the spatial resolutions related to the GNSS and UAV surveys, respectively: equal to 20 cm and 5 cm. Then, it was possible to compute the DEMtoDEM differences over time, thus defining the volume changes

estimated through the two different survey techniques. The maps of height variation have been computed over the common area (9.616 m²) for all the involved surveys, excluding a central spot where the lack of points of the GNSS surveys could have affected the interpolation results. Note that the limited spatial extension of the common area was bounded to the use of surveys performed for different specific purposes (regular monitoring activities, monitoring of beach nourishment evolution, European projects). In particular, the 2020 survey campaign was part of the European Project H2020 OPERANDUM (OPEn-air laboRAtories for Nature based solUtions to Manage environmental risk) [225] for the study of Natural-Based Solutions as possible structures for the mitigation of extreme weather events. The purpose of this survey was to obtain data for a deep analysis of the selected area to set up the project of an artificial dune strengthened by a natural and biodegradable structure. Furthermore, for the DEMtoDEM computation, we excluded data in the nearshore area since affected by the delay between the 2020 surveys.

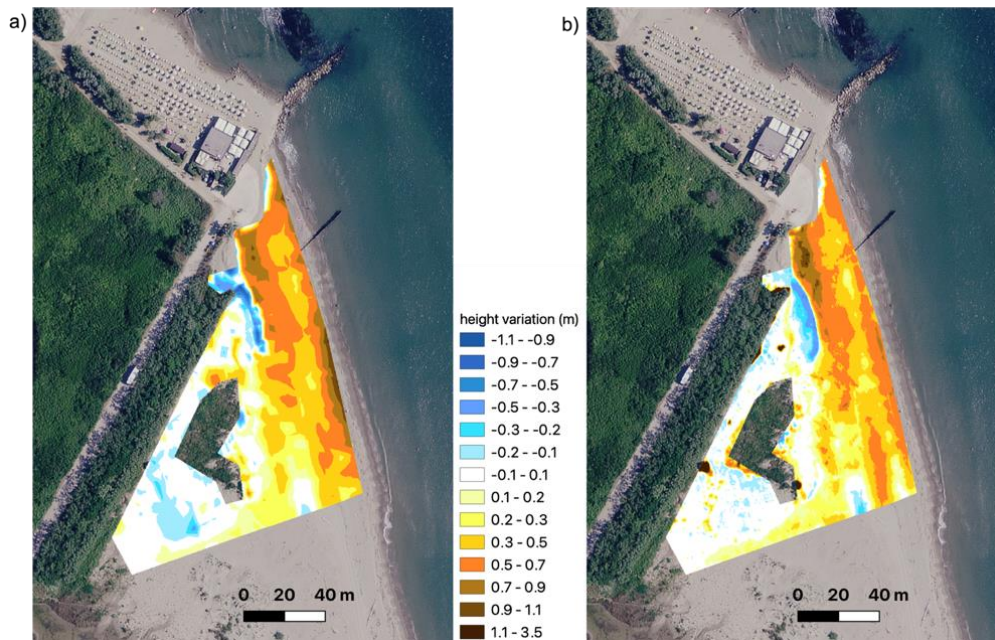


Figure 5.23- Maps of height variations between 2019 and 2020 for GNSS (a) and photogrammetric UAV surveys (b).

Looking at Figure , regardless of the different spatial resolutions of the two datasets (a – GNSS; b - UAV), the overall sand variations are very similar. A general height

increase between the two survey campaigns can be observed, with values from 30 cm to 70 cm mostly concentrated along the shore.

Some height differences of about 10-50 cm are located near the vegetated area, and relatively homogeneous values are distributed on the rest of the area. Both the sand monitoring analysis denoted an accretion situation, with very similar results. Positive volumes of 2.238 m³ and 2.233 m³ have been obtained for GNSS and UAV, respectively, with differences of about the 0.2%. It should be stressed that such a high coherence in the definition of sand's volume changes using the two techniques can only be reached by paying particular attention to vegetated areas, which may strongly affect UAV measurements if not correctly managed during the processing phase (data filtering). In fact, as described in Chapter 3.3, photogrammetric applications inherently provide surface geometries (DSM) that cannot be directly compared to GNSS datasets (DTMs).

Moreover, obtained results also showed that the lower spatial resolution of the GNSS survey with respect to the UAV photogrammetric one does not significantly impact the estimated volumes if the terrain is quite regular or flat. In general, this argument can be employed for accuracy-efficiency analysis since, as long as the computation is not dependent on the spatial resolution, it is possible to employ coarser data sources for the same application. This way, advantages from a practical point of view can be achieved thanks to reduced time and processing effort. Lastly, all the described results could benefit from the support of a common RGC benchmark, which ensured the alignment to the same reference system. This is not commonly assumed, especially when dealing with data acquired from different operating companies, which can lead to potentially critical issues related to the reference system.

Chapter 6

6 Statistical analysis of geomatic data accuracy

Coastal hydro-morphodynamic analysis and flood risk assessments rely on topographic and bathymetric datasets, or, in general, to Digital Elevation Models (DEMs), as one of the main inputs for numerical investigations [154][50]. As seen in Chapter 5.1, high resolution maps, achievable by means of different geomatic techniques, require both computational, time and cost. On the other hand, there is an increasing availability of public DEMs at lower resolutions which can be employed for these purposes, clearly ensuring a significant reduction of the associated computational burden. Nevertheless, it is known that the resolution, and thus the accuracy, of the topographic dataset, are critical parameters that significantly affect the model's results [154][50]. Please refer to Chapter 5.1, where the topic of DEMs' uncertainty concerning the resolution has been deeply explained.

In particular, concerning numerical modelling applications on coastal areas, selecting the appropriate strategy for the input bathymetric data could be challenging, aiming to find the proper balance between the accuracy of the final results and a logistic

convenience. For example, the findings by [154] confirmed that, in the case of coastal flood assessment, the chosen publicly available DEMs did not meet the accuracy requirement, resulting in an overestimated land elevation and thus underestimating the flooded area. Based on the approaches proposed by [50], this analysis aims to provide a proper modelling framework of the elevation errors computed between a public bathymetry and a set of ground truth points accurately surveyed in the field using the GNSS-RTK technique and multibeam echosounder. Indeed, the study presented in [50] analysed the impact of the DEM's resolution on coastal flood risk assessment. This can help in selecting a suitable input DEM for more efficient analysis and reducing the models' uncertainty.

The issue regarding the optimal choice in terms of input DEM can be preferably addressed using a probabilistic approach, revealing the spatial variability of the induced errors [50][79]. Therefore, having a dataset of collected points available to be used as ground truth, the elevation errors can be statistically modelled considering their associated spatial structure. This modelling phase involves, as a first step, the fitting of a variogram and, secondly, the interpolation of the sample values through the kriging generation. The Ordinary kriging algorithm was chosen, ensuring a good trade-off between accurate computation and not too many related parameters. Since this geostatistical interpolator provides both the estimated values and the associated variances, obtained results can be used within a particular Monte-Carlo-based approach named Sequential Gaussian Simulation (SGS). This algorithm introduces a certain level of randomness to the input dataset by simulating a chosen number of equiprobable realizations of the input variable. Using the outputs estimated by the kriging modelling, the probability distribution functions of each grid's cell are generated assuming a normal distribution and a random value honouring it is extracted. Multiple grids of simulated errors are obtained by applying the same approach to each cell and repeating the process several times. New possible DEMs realizations are finally computed by summing these simulations to the original input

DEM. The complete workflow is shown in Figure and will be deeply explained throughout this chapter.

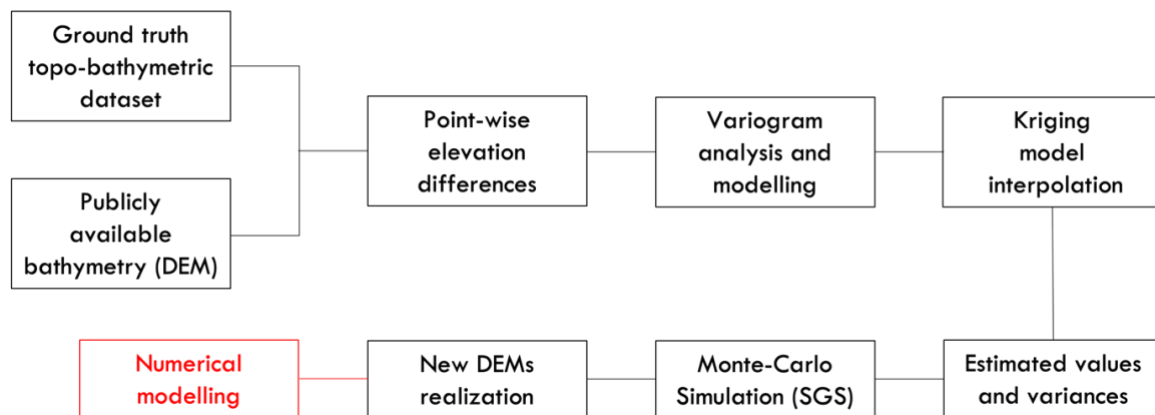


Figure 6.1 – Workflow of the analysis.

Although the process has been applied for one selected location, the same approach can be used for other case studies, indicating the suitability of public datasets for numerical modelling purposes, in terms of associated uncertainty. In fact, this method can find possible final applications in the evaluation of the impact of the bed level data's accuracy on the results obtained from coastal hydro-morphodynamic models. The findings of such analysis, if revealing any differences in the modelling outcomes, could be helpful for the planning and investment decisions related to particular coastal studies. Furthermore, note that such analysis is strictly connected with one of the central ideas of this thesis, being the proper management of the altimetric reference systems when comparing different sources of 3D data.

The study presented in this chapter has been carried out in collaboration with the Technical University of Delft (TUDelft), where I spent about three months working at the Department of Hydraulic Engineering, with dr. Alessandro Antonini. The main target was combining geomatic aspects with some operations commonly applied in the field of hydraulic engineering, resulting in a trait d'union between our two fields of study. A deep research and bibliographic study were necessary before starting the processing activities. Moreover, most of the computations have been performed through python scripts, requiring an initial phase of approaching the language.

6.1 Elevation differences

The examined case study area consists of a coastal stretch (about 2.000 m long) located along the Adriatic coast of the Emilia-Romagna region in Italy (Figure a). The current sandy beach is among objects of the monitoring activities managed by Arpae, which consist of repeated geomatic survey campaigns and nourishment interventions [158]. Reliable 3D data, both for the subaerial and subaqueous beach, are therefore available from topo-bathymetric surveys performed using GNSS-RTK and multibeam echo sounder in the selected area (Figure b). Their standard configuration is visible by looking at the spatial distribution of the acquired points: topo-bathymetric surveys realized through the mentioned techniques are typically collected following cross-shore and along-shore transects. Note that this specific configuration can make the following analysis challenging due to its pattern, particularly considering the presence of some isolated longer transects. Concerning other specifications about the adopted surveying techniques, please refer to Chapter 3, which explains them in detail.

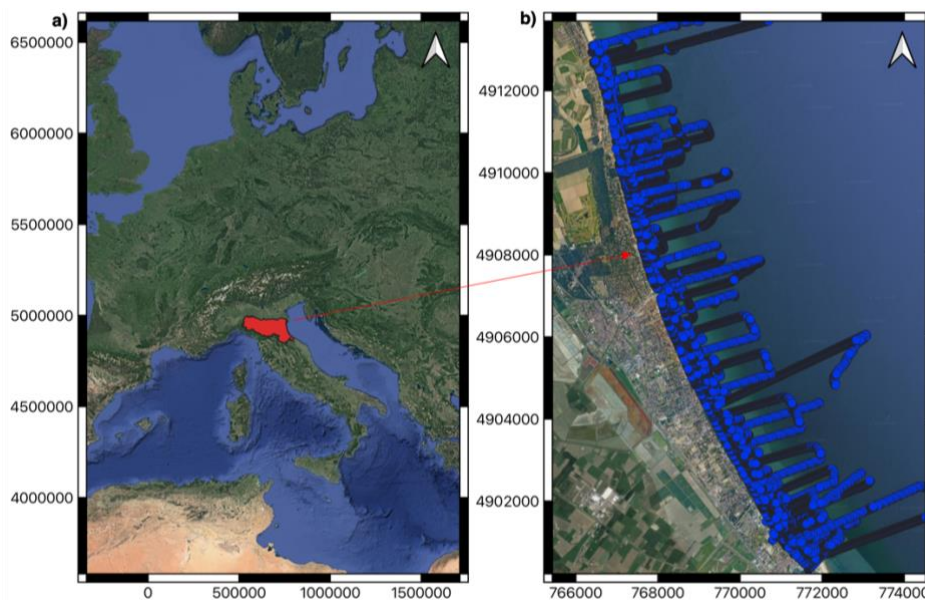


Figure 6.2 - Emilia-Romagna region in Italy (a), GNSS and multibeam survey along the Northern Adriatic coast (b).
Base map: Google Satellite. Coordinates in ETRS89-WGS84.

The GNSS-multibeam data source was selected to be used as ground truth for the following analysis (Figure a), while the publicly available bathymetry for the comparison was downloaded from the EMODnet service [214] considering the

corresponding area (Figure b). As a first step, the point-wise elevation differences between the two data sources have been computed. To do this, the alignment to the same common reference system has to be ensured. In this case, the WGS84 in geographic coordinates (lat, lon), i.e. the one of the EMODnet bathymetry, was selected. As for the altimetric aspect, additional considerations were necessary to consider any possible difference in the zero references assumed for the sea level. Usually, publicly available bathymetries are aligned to the Low Astronomical Tide (LAT) for reasons related to nautical applications (see Chapter 2.3). However, the EMODnet service provides two different products aligned to the MSL and the LAT, respectively. Thus, it was possible to select the Mean Sea Level as the common reference for the two data sources. For the GNSS-multibeam dataset, this fact was ensured by one supporting RGC benchmark (see Chapter 4.1), whose height has been obtained from spirit levelling campaigns realizing the alignment to the mean sea level in Italy.

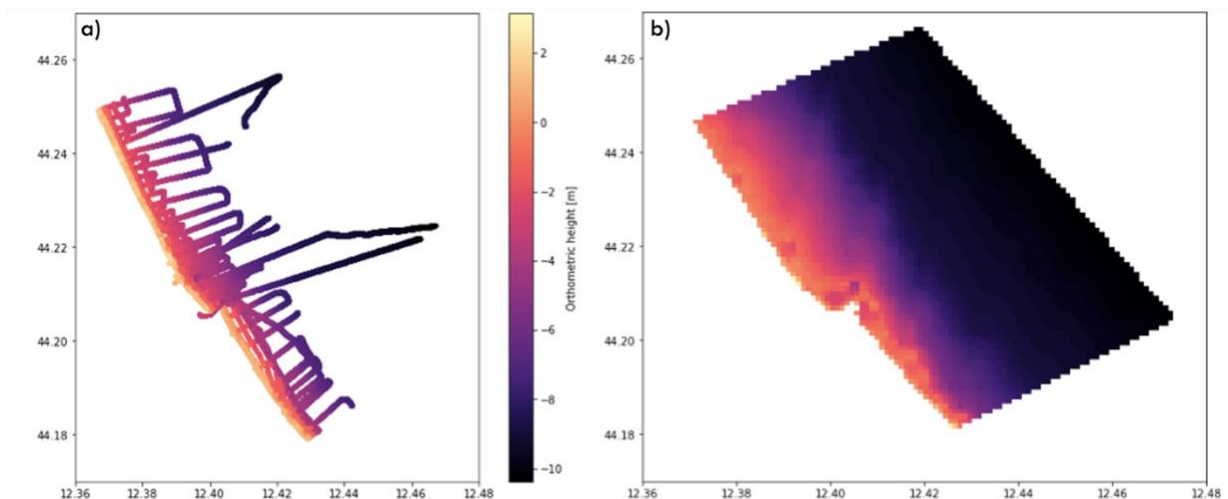


Figure 6.3 – Considered datasets in the selected area: ground truth topo-bathymetric data (a) and publicly available bathymetry from EMODnet service [214] (b).

The GNSS-acquired point closer to the centre of each bathymetry’s pixel was selected following a GIS-based nearest neighbour approach. Then, the elevation differences between the two data sources were computed and graphed through a python script.

Looking at the spatial distribution of the height differences (Figure), it can be observed that the highest absolute values are clearly located at the lower depths. In these areas, particular patterns, probably due to defence structures, can be lost at a larger spatial scale. Moreover, a band of higher difference around the breaking water depth is also present.

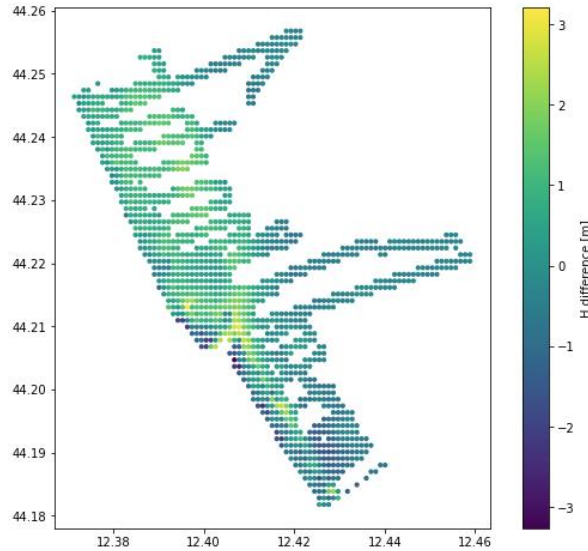


Figure 6.4 – Spatial distribution of the computed elevation differences.

Once the differences between the measured points (ground truth) and the DEM values are calculated, the DEM's vertical accuracy can be quantified by applying the error statistics. Descriptive statistical metrics have been evaluated: differences' minimum and maximum values, mean value (Eq 6.1), root mean square error (Eq 6.2), and standard deviation (Eq 6.3).

$$mean = \frac{\sum(H_p - H_{cell})}{n} \quad Eq\ 6.1$$

$$RMSE = \sqrt{\frac{\sum(H_p - H_{cell})^2}{n}} \quad Eq\ 6.2$$

$$SD = \sqrt{\frac{\sum((H_p - H_{cell}) - mean)^2}{n-1}} \quad Eq\ 6.3$$

Where H_p is the orthometric height of the GNSS-multibeam surveyed point; H_{cell} is the orthometric height extracted at the centre of each pixel; n is the number of considered points, which is equal to 1412.

Table shows the computed statistical parameters related to the elevation differences, resulting in a mean value of about 25 cm, with positive and negative peaks up to 3 meters. As mentioned, higher values basically correspond to shallow water, where the public DEM suffers for its coarseness.

Table 6.1– Statistical parameters related to the computed elevation differences: minimum value (min), maximum value (max), mean value (mean), root mean square error (RMSE), and standard deviation (SD). Values are expressed in meters.

| min (m) | max (m) | mean (m) | RMSE (m) | SD (m) |
|---------|---------|----------|----------|--------|
| -3.26 | 3.21 | 0.24 | 0.88 | 0.85 |

In this context, the mean value can indicate whether the dataset is under or overestimated with respect to the ground truth [154], while the standard deviation quantitatively describes the spread of the obtained values, i.e. the variability of the selected dataset. Moreover, the RMSE is used to quantify the coherence between two data sources. It should be underlined that non-spatial statistics can give an overall metric of the DEM’s quality, implying a hypothesis of spatial homogeneity so it cannot account for any local variations of the errors [79]. The spatial structure of the errors, allowing for a better interpretation of the DEM’s uncertainty, is the topic of the following paragraphs.

6.2 Variogram analysis

After computing the elevation differences between the two datasets, the second step of the workflow involves the fitting of the best variogram. Before diving into the product obtained for the considered case study, the theory behind this computation will be briefly explained in the following paragraphs.

The semivariance represents the parameter used to measure the degree of spatial dependence (or autocorrelation) between a measured set of samples, that is, half the variance of the increment of the regionalized variable [166]. The semivariogram is the plot of the semivariance values as a function of the increasing distance between the

observed points; for simplicity, it is commonly named “variogram”. As stated by the basic principle of Geography (*Tobler’s First Law of Geography: “everything is related to everything else, but near things are more related than distant things”*), a smaller distance leads to a lower semivariance, while a more significant distance results in a higher semivariance (Figure). This means that the computed value of this parameter is strongly dependent on the distance between the considered points: closer things are generally affected by a smaller variability and are therefore more predictable.

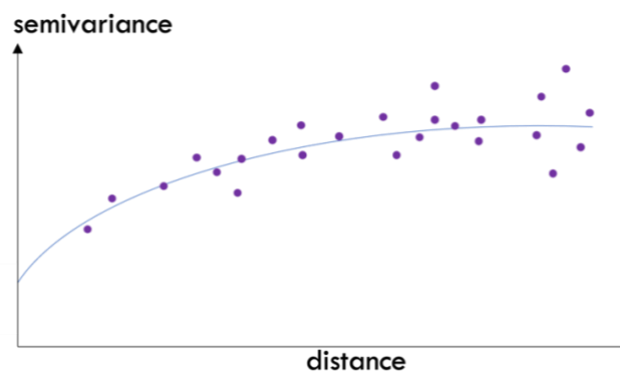


Figure 6.5 – The relationship between semivariance value and distance among the considered points.

Moreover, this semivariance increases with the distance only until it reaches its upper value, named *sill* (Figure). In fact, at a certain distance away from a point, the semivariance will equal the variance around the average value and will, therefore, no longer increase, causing an occurring flat region on the semivariogram [12]. The *range* parameter represents the distance from the point of interest where the curve starts being flat (where it reaches its asymptotic level), meaning that within this distance, the correlation decreases for larger lags, while after this distance, the correlation is the same. Range and sill parameters are connected since the sill is the y-value at which the curve reaches a distance equal to the range (Figure). An acceptable range has to be considered when estimating the values related to unknown points, as all the samples located within the range region will influence the estimations. In fact, to determine the unknown values, a specific neighbourhood is considered for each location, and different weights are assigned to all known samples within the range area.



Figure 6.6 - Range, sill, and nugget parameters used to describe variogram models.

The *nugget* parameter is the value at which the semivariogram asymptotically intercepts the y-axis, resulting in a discontinuity at the curve's origin (Figure). "Theoretically, at zero separation distance, the semivariogram value is 0. However, at an infinitely small separation distance, the semivariogram often exhibits a nugget effect, which is a value greater than 0" [199]. This behaviour can be addressed primarily to possible measurement errors due to the inherent characteristics of the employed instruments or to other sources of spatial variations at distances smaller than the sampling span. Due to the definition of the nugget, coinciding in the small scale variability/noise in the variable that the model cannot estimate, its associated value will include any spatial variations at scales smaller than the sampling distance of the dataset. Different natural phenomena to be investigated can be affected by unpredictable spatial variability across different scales. For this reason, a significant aspect of geostatistical analysis is related to understanding the spatial variation's scale, which address the computation. Using a non-zero nugget in the variogram modelling results in a non-zero variance concerning two observations having a small selected interdistance, and a slight reduction of the correlation between neighbouring samples. It means that also a pair of observations chosen within an arbitrary (small) distance can assume different values.

It is essential to underline that variations in the nugget value directly impact the kriging estimates: a non-zero nugget effect, i.e. a semivariogram's origin different from zero, leads the kriging not to be an exact interpolator. As the nugget value increases,

the kriging model becomes smoother, with estimated values approaching the simple mean of the samples used. Therefore, this can be seen as a decrease in efficiency of the spatial prediction since the chosen spatial model is less allowed to influence the estimation. Conversely, if the nugget parameter is under-estimated, the kriging model becomes too selective and, therefore, less smoothed [195].

The semi-variance value can be computed using several estimators. Usually, they operate from an array of pairwise differences and return the semi-variance values for the whole array. One of the most common operators is the *Matheron*, which calculates the semi-variance as (Eq 6.4) [97]:

$$\gamma(h) = \frac{1}{2N(h)} * \sum_{i=1}^{N(h)} (Z(x_i) - Z(x_{i+h}))^2 \quad \text{Eq 6.4}$$

Where:

$\gamma(h)$ is the Matheron estimator;

$Z(x_i)$ is the variable's value at the i -th point;

$Z(x_{i+h})$ is the variable's value at the point $i + h$;

$N(h)$ is the number of pairs separated by a h -distance;

$Z(x_i) - Z(x_{i+h})$ is precisely the input array.

Another significant aspect when computing a variogram is the discretization of the existing distances within defined classes. Considering all the available samples, each pair of locations is characterized by a unique distance, but reasonably "it is fairly unlikely to find two pairs of observations where the separating distance between the coordinates matches exactly the same value" [203]. Therefore, since the number of pairs is commonly quite high, the paired locations must be grouped into lag bins instead of plotting each pair. This grouping operation, called binning, is crucial and has significant effects on the obtained variogram, as it leads to one estimated variance describing all the values at a given range of distances. The proper selection of the lag value is a trade-off between holding enough representative members for each bin and

having a reasonable resolution at the scale of interest [203]. “For example, if the lag size is too large, short-range autocorrelation may be masked. If the lag size is too small, there may be many empty bins, and sample sizes within bins will be too small to get representative averages for bins” [199]. Depending on the specific analyzed case, there are different approaches to address this issue. For example, when dealing with evenly distributed samples, a good practice could be choosing their spacing as the lag size. On the other hand, choosing the suitable bin dimension becomes critical when the data are irregularly distributed. Some practical approaches can be arbitrarily adopted. For instance, the average distance between each point and its nearest neighbours can be considered, ensuring at least a few representative points for each lag [181]. However, depending on the total range covered by the fitting curve compared to the empirical variogram’s extent, one can subjectively increase or decrease the lag dimension. A non-negligible problem arises when dealing with clustered points, which typically requires considering smaller bins to reach the same level of accuracy in the semivariogram estimation [181]. The computing of the distance between samples is handled by means of a function which can be given as an input argument for the variogram modelling. Generally, the default function coincides with the Euclidean and the computed distances for each point location are stored in a matrix.

In order to determine the lag size, different binning functions which operate in the range $[0, \text{maxlag}]$ are available. They are based on different approaches, such as:

- finding n bins with the same width;
- finding n bins with the same data count;
- using the square root of distance as n of bins;
- using the K-Means clustering to obtain the bins;
- ...

In our analysis, the K-Means algorithm [69] was selected. This method is relatively efficient, although it requires specifying the number of clusters in advance since it cannot be a-priori-determined. Specifically, this method splits a certain number (n) of observations into k clusters based on the similarity between each observation and the

cluster's average [207]. The algorithm works iteratively, repeating two different steps: 1) each value is associated with the cluster with the closest centroid, 2) the new value of the centroid is recalculated. Therefore, the K-Means approach minimises the intra-cluster variance [202].

Once the pairwise dissimilarities are plotted with the chosen lag, the empirical variogram is obtained, where the x-axis represents the distance and the y-axis is the semivariance value. This provides information about the spatial autocorrelation of the considered datasets. The following step consists of finding a curve that properly fits the points and obtaining an accurate continuous description where the samples are not present. Fitting a model is also known as "spatial modelling" or "variography". Its primary principle states that closer points have similar values and smaller semivariance, whereas more dissimilarity is found with increasing distance [38]. The empirical variogram can be modelled using several existing analytical models, each with a different associated degree of complexity and specific parameters (Figure), or even defining a personalized curve. The selected function, which has to result in the minimum difference with the given experimental values, will then be applied to obtain the prediction of the unknown values. In any case, the choice of the fitting model is based on the spatial autocorrelation of the known samples and the available prior knowledge about the analyzed phenomenon [199]. Therefore, different models can be typically adopted to fit different types of phenomena. One of the most impacting factors is the shape of the curve near the origin, as steeper curves in this area lead to a higher influence of the closest points on the final prediction.

Among the standard models, the spherical is one of the most used and shows a progressive decrease of spatial autocorrelation (equivalently, an increase of semivariance) until a certain distance beyond which autocorrelation is zero [181]. Concerning the exponential model, the spatial autocorrelation decreases exponentially with increasing distance and completely disappears only at an infinite distance [181].

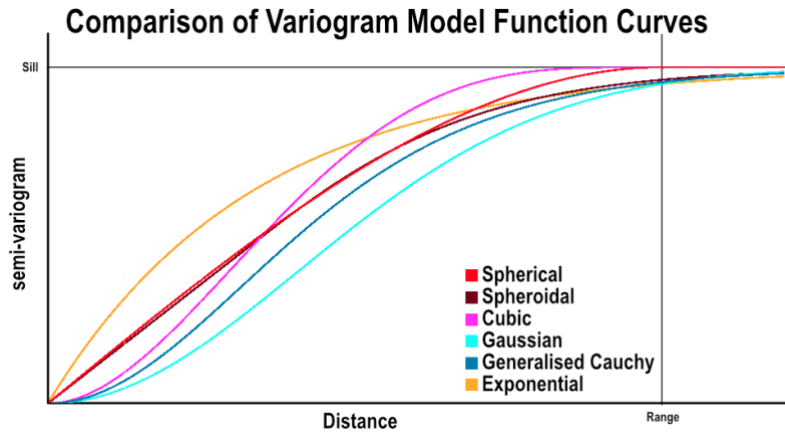


Figure 6.7– Different analytical semivariogram models. Source: [192].

The fitting procedure of the empirical variogram (observations) can be done by-eye, using least squares, weighted least squares, or restricted maximum likelihood methods [107]. Among these, the Trust Region Reflective function (TRF) can be employed, ensuring a robust computation. This function belongs to the Least Square methods, which, “in general, is the problem of finding a vector x that is a local minimizer to a function that is a sum of squares” [223] (Eq 6.5):

$$\min_x \|F(x)\|_2^2 = \min_x \sum_i F_i^2(x) \quad \text{Eq 6.5}$$

Table and Figure , respectively, show the chosen parameters for the present analysis and the computed variogram model with the bins’ histogram. Note that a random set of points (100) has been excluded from the modelling computation and will be used as test points in the subsequent processing steps.

Table 6.2 – Chosen parameters for the variogram modelling.

| | |
|-------------------------|-----------|
| estimator | Matheron |
| model | spherical |
| binning function | kmeans |
| fit method | TRF |
| number of lags | 15 |
| range | 600 |
| sill | 0.66 |
| nugget | 0.25 |

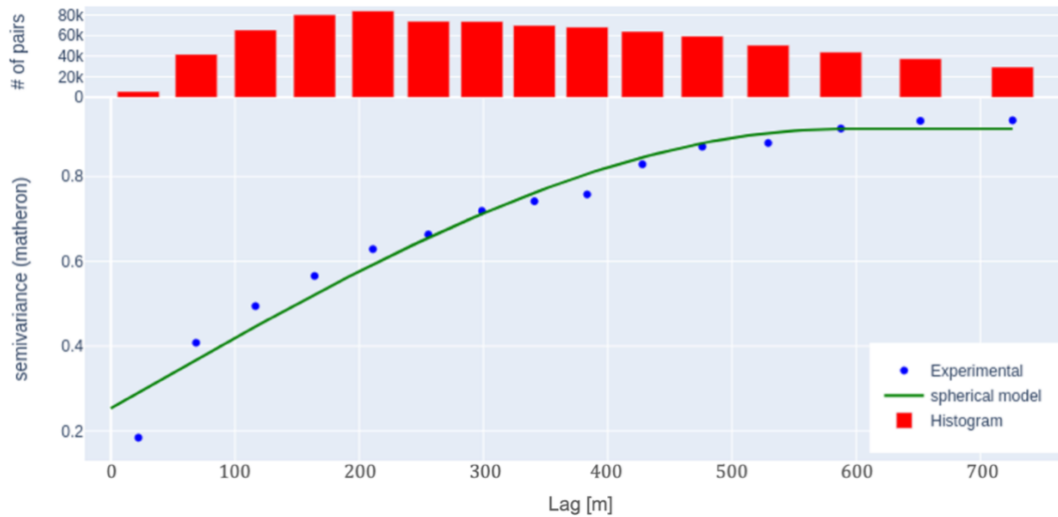


Figure 6.8 – Obtained variogram for the considered dataset. Experimental variogram (blue dots), fitting model (green line) and bins' histogram (red bars).

Two additional parameters have been identified in order to quantify the variogram prediction's error, i.e. the goodness of the fit: the Root Mean Square Error (RMSE) and the Nash and Sutcliff coefficient (NSE) [103]. In general, an RMSE=0 indicates a perfect fit. Concerning the NSE, it is a dimensionless indicator that “represents the complement to unity of the ratio between the mean square error of observed vs. predicted values and the variance of the observations” [128]. Therefore, NSE values close to zero refer to bad predictive performances of the model, whereas values close to 1 refer to good model fitting. Even if there are no general standards to discern whether an estimation is reliable, it is always recommended to use more than a single indicator and to combine them with the visual observation of the results [128]. The study by [128] defined a range of values characterizing different efficiency levels of the model's fitting. According to their classification, the fitted model exhibits excellent performance, with an NSE value higher than 0.90 (Table). Nevertheless, when using this index, it should be considered that its value is affected by the possible presence of outlier, model bias, or repeated data, leading the interpretation of the model's performance to be subjective [128].

Table 6.3 – Parameters to estimate the goodness-of-fit.

| Root Mean Square Error (m) | Nash and Sutcliff coefficient |
|----------------------------|-------------------------------|
| 0.0391 | 0.9649 |

6.3 Kriging

The interpolation process, in general, is a procedure that aims at generating a continuous surface from a scattered set of sample values, thus predicting a variable's values at unsampled locations. Whatever the interpolation approach, it is clear that the final accuracy reached by the method is strongly related to the number of input observations used for the computation, particularly their spatial density. Hypothetically, having an input dataset of perfectly regular points available, with an isotropic interdistance, even using different algorithms, the obtained results would be very similar. The denser the input samples, the less impacting the interpolation method is, both in terms of estimation and representation. This is reasonable because there are fewer unknown values to be determined by the interpolation. Different interpolation methods can lead to significant differences in the results, whether the input samples result scattered or unevenly spaced, for example, with the presence of separated clusters. Furthermore, very irregular configurations of the input samples can force the model to follow their distribution even if it is only related to how the data have been acquired.

Therefore, proper considerations must be done to discriminate the most reliable approach for the selected purpose. In general, however, all interpolation methods are affected by errors if their capabilities are overestimated since there are no physical or mathematical laws that describe the real data structure when data are missing, which is inherent in the uncertainty related to the process of estimating a surface. Moreover, another source of error can be related to the prior knowledge of the phenomenon's behaviour with changing the distance. Only some interpolation methods can consider this aspect, although the study and definition of this relation remain up to the user.

The kriging algorithm belongs to the class of geostatistical interpolators since the process requires a structural analysis (variography) of the considered variable to determine the spatial autocorrelation and auto-covariance among the measured

points. These parameters can be determined after specific analysis and considerations, which imply significant issues, as seen in Chapter 6.2. Differently from other interpolation methods, in this case, the weighing of sampled values used for the new estimations depends on their overall spatial structure and not only on the existing distance between measured points and the prediction locations. Reasonably, in any case, the closer the surrounding sample values, the more they influence the unknown points. However, the weight assigned to each sample comes from a sophisticated process which links the distance between the measured point and the prediction location with the spatial relationship existing among the points around each location. The semivariogram is the instrument employed to determine the spatial structure of the input dataset, i.e. the curve which relates pair of points' distances and the computed semivariance between them [33]. "Because of this, geostatistical techniques not only have the capability of producing a prediction surface but also provide some measure of the certainty or accuracy of the predictions" [181] (Figure). Actually, Kriging modelling is a multistep process consisting of two main steps. The first phase is the so-called variography, which aims to define the variogram and the covariance relations to uncover the spatial dependency rules among the considered dataset. The second phase consists on predicting the unknown values for each defined location, so on creating the continuous interpolated surface itself. Finally, the computing of the relative variance surface is an optional step.

"The general formula is formed as a weighted sum of the data" [77] (Eq 6.6):

$$\hat{Z}(s_0) = \sum_{i=1}^n \lambda_i Z(s_i) \quad \text{Eq 6.6}$$

Where:

$Z(s_i)$ is the measured value at the i -th location;

λ_i is the computed weight related to the value $Z(s_i)$;

s_0 is the location of the new predicted value;

n is the total number of measured samples.

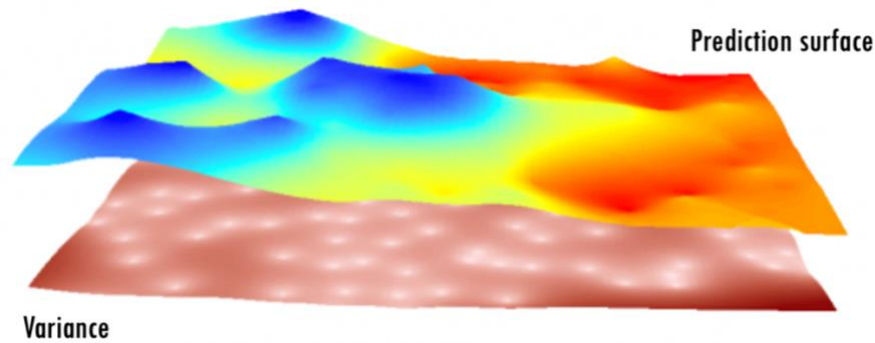


Figure 6.9 – Example of kriging model: prediction surface and associated errors map. Source: [191] (modified).

Kriging methods can be classified into three main approaches:

- Ordinary Kriging: it is commonly employed as default as it can be widely applied for several analysis [155]. The central assumption is that of a stationary phenomenon, which means that the values' mean and variance are constant within the local field. Then, these constant values are assumed to be unknown.
- Universal Kriging: in this case, the stationarity assumption is modified, allowing the mean of the values to change in different locations of the considered field while the variance is maintained as a constant. It is used when data are known to be affected by a prevalent spatial trend that can be described and proved in scientific terms [227]. Usually, this means that a polynomial function can be used to model this trend.
- Simple Kriging: it is the simplest method from an analytical point of view, but this leads to its inapplicability on a general level due to the overly limiting hypothesis. In fact, it assumes to have known both the random field's expectation and the covariance function.

As previously mentioned, a standard procedure to evaluate the kriging model reliability is to use a certain number of points as test data while the remaining ones are employed as training data for the model computation. Therefore, before computing the variogram and the kriging model, we selected a set of 100 test points for this purpose. After computing the variogram model considering a total of 1312 points, it was necessary to define a grid including the coordinates of the desired predictions

locations. In this regard, the grid was defined using the same spatial resolution and pixel coordinates of the original EMODnet bathymetry, to ensure coherence of the spatial structure in the following steps of the analysis. Once the coordinates of the new estimates have been defined, Ordinary Kriging interpolator is applied to compute the corresponding values [50]. Therefore, two different matrixes have been obtained, for the Kriging estimates and the associated variances, respectively. An example of (part of) the matrix related to the kriging estimates is shown in Figure , where the first two columns contain the coordinates of the ' locations and the third represents the corresponding estimated values. Note that 8840 pixel coordinates have been considered for the defined grid.

An automatic procedure was necessary to convert the obtained maps into raster format (.tif), allowing further considerations in a GIS environment. Figure shows the two maps imported into QGIS software, together with their associated colour scales: a) refers to the Kriging model, while b) refers to the variances associated with each cell.

| 1 | pixel_lon | pixel_lat | kriging_estimate |
|----|-------------|-------------|------------------|
| 2 | 12.36614585 | 44.17968764 | -0.23716151 |
| 3 | 12.36718751 | 44.17968764 | -0.23981035 |
| 4 | 12.36822918 | 44.17968764 | -0.24266941 |
| 5 | 12.36927085 | 44.17968764 | -0.24575186 |
| 6 | 12.37031251 | 44.17968764 | -0.24907120 |
| 7 | 12.37135418 | 44.17968764 | -0.25264114 |
| 8 | 12.37239585 | 44.17968764 | -0.25647551 |
| 9 | 12.37343751 | 44.17968764 | -0.26058819 |
| 10 | 12.37447918 | 44.17968764 | -0.26499291 |
| 11 | 12.37552085 | 44.17968764 | -0.26970320 |
| 12 | 12.37656251 | 44.17968764 | -0.27473221 |
| 13 | 12.37760418 | 44.17968764 | -0.28009254 |
| 14 | 12.37864585 | 44.17968764 | -0.28579612 |
| 15 | 12.37968751 | 44.17968764 | -0.29185405 |
| 16 | 12.38072918 | 44.17968764 | -0.29827645 |
| 17 | 12.38177085 | 44.17968764 | -0.30507227 |
| 18 | 12.38281251 | 44.17968764 | -0.31224924 |
| 19 | 12.38385418 | 44.17968764 | -0.31981364 |
| 20 | 12.38489585 | 44.17968764 | -0.32777021 |
| 21 | 12.38593751 | 44.17968764 | -0.33612202 |
| 22 | 12.38697918 | 44.17968764 | -0.34487023 |
| 23 | 12.38802085 | 44.17968764 | -0.35401389 |
| 24 | 12.38906251 | 44.17968764 | -0.36354957 |
| 25 | 12.39010418 | 44.17968764 | -0.37347093 |
| 26 | 12.39114585 | 44.17968764 | -0.38376801 |
| 27 | 12.39218751 | 44.17968764 | -0.39442639 |
| 28 | 12.39322918 | 44.17968764 | -0.40542595 |
| 29 | 12.39427085 | 44.17968764 | -0.41673938 |
| 30 | 12.39531251 | 44.17968764 | -0.42833022 |

Figure 6.10 – Example of the kriging matrix, containing the coordinates of the predictions locations (pixel_lon, pixel_lat) and the estimated value (kriging_estimate).

Most of the higher elevation differences in the map in Figure a are clearly located at shallow depths, up to the bathymetry of 5 meter. This behaviour can be mainly addressed to the loss of local patterns concerning the EMODnet bathymetry, which has a spatial resolution of about 100 m.

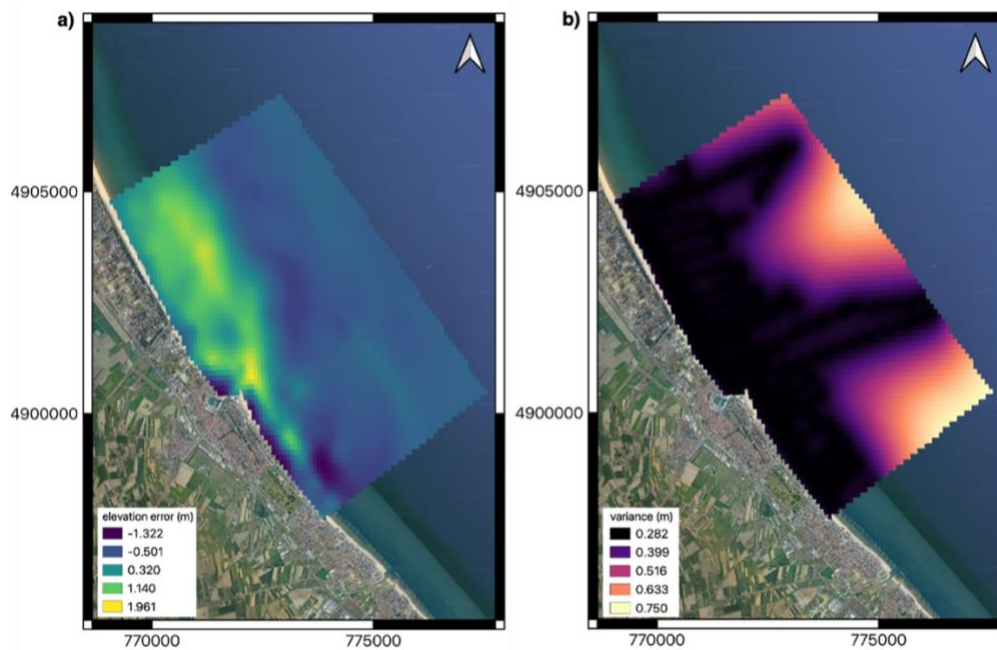


Figure 6.11 – Kriging model of the elevation differences (a) and associated variance map (b).

On the other hand, Figure b shows a very distinct trend in the pixels' variances, where the lower values evidently follow the spatial distribution of the sample values, i.e. the GNSS-multibeam acquired points. This conduct is not surprising since any interpolator suffers when the sample points are unevenly distributed. Nevertheless, in this case, we are dealing with topo-bathymetric data; therefore, it is known that at a certain distance from the shoreline, height values are alike to be similar. For this reason, this fact should be considered when assessing the variance related to each estimation. A possible approach could be to teach the kriging interpolator so that its predictions at a certain distance would be more related to each other even if no samples are present (Figure).

Further developments of this analysis will address this issue, trying to realize a set of different variograms locally valid for each defined depth band and finally reassemble them to obtain the complete model. In fact, it is known that this approach could solve the issue of properly representing the spatial structure [79]. Another option to deal with this behaviour could be using a directional variogram, which can represent better model for beach bathymetries with respect to a unidirectional one. The overall workflow has been completed even if the mentioned computations were not

developed within the present study remaining the topic of possible future developments.

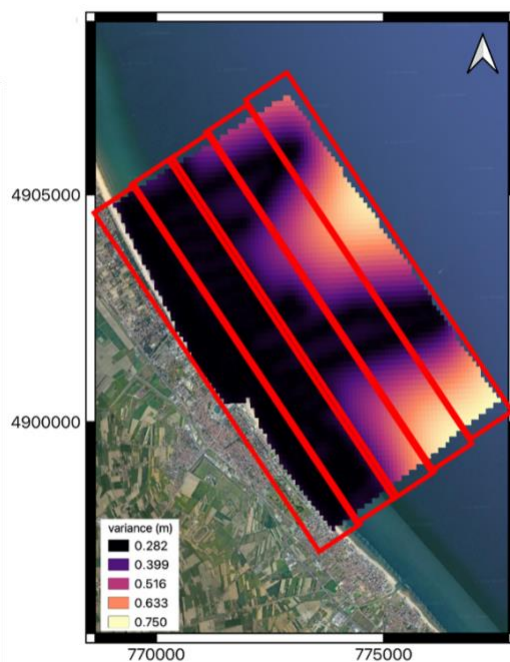


Figure 6.12 – Possible approach to avoid an over-separation in the variance values, through the definition of different depth bands where computing the variograms independently.

Concerning assessing the kriging model's error, the point-wise differences between the test points values and the model estimates have been computed, together with the related frequency histogram. After sampling the Kriging model on the test points' locations, the corresponding values have been extracted. Figure shows the frequency histogram of the computed differences and their spatial distribution in the analysed area.

The main statistical parameters associated with this computation are listed in Table . Although maximum (absolute) values of about 2 meters are present, they are related only to less than ten test points, while the mean of the computed difference is equal to 7 centimetres.

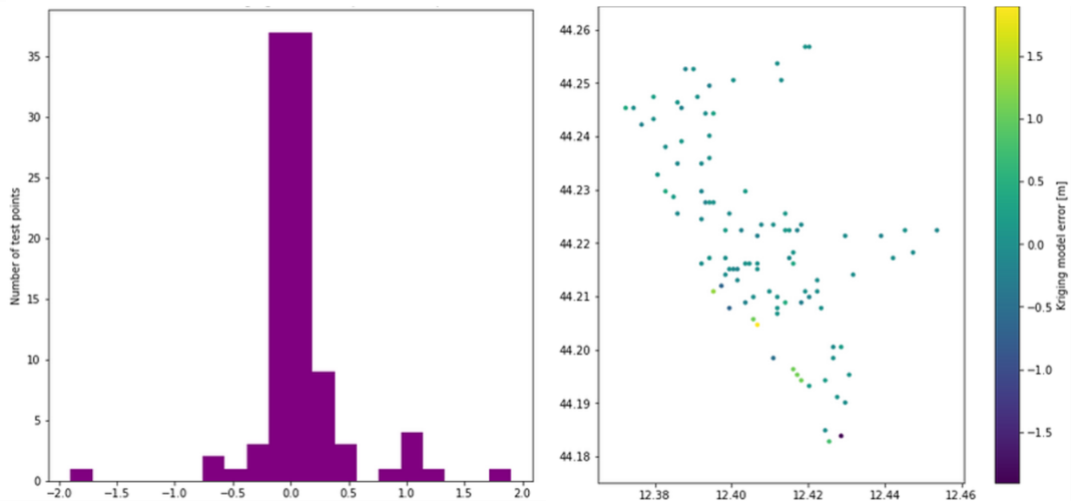


Figure 6.13 – Histogram of the differences between test point values and corresponding estimates from the kriging model and their spatial distribution.

Table 6.4 – Statistical parameters related to the interpolation’s errors: minimum (min) and maximum (max) values, mean value, and standard deviation (SD). Values are expressed in meters.

| Min (m) | Max (m) | Mean (m) | SD (m) |
|---------|---------|----------|--------|
| -1.90 | 1.89 | 0.07 | 0.41 |

6.4 Monte-Carlo simulation

“Monte Carlo Simulation, also known as the Monte Carlo Method or a multiple probability simulation, is a mathematical technique used to estimate the possible outcomes of an uncertain event” [68]. Its name is due to the similarity with the game of roulette. The Monte-Carlo simulation can be applied in the context of sensitivity analysis, quantifying the impact of several different inputs on a process’ outcome. Moreover, it can be used to determine the possible relation between any different input variables used for a specific analysis. For these reasons, it finds many different applications in many real-life scenarios, not only including scientific research.

Basically, by applying a Monte-Carlo chain, a series of outcomes is predicted based on an estimated range of possible input values having their inherent uncertainty. As a result, it provides a model of possible results, together with the probability of occurring of each expected outcome [196]. Due to its random nature, this process yields different results each time a new run is launched [229].

The standard procedure is structured into three steps:

- identification of the variable object of the predictions to be realized;
- determination of the probability distribution function leveraging the variable;
- run of the simulation, i.e. generation of a certain number (n_s) of random values of the variable.

In particular, the second step usually requires research about the common hypothesis applied for similar analysis or the study of historical data of the chosen phenomenon. The purpose is to define the possible range where the values are alike to vary and also quantify their associated probability. Concerning the third step, the number of simulations must be chosen to ensure a proper balance between an expensive computational burden and a good representativity of the input sample. In fact, hypothetically, the simulations can be repeated thousands of times, producing very high numbers of possible outcomes that become hard to handle. On the other hand, all the procedures which follow a Monte Carlo approach involve long and heavy computations due to the long rate of convergence required in order to reach stable and reliable results [229]. Reasonably, the higher the number of samples, the lower difference is expected between different random realizations, because of the reduced associated noise (variance). Besides, indeed, the original input dataset's inherent diversity impacts the resulting similarity among different realizations. Even if these processes are commonly managed using automatic procedures due to the massive amounts of data involved, it is always a good practice to check the obtained simulations to avoid mistakes in the following analysis. In particular, considering the basic concept of the Monte-Carlo method, four different requirements of the obtained simulation can be identified:

- the simulated outputs should be reasonable, both in terms of their associated values and in terms of spatial distribution;
- the semivariogram of the simulations should approximately reproduce the one related to the original input data;

- depending on the employed model, it could be required that the histogram of the simulations approximately equals the one related to the original input data;
- if constraints are present, they must be honoured by the simulations.

Among the possible available geostatistical methods based on the Monte-Carlo approach, Sequential Gaussian Simulation (SGS) can be used when the spatial structure of the considered variable is known. This has already been applied in other studies to generate different equally probable realizations of a DEM, based on the spatial variability of the elevation errors [50][79]. In fact, the SGS method uses the outputs estimated by the kriging modelling, i.e. the mean and variance of the selected variable, to introduce a certain level of randomness to the input dataset. The assumption of a normal variable distribution is required to apply the SGS approach, which results highly dependent on the actual distribution of the input dataset [50]. Within the general workflow, the associated probability distribution function is generated for each computational cell of kriging's grid, and then a random (possible) value is extracted within this distribution and assigned to the corresponding cell. When applied to all the grid's cells and after repeating the whole process several times, it results in multiple equiprobable grids of simulated errors. Finally, by adding each specific simulation to the original DEM, a certain number of new DEM realizations are obtained.

In the context of our analysis, having available for each cell of the defined grid both the estimated values and the associated variances (and thus the standard deviations), it was possible to generate the associated probability density functions in the hypothesis of a normal distribution. This way, each pixel has its probability density function, allowing for a resampling process according to the Sequential Gaussian Simulation. In this step, it was, therefore, necessary to define the sampling approach and the chosen number of simulations to avoid any possible unnecessary computational effort. We identified two main options regarding the sampling process: classic random sampling and Latin Hypercube Sampling (LHS). The first one

generates new samples without considering the previously generated sample points [105]. This means that, hypothetically, all the simulations could be located only in a limited area of the considered field, therefore being less representative of the overall samples distribution (Figure a). Moreover, for this process, it is not necessary to know how many samples will be generated before starting. On the other hand, the LHS approach is based on the definition of a square grid with a certain number of rows and columns, with one sample in each row and each column [87] (Figure b). To do this, the range of the variable is divided into bins with the same associated probability, forcing the number of divisions. For this reason, using the LHS approach, the desired number of sample points must be given as input, although it is possible to take the random samples individually, only considering how many of them were already taken.

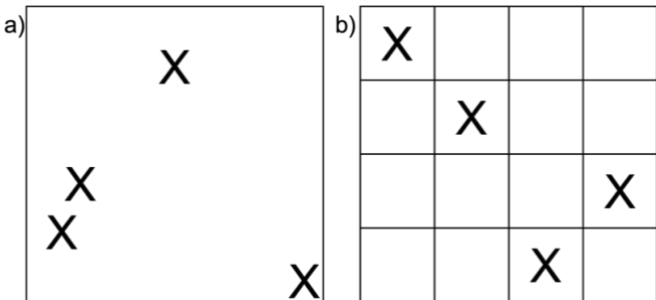


Figure 6.14 – Random sampling (a) and Latin Hypercube sampling (b) principles.

Since the LHS method can lead to a faster convergence, we opted for it in our application’s context, following the scheme in Figure . Thus, a new matrix of possible elevation errors has been obtained for each simulation. These new matrixes are organized into three columns containing the longitude and latitude coordinates of the pixels’ centres and the associated simulated values. Each matrix has been transformed into .tif format allowing the following processing in a GIS environment, by applying an automatic procedure in python. The number of simulations is commonly subjective, depending on the final purpose and the computational effort that is possible to reach, but it is known that commonly a large number is required to reach stable results and reliable estimation of distribution function [71].

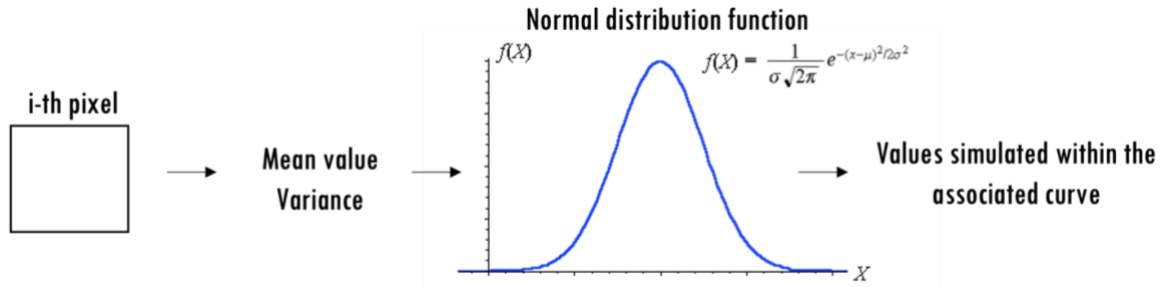


Figure 6.15 – Steps of the processing to extract the simulated value.

We identified two different methods (hereinafter named A and B) to ensure whether the chosen number of simulations is suitable for our specific analysis, both related to the reaching of convergence.

Method A can be summarized as follow:

- a certain number (n_s) of simulations is produced;
- the value x_i^n , $n = [1, n_s]$, of each pixel (i) for each simulation is considered;
- as the number of simulations increases, the mean of the current n_s values x_i^n is considered independently for each pixel i , according to Eq 6.7:

$$n = [1, \dots, n_s] \quad \bar{x}_i^n = \frac{\sum_{j=1}^n x_i^j}{n} \quad \text{Eq 6.7}$$

- then, the variation coefficient (ϕ_i^n) with the increasing number of simulations is computed considering the ratio between the \bar{x}_i^n value and the kriging estimate x_i^k of each pixel, according to Eq 6.8:

$$\phi_i^n = \frac{\bar{x}_i^n}{x_i^k} \quad \text{Eq 6.8}$$

- a graph of the variation coefficient with the change in the number of simulations is produced for each pixel, thus allowing to graphical estimate when it reaches its convergence, i.e. when the curve starts being almost flat.

Method B is structured in the following steps:

- a certain number (n_s) of simulations is produced;
- for each simulation, starting from the value x_i^n , $n = [1, n_s]$, of each pixel (i), the mean considering the total number of simulations is computed, named \bar{x}_i (Eq 6.9);

$$\bar{x}_i = \frac{\sum_{n=1}^{n_s} x_i^n}{n_s} \quad \text{Eq 6.2}$$

- each \bar{x}_i value is compared with the corresponding one given as input for the simulation, i.e. kriging's estimate x_i^k . After, the difference (Δ_i) is computed according to Eq 6.10. For the inherent definition of a normal distribution with associated mean and variance, the mean of the obtained values should match the input mean of the distribution.

$$\Delta_i = \bar{x}_i - x_i^k \quad \text{Eq 6.10re}$$

According to the described approach, a number equal to 1000 simulations was chosen, resulting in a mean difference at the 10^{-4} cm level for Method B (Figure B). Note that Figure A refers to a specific pixel since, according to Method A, one graph is obtained for each pixel.

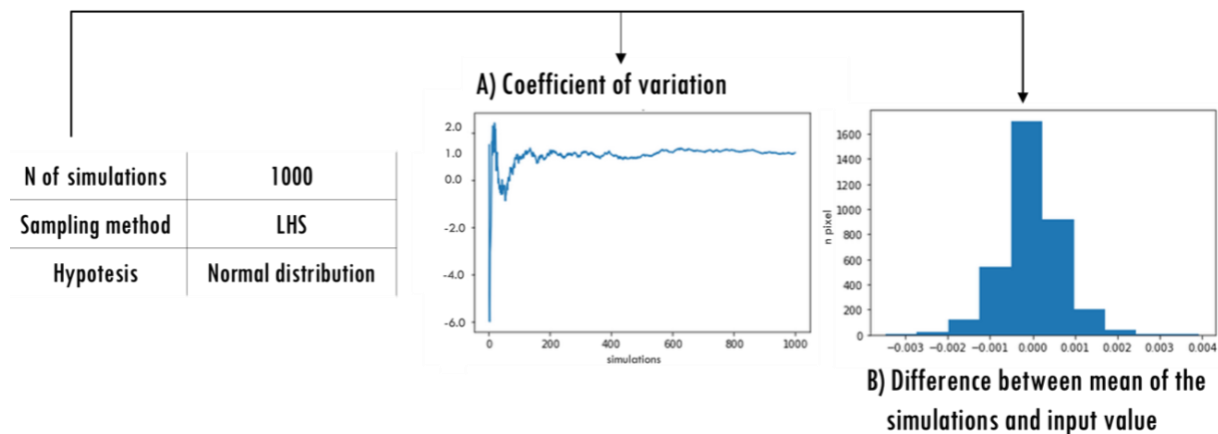


Figure 6.16 – Methods A and B to assess the reaching of convergence for the selected number of simulations. Note that A) refers to a specific pixel chosen as example, while B) refers to all the pixels.

Once a raster map was realized for each simulation, it was possible to compute the n_s new DEM's realizations simply by adding the simulation matrix with the original EMODnet bathymetry. This easy computation was possible thanks to the special attention given in the whole process to the correct grid definition, always using the same pixel coordinates for all the processes, i.e. the same spatial structure. Moreover, the same attention must be addressed to the reference system used for all the data sources implied in the computation to avoid mistakes in the results. As already mentioned, this final step of the workflow allows considering the uncertainty

associated with the DEM in any possible analysis based on it as an input data source [79]. Figure shows an example of a map of simulated elevation errors and the relative newly computed DEM.

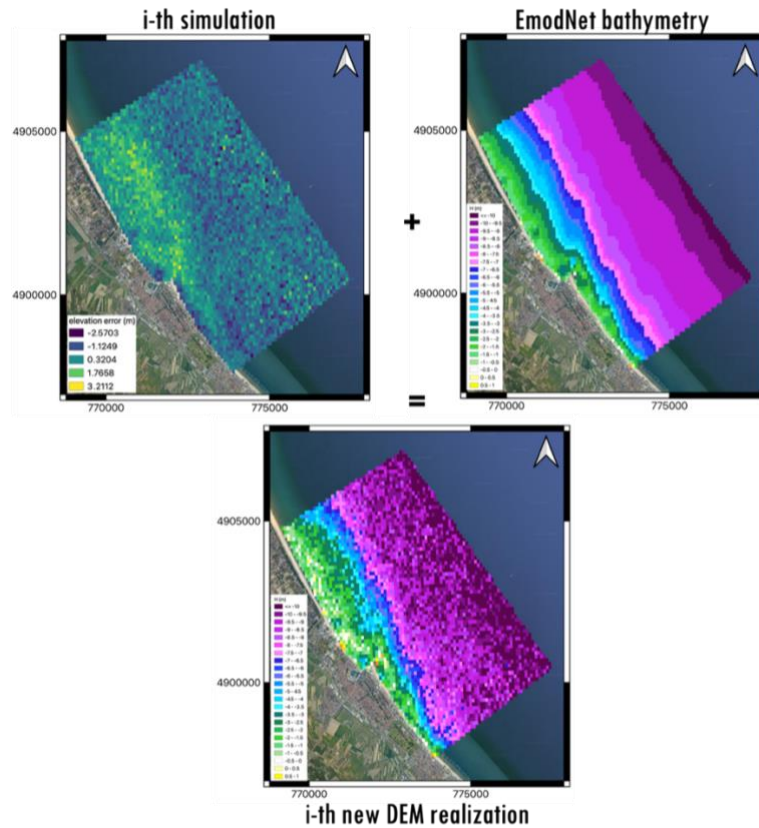


Figure 6.17 – Processing for the realization of the new DEM, starting from the computed map of simulated elevation errors.

6.5 Considerations

This analysis' main goal was to quantify how the accuracy of the geomatic data can affect the final results of numerical modelling. Even if the study in this sense is not complete, detailed computations have addressed the statistical analysis of height differences between a publicly available bathymetry and a GNSS-multibeam dataset over a common area. The arose considerations from the performed analysis are reported in the paragraphs below. In this kind of analysis, the configuration of the input points plays a fundamental role, i.e. the spatial distribution and the density of the samples. Therefore, some of the adopted parameters, especially those related to the variogram modelling, should be at least reconsidered if varying the ground truth

dataset. Moreover, another possible approach to generalize the processing could be to vary only the configuration of the samples starting from the same input dataset, applying different possible setups. These variations could include different values of inter distance among the points, the presence of clusters, or the use of different total samples considered as training points for the variogram and kriging models.

Indeed, since this specific analysis has been performed to support hydraulic modelling studies, some aspects must be taken into account. The first consideration is related to the input parameters required to run hydro-morphodynamic models. These commonly include the bathymetry, the granulometric distribution of the material, the present defence structures, the wave climate, the wind, and the sea level changes due to tides and currents. All the listed parameters can affect the model's result at different levels, mainly depending on the considered spatial scale. For this reason, even the bathymetric model used as input can be relevant at particular modelling scales rather than others or at least can have different impacts according to the selected scale. The change in the spatial scale involved in the analysis could be another aspect to be addressed by creating different scenarios at different scales.

Moreover, the specific phenomenon to be investigated can make the bathymetric data discriminative only within a certain distance from the shoreline. This is particularly true for morphodynamic studies, where the impacting area is only the one within the depth of closure. One practical objective of such analysis is related to the managing and planning the surveys on the field. In fact, following this approach, it would be possible to observe whether the numerical modelling results are affected by any variation in the input bathymetry and to quantify any induced change. Obtained considerations could be therefore used to evaluate how the topo-bathymetric survey campaigns should be configured for a specific modelling analysis, allowing for a more efficient organization of the entire project. Reasonably, even the computational effort associated with different input datasets should be considered, as the described analysis can involve a large amount of data.

Hereafter, the list of the employed public python libraries is shown:

- NumPy: fundamental package for scientific computing;
- Pandas: for any data analysis and manipulation;
- GeoPandas: to manage geospatial data;
- GDAL: for GIS-based analysis, manipulating geospatial raster and vector data;
- Rasterio: to manage raster data;
- Fiona: for GIS-based analysis;
- SciKit GStat: for the variogram computing;
- gstools.krige.Ordinary: for the kriging process.

Conclusions

Recently, we are experiencing an increase in publicly available and accessible spatial data sources. This is mostly related to European policies aiming to enhance and simplify the use of spatial information, and, also, with a view of awareness on environmental-related subjects. Reasonably, this fact is also connected with the technological development, which makes available more and more possibilities both in terms of techniques and processing tools. Advancements in the performance of instrument and approaches usually lead to higher associated spatial resolutions and accuracies. On the other hand, proper management of these data must be ensured to avoid useless computation effort, or, worse, erroneous analyses. This is even more true considering that environmental themes are of public interest and, therefore, usually involve users outside the scientific community.

Among the environmental heritages, sandy coasts represent critical areas due to the inherent link between land and sea, which should be properly considered during all the related analyses. Indeed, coastal monitoring activities are structured into several steps, starting with field surveys, processing acquired data, and finally evaluating the obtained products.

In particular, concerning the present thesis, monitoring activities are framed in the context of middle/long-term studies related to the erosion process and associated defence interventions. These kinds of analyses should always be addressed by

combining engineering solutions and management policies since the economic role and the tourist impact of coastal areas cannot be neglected.

Throughout this study, the primary aspects of coastal monitoring have been analysed, with particular attention to the proper management of the reference systems during the entire process. About this, in coastal areas, the altimetric aspect has a fundamental role since there is a need for 3D information about both emerged and submerged beaches. Thus, topo-bathymetric maps are commonly required as essential products representing the beach's heights and depths. Among the suitable geomatic techniques for coastal applications, the most efficient choice depends on the specific area's morphology and monitoring purpose. Reasonably, some techniques are known to have higher performance in specific conditions, but it is impossible to discern if a technique generally works better than another due to the amount of impacting parameters entering the discussion. For these reasons, an accuracy-efficiency trade-off should always be ensured to calibrate the survey's accuracy and spatial resolution according to the final use of the data, i.e. the derived products demanded the analysis.

Moreover, the economic point of view should also be contemplated, considering that an increase in the final accuracy results from higher-level instruments, longer time on the field, higher amounts of acquired data and processing effort, each with associated costs. Apart from a cost-benefit analysis, reaching the highest possible accuracy is not always desirable. If the analysis does not strictly rely on high-resolution data, their use can even represent a useless source of confusion. The equilibrium point arises when the increase in performance evidently becomes an additional value for the achievable products. This performance concerns both the technique's accuracy and the processing approach employed, which sometimes introduces additional sources of error.

After these considerations, clearly, a precise understanding of the investigated phenomenon represents the fundamental crux of coastal monitoring, reflecting both the magnitude of the expected measurements and the products needed for the

evaluations. The same thought can also be applied in the context of numerical modelling, which is becoming an affirmed method for supporting coastal studies. Also, in this context, several models are currently available with different associated complexity and always rely on several parameters as input data. Understanding the impact of different parameters on the models' results is undoubtedly not straightforward due to their inherent relationships in the analysed processes. However, identifying the effects of different levels of accuracy on numerical analysis can represent a helpful instrument to properly manage and organize the in situ surveys for each specific application.

This study finds its practical application in the activities performed by Arpae, the Regional agency for prevention, environment and energy of Emilia-Romagna, which is involved in the identification of the coastal dynamics and the main impacting parameter on the littoral evolution. Arpae periodically realizes topo-bathymetric surveys to monitor the coastal erosion and plan associated defence interventions subsequently. Along the Emilia-Romagna littoral, the importance of proper management also results in maintaining an area with great economic relevance. Therefore, the realization of defence interventions also needs proper planning of the associated monitoring activities to evaluate their efficiency over time.

References

Articles

- [1] Aguzzi, M., Costantino, R., De Nigris, N., Morelli, M., Romagnoli, C., Unguendoli, S., Vecchi, E. Stato del litorale emiliano-romagnolo al 2018: Erosione e Interventi di Difesa; ARPAE Emilia-Romagna: Emilia-Romagna, Italy. 2020.
- [2] Aguzzi, M., De Nigris, N., Mallegni, R., Preti, M. Nuovi indicatori per lo studio e la gestione della costa emiliano-romagnola. *Studi Costieri*, 20. 2012, pp. 95–109.
- [3] Aguzzi, M., De Nigris, N., Morelli, M., Paccagnella, T., Unguendoli, S. Il monitoraggio di Arpae sulle spiagge, *Ecoscienza*, 3. 2017, pp. 94–95.
- [4] Aguzzi, M., et al. Stato del litorale emiliano-romagnolo al 2012, Erosione e interventi di difesa, Bologna, Arpae Emilia Romagna, I quaderni di Arpae, 2016.
- [5] Andersen, O.B., Knudsen, P. DNSC08 mean sea surface and mean dynamic topography models, *J. Geophys. Res.* 114. 2009. doi:10.1029/2008JC005179.
- [6] Andriolo, U., Gonçalves, G., Sobral, P., Fontán-Bouzas, Á., Bessa, F. Beach-dune morphodynamics and marine macro-litter abundance: An integrated approach with Unmanned Aerial System. *Sci. Total Environ.* 749, 2020.
- [7] Archetti, R., Zanuttigh, B. Integrated monitoring of the hydro-morphodynamics of a beach protected by low crested detached breakwaters, *Coastal Engineering*, 57, 10. 2010, pp. 879-891. doi:10.1016/j.coastaleng.2010.05.002.
- [8] Aykut, N.O., Güral, E., Akpınar, B. Performance of single base RTK GNSS method versus network RTK. *Earth Sci Res J* 19(2). 2015, pp. 135-139. doi:10.15446/esrj.v19n2.51218.
- [9] Bange, H.W., et al. World Ocean Review 2015: living with the oceans 5. Coasts-a vital habitat under pressure. *Maribus*. 2017.
- [10] Barbano, A., et al. Caratteristiche della Costa Italiana: le Unità Fisiografiche e le Profondità di Chiusura. *Atti della I Conferenza Nazionale Coste: Prevenire, Programmare, Pianificare, Maratea*, 9. 2008.
- [11] Barbarella, M., Barzaghi, R., Dominici, D., Fiani, M., Gandolfi, S., Sona, G. A comparison between the Italgeo'95 and GPS/Leveling data along the coast of Italy. *J. Phys. Chem. Earth* 23(1). 1998, pp. 81–86.
- [12] Bárdossy, A. Introduction to geostatistics." Institute of Hydraulic Engineering, University of Stuttgart. 1997.
- [13] Barnard, P.L., et al. Coastal vulnerability across the Pacific dominated by El Niño/Southern oscillation. *Nature Geoscience* 8.10. 2015, pp. 801-807.

- [14] Barzaghi, R., Borghi, A., Carrion, D., Sona, G. Refining the estimate of the Italian quasi-geoid. *Bollettino di Geodesia e Scienze affini*, 3. 2007, pp. 146–157.
- [15] Barzaghi, R., Carrion, D. Testing EGM2008 in the central mediterranean area, external quality evaluation. *Reports of EGM08. Newton’s Bull* 4. 2009, pp. 133–143.
- [16] Beachmed. 2° Quaderno Tecnico, Fase “B”. Beachmed Project: Recupero ambientale e mantenimento dei litorali in erosione con l’utilizzo di depositi sabbiosi marini, Roma, July. 2004.
- [17] Bello-Pineda, J., Hernández-Stefanoni, J.L. Comparing the performance of two spatial interpolation methods for creating a digital bathymetric model of the Yucatan submerged platform. *Executive editor: Gonzalo Velasco*, 1(3). 2006, pp. 247-254.
- [18] Benedetti, G., Bitelli, G., Bonsignore, F., Draghetti, T., Unguendoli, M., Zavatti, A. Emilia-Romagna subsidence monitoring network. First results. *Proceedings third congress on regional geological cartography and information systems. Munich*, 24/27 October. 2000, pp. 36–40.
- [19] Bertoni, D., Armaroli, C., Ciavola, P. Fast retreat of a barrier system due to reduced sediment supply (Bellocchio, Northern Adriatic Sea, Italy). *Proceedings of the 3rd CM2 Coastal Maritime Mediterranean Conference, Ferrara, Italy*, 25–27 November. 2015, pp. 7–10.
- [20] Bitelli, G., et al. Updating the subsidence map of Emilia-Romagna region (Italy) by integration of SAR interferometry and GNSS time series: the 2011–2016 period. *Proc. IAHS* 382. 2020, pp. 39–44.
- [21] Bjelotomic Oršulic, O., Markovinovic, D., Varga, M., Bašić, T. The impact of terrestrial gravity data density on geoid accuracy: case study Bilogora in Croatia. *Surv. Rev.* 52(373), 2020, pp. 299–308.
- [22] Bremer, M., Sass, O. Combining airborne and terrestrial laser scanning for quantifying erosion and deposition by a debris flow event. *Geomorphology* 138.1. 2012, pp. 49-60.
- [23] Brunel, C., François, S. Potential influence of sea-level rise in controlling shoreline position on the French Mediterranean Coast. *Geomorphology* 107.1-2. 2009, pp. 47-57.
- [24] Brunier, G., Fleury, J., Anthony, E.J., Gardel, A., Dussouillez, P. Close-range airborne Structure-from-Motion Photogrammetry for high-resolution beach morphometric surveys: Examples from an embayed rotating beach. *Geomorphology* 261. 2016, pp. 76–88.
- [25] Carli, S., et al. *Tecniche Di Monitoraggio Dell’evoluzione Delle Spiagge, Regione Toscana, Il Piano Regionale di gestione integrata della costa ai fini del riassetto idrogeologico, Erosione costiera, Firenze, Edifir*. 2004, pp. 125–165.
- [26] Casella, E., Rovere, A., Pedroncini, A., Stark, C.P., Casella, M., Ferrari, M., Firpo, M. Drones as tools for monitoring beach topography changes in the Ligurian Sea (NW Mediterranean). *Geo-Mar. Lett.* 36. 2016, pp. 151–163.

- [27] Choy, S., Kuckartz, J., Dempster, A.G., Rizos, C., Higgins, M. GNSS satellite-based augmentation systems for Australia. *GPS Solutions* 21 (3). 2017, pp. 835–848. doi:10.1007/s10291-016-0569-2.
- [28] Cina, A., Dabove, P., Manzano, A.M., Piras, M. Augmented positioning with CORSs network services using GNSS mass-market receivers. *Proc. IEEE/ION Position, Location and Navigation Symp.-PLANS*. 2014, pp. 359–366.
- [29] Cipriani, L.E., Wetzel, L., Aminti, D.L., Pranzini, E. Converting seawalls into gravel beaches, first international management of coastal recreational resources. *Beaches, Yacht Marinas and Coastal Ecotourism, Malta, 20/23 October*. 2004, pp. 3–12.
- [30] Cohen, O., Héquette, A. Recent Advances in Coastal Survey Techniques: From GNSS to LiDAR and Digital Photogrammetry- Examples on the Northern Coast of France. *Spatial Variability in Environmental Science-Patterns, Processes, and Analyses*, IntechOpen London, UK. 2020.
- [31] Colomina, I., Pere, M. Unmanned aerial systems for photogrammetry and remote sensing: A review. *ISPRS J. Photogramm. Remote Sens.* 92. 2014, pp. 79–97.
- [32] Corchete, V. The high-resolution gravimetric geoid of Italy: ITG2009. *J. Afr. Earth Sci.* 58. 2010, pp. 580–584.
- [33] Cressie, N. Fitting variogram models by weighted least squares. *Journal of the international Association for mathematical Geology* 17.5. 1985, pp. 563-586.
- [34] Crossland, C.J., Kremer, H.H., Lindeboom, H.J., Marshall Crossland J.I., Le Tissier, M.D.A. Coastal fluxes in the anthropocene. *The Land-Ocean Interactions in the Coastal Zone Project of the International Geosphere-Biosphere Programme*, Springer. 2005.
- [35] de Sanjosé Blasco, J.J., et al. Application of multiple geomatic techniques for coastline retreat analysis: The case of Gerra Beach (Cantabrian Coast, Spain). *Remote Sensing* 12.21. 2020.
- [36] de Sanjosé Blasco, J.J., et al. Monitoring retreat of coastal sandy systems using geomatics techniques: Somo Beach (Cantabrian Coast, Spain, 1875–2017). *Remote Sensing* 10.9. 2018.
- [37] Delacourt, C., et al. DRELIO: An unmanned helicopter for imaging coastal areas. *J. Coast. Res.* 2. 2009, pp. 1489–1493.
- [38] Deutsch, C.V. *Geostatistics*, Robert A. Meyers, *Encyclopedia of Physical Science and Technology (Third Edition)*, Academic Press. 2003, pp. 697-707. doi:0.1016/B0-12-227410-5/00869-3.
- [39] Dix, M., et al. Accuracy evaluation of terrestrial LiDAR and multibeam sonar systems mounted on a survey vessel. *Journal of Surveying Engineering* 138.4. 2012, pp. 203-213.
- [40] Drummond, C.D., Harley, M.D., Turner, I.L., Matheen, N., Glamore, W.C. UAV applications to coastal engineering. *Eng. Aust. IPENZ*. 2015, pp. 267–272.
- [41] Duo, E., et al. Local-scale post-event assessments with GPS and UAV-based quick-response surveys: a pilot case from the Emilia–Romagna (Italy) coast. *Natural Hazards and Earth System Sciences* 18.11. 2018, pp. 2969-2989.

- [42] Duvat, V. Interest of quality-based policies for Integrated Coastal Zone Management implementation: Lessons learnt from a French case study. *Ocean Coast. Manag.* 54. 2011, pp. 831–843.
- [43] El Kafrawy, S.B., et al. Performance evaluation of shoreline extraction methods based on remote sensing data. *Journal of Geography, Environment and Earth Science International* 11.4. 2017, pp. 1-18.
- [44] Emilia-Romagna, A.R. Misura della rete regionale di controllo della subsidenza, misura di linee della rete costiera non comprese nella rete regionale, rilievi batimetrici. *Relazione Finale*. 2001.
- [45] Emilia-Romagna, A.R. Rilievo della Subsidenza nella pianura Emiliano-Romagnola. *Relazione finale*. 2012.
- [46] Emilia-Romagna, A.R. Rilievo della Subsidenza nella pianura Emiliano-Romagnola. *Relazione finale*. 2018.
- [47] EMODnet Thematic Lot n°0 – Bathymetry – High Resolution Seabed Mapping (HRSM2), EMODnet Phase III – Quarterly Progress Report (5). 2020.
- [48] EuroSION. Living with Coastal Erosion in Europe: Sediment and Space for Sustainability. Part IV - A guide to coastal erosion management practices in Europe: Lessons Learned, Final Version, 22 May. 2004
- [49] Fabbri, M., Magnani, C., Regina, N. Erosione costiera e subsidenza, in *Progetto Mare, L'Adriatico in Romagna: caratteristiche, controllo e risorse dell'ecosistema marino*. 2001.
- [50] Fereshtehpour, M., Karamouz, M. DEM resolution effects on coastal flood vulnerability assessment: Deterministic and probabilistic approach. *Water Resources Research* 54.7. 2018, pp. 4965-4982.
- [51] Fiani, M., Prezioso, G., Troisi, S., Turturici, L., Wirz, M. Una rete GPS per il monitoraggio delle variazioni morfologiche delle coste, *Bollettino SIFET* 1. 2003, pp. 35-52.
- [52] Frazer, L.N., Anderson, T.R., Fletcher, C.H. Modeling storms improves estimates of long-term shoreline change. *Geophysical Research Letters* 36.20. 2009.
- [53] Gabrlik, P. The use of direct georeferencing in aerial photogrammetry with micro UAV. *IFAC-PapersOnLine* 48.4. 2015, pp. 380-385.
- [54] Gaeta, M.G., Bonaldo, D., Samaras, A.G., Carniel, S., Archetti, R. Wave-2D Hydrodynamics Modeling at the Reno River Mouth (Italy) under Climate Change Scenarios. *Water* 10. 2018.
- [55] Gandolfi, S., De Nigris, N., Morelli, M., Tavasci, L., Poluzzi, L., Cenni, N. La Rete Geodetica Costiera della Regione Emilia- Romagna. *ASITA*. 2017, pp. 599–604.
- [56] García-Rubio, G., Huntley, D., Russell, P. Assessing shoreline change using satellite-derived shorelines in Progreso, Yucatán, México. *Coastal Engineering Proceedings* 33. 2012, pp. 79-79.

- [57] Gibbs, M. Coastal climate risk and adaptation studies: The importance of understanding different classes of problem. *Ocean Coast. Manag.* 103. 2015, pp. 9–13.
- [58] Gibeaut, J.C., Gutierrez, R., Kyser, J.A. Increasing the accuracy and resolution for coastal bathymetric surveys, *Coastal Surveys*. *J Coastal Res* 14. 1998, pp.1082–1098.
- [59] Gómez-Pazo, A. et al. Open Digital Shoreline Analysis System: ODSAS v1. 0. *Journal of Marine Science and Engineering* 10.1. 2021.
- [60] Gonçalves, J.A.; Henriques, R. UAV photogrammetry for topographic monitoring of coastal areas. *ISPRS J. Photogramm. Remote Sens.* 104. 2015, pp. 101–111.
- [61] Gonçalves, R.M., Awange, J.L. Three Most Widely Used GNSS-Based Shoreline Monitoring Methods to Support Integrated Coastal Zone Management Policies. *J. Surv. Eng* 143. 2017.
- [62] Grządziel, A. The Importance of Under-Keel Sound Velocity Sensor in Measuring Water Depth with Multibeam Echo sounder. *Energies* 14. 2021. doi:10.3390/en14175267.
- [63] Gumus, K., Selbesoglu, M.O., Celik, C.T. Accuracy investigation of height obtained from Classical and Network RTK with ANOVA test. *Elsevier Meas* 90. 2016, pp. 135–143. doi:10.1016/j.measurement.2016.04.045.
- [64] Hagenaaars, G., et al. On the accuracy of automated shoreline detection derived from satellite imagery: A case study of the sand motor mega-scale nourishment. *Coastal Engineering* 133. 2018, pp. 113-125.
- [65] Hallermeier R.J. Seaward Limit of Significant Sand Transport by Waves: An Annual Zonation for Seasonal Profiles. *Coastal Engineering Technical Aid*, Coastal Engineering Research Center, U.S. Army Engineer Waterways Experiment Station, Vicksburg, MS, CETA 81-2. 1981, p. 23.
- [66] Hallermeier, R.J. A Profile Zonation for Seasonal Sand Beaches from Wave Climate. *Coastal Engineering*, 4,. 1981, pp. 253-277.
- [67] Harley, M.D., et al. Shoreline change mapping using crowd-sourced smartphone images." *Coastal Engineering* 150. 2019, pp. 175-189.
- [68] Harrison, R.L. Introduction to monte carlo simulation. *AIP conference proceedings*. 1204, 1. American Institute of Physics. 2010.
- [69] Hartigan, J.A., Wong, M.A. Algorithm AS 136: A K-Means Clustering Algorithm. *Journal of the Royal Statistical Society. JSTOR, Series C (Applied Statistics)*, 28, 1. 1979, pp. 100–08. doi:10.2307/2346830.
- [70] Heck, B. Problems in the definition of vertical reference frames. *V Hotine-Marussi Symposium on Mathematical Geodesy*. Springer, Berlin, Heidelberg. 2004.
- [71] Heuvelink, G.B.M. Analysing uncertainty propagation in GIS: why is it not that simple. *Uncertainty in remote sensing and GIS*. 2002, pp. 155-165.
- [72] Hoffmeister, D., Tilly, N., Curdt, C.; Aasen, H.; Ntageretzis, K., Hadler, H., Timo, W., Andreas, V., Georg, B. Terrestrial laser scanning for coastal geomorphologic research

- in western Greece. *Int. Arch. Photogramm. Remote Sens. Spat. Inf. Sci.* 39. 2012, pp. 511–516.
- [73] Hofmann-Wellenhof, B., Lichtenegger, H., Wasle, E. *GNSS– global navigation satellite systems: GPS, GLONASS, Galileo, and more.* New York: Springer. 2007.
- [74] IDROSER Spa. Progetto di piano per la difesa dal mare e la riqualificazione ambientale del litorale della Regione Emilia-Romagna, Relazione generale. 1996, pp. 365.
- [75] James, M.R., Ilic, S., Ruzic, I. Measuring 3D coastal change with a digital camera. *Proc. Coast. Dyn.* 2013, pp. 24–28.
- [76] Jaud, M., Grasso, F., Le Dantec, N., Verney, R., Delacourt, C., Ammann, J., Deloffre, J., Grandjean, P. Potential of UAVs for Monitoring Mudflat Morphodynamics (Application to the Seine Estuary, France). *ISPRS Int. J. Geo-Inf.* 2016.
- [77] Jiang, F., Hirohata, M. Numerical simulations for time-dependent corrosion surface of unpainted structural steel plates using spatio-temporal data. *IOP Conference Series: Materials Science and Engineering.* 1252, 1. 2022.
- [78] Karaki, A.A., et al. Multi-Platforms and Multi-Sensors Integrated Survey for the Submerged and Emerged Areas. *Journal of Marine Science and Engineering* 10.6. 2022.
- [79] Karamouz, M., Fereshtehpour, M. Modeling DEM errors in coastal flood inundation and damages: a spatial nonstationary approach. *Water Resources Research* 55.8. 2019, pp. 6606-6624.
- [80] Karunarathna, H., et al. An analysis of cross-shore profile evolution of a sand and a composite sand-gravel beaches. *Coastal Engineering* 2. 2012.
- [81] Klemas, V. Beach profiling and LIDAR bathymetry: An overview with case studies. *Journal of Coastal Research* 27.6. 2011, pp. 1019-1028.
- [82] Komar, P.D. *Handbook of coastal processes and erosion 1*, CRC Press, Boca Raton. 1983, pp. 1–18.
- [83] La Monica, G.B., et al. A new approach to detect shoreline from satellite images. 2008, pp. 61-74.
- [84] Landau, H. et al. Virtual Reference Station Systems. *Journal of Global Positioning Systems* 1. 2002.
- [85] Langley, R.B. RTK GPS. *GPS World* 9 (9). 1998, pp. 70–76.
- [86] Li, R., Zheng, S., Wang, E., Chen, J., Feng, S., Wang, D., Dai., L. Advances in BeiDou navigation satellite system (BDS) and satellite navigation augmentation technologies. *Satell. Navig.* 1 (1). 2020, pp. 1–23. doi:10.1186/s43020-020-00010-2.
- [87] Loh, W.M. On Latin hypercube sampling. *The annals of statistics* 24.5. 1996, pp. 2058-2080.
- [88] López, I., Aragonés, L., Villacampa, Y. Analysis and modelling of cross-shore profile of gravel beaches in the province of Alicante. *Ocean Engineering* 118. 2016, pp. 173-186.

- [89] Luijendijk, A., et al. The state of the world's beaches. *Scientific reports* 8.1. 2018, pp. 1-11.
- [90] Maleika, W. Development of a method for the estimation of multibeam echo sounder measurement accuracy. parameters (difficult to estimate and usually neglected) 2. 2012.
- [91] Maleika, W., Pałczyński, M., Frejlichowski, D. Multibeam echo sounder simulator applying noise generator for the purpose of sea bottom visualisation. *International Conference on Image Analysis and Processing*. Springer, Berlin, Heidelberg, 2011.
- [92] Mancini, F., et al. Using Unmanned Aerial Vehicles (UAV) for High-Resolution Reconstruction of Topography: The Structure from Motion Approach on Coastal Environments. *Remote Sens.* 5, 2013, pp. 6880–6898.
- [93] Mancini, F., Grassi, F., Cenni, N. A workflow based on SNAP–StaMPS open-source tools and GNSS data for PSI-based ground deformation using dual-orbit sentinel-1 data: accuracy assessment with error propagation analysis. *Remote Sens.* 13. 2021. doi:10.3390/rs13040753.
- [94] Mangor, K., et al. *Shoreline management guidelines*. 2004.
- [95] Martínez, C., et al. Coastal erosion in central Chile: A new hazard? *Ocean & coastal management* 156. 2018, pp. 141-155.
- [96] Maso, M. Misure laserscanning e batimetria multibeam sull'asta principale del fiume Brenta. *Perugia*, 5– November 2002, ASITA 2002, II, 2002, pp. 1515–1520.
- [97] Matheron, G. *Traité de Géostatistique Appliqué*, Tonne 1. *Memoires de Bureau de Recherches Géologiques et Minières*, Paris. 1962.
- [98] Matsumoto, Y., Kokuta, S., Mori, H., Yamano, H. Shallow water multibeam echosounding in Japan Hydrographic department, In: F.I.G. International conference, Seoul, Korea, 6/11 May. 2001.
- [99] Mattivi, P., et al. TWI computation: a comparison of different open source GISs. *Open Geospatial Data, Software and Standards* 4.1. 2019, pp. 1-12.
- [100] MATTM-Regioni, T.N.E.C. *Linee Guida per la Difesa Della Costa Dai Fenomeni di Erosione e Dagli Effetti Dei Cambiamenti Climatici*. Versione Settembre. 2018.
- [101] Milan, D.J., Heritage, G.L., Large, A.R., Fuller, I.C. Filtering spatial error from DEMs: Implications for morphological change estimation. *Geomorphology* 125. 2011, pp. 160–171.
- [102] Moritz, H. *Advanced physical geodesy*. *Advances in Planetary Geology*. 1980.
- [103] Nash, J.E., Sutcliffe, J.V. River flow forecasting through conceptual models part I - A discussion of principles. *Journal of Hydrology* 10 (3). 1970, pp. 282–290. doi:10.1016/0022-1694(70)90255-6.
- [104] Nicholls, R.J., Birkemeier, W.A., Hallermeier, R.J. Application of the depth of closure concept. *Coastal Engineering* 1996. 1997, pp. 3874-3887.

- [105] Olken, F. Random sampling from databases. Diss. University of California, Berkeley. 1993.
- [106] Oluyori, P.D., Ono, M.N., Eteje, S.O. Computations of Geoid undulation from comparison of GNSS/levelling with EGM 2008 for Geodetic applications. *Int. J. Sci. Res. Publ.* 8(10). 2018, pp. 235–241. doi:10.29322/IJSRP.8.10.2018.p8230.
- [107] Pardo-Iguzquiza, E., Chica-Olmo, M. Geostatistics with the Matern semivariogram model: A library of computer programs for inference, kriging and simulation. *Computers & Geosciences* 34.9. 2008, pp. 1073-1079.
- [108] Parisot, J.P., et al. Treatment of topographic and bathymetric data acquired at the Truc-Vert Beach during the ECORS Field Experiment. *J. Coast. Res.* SI56. 2009, pp. 1786–1790.
- [109] Pavlis, N.K., Holmes, S.A., Kenyon, S.C., Factor, J.K.: The development and evaluation of the Earth Gravity Model 2008 (EGM2008). *J. Geophys. Res. Solid Earth* 117. 2012. doi:10.1029/2011JB008916.
- [110] Pellegrinelli, A. La definizione di un livello medio mare locale, *Ecoscienza*, 6. 2019, pp. 61–62.
- [111] Pepe, M., Prezioso, G., Santamaria, R. Confronto, su territorio campano, tra modello geoidico EGM2008 e modello di ondulazione da grigliati. 2006.
- [112] Peppia, M.V., et al. Photogrammetric assessment and comparison of DJI Phantom 4 pro and phantom 4 RTK small unmanned aircraft systems. *ISPRS Geospatial Week*. 2019.
- [113] Perini, L., Calabrese, L., Salerno, G., Luciani, P. Mapping of flood risk in Emilia-Romagna coastal areas. *Nat. Hazards Earth Syst. Sci. Discuss.* 3. 2015, pp. 4315–4352.
- [114] Perini, L., Lorito, S., Calabrese, L. Il Catalogo delle opere di difesa costiera della Regione Emilia-Romagna. *Studi Costieri* 15. 2008, pp. 39–56.
- [115] Perroy, R.L., Bookhagen, B., Asner, G.P., Chadwick, O.A. Comparison of gully erosion estimates using airborne and ground-based LiDAR on Santa Cruz Island, California, *Geomorphology*, 118, 3–4. 2010, pp. 288–300. doi:10.1016/j.geomorph.2010.01.009.
- [116] Phillips, M.R., Jones, A.L. Erosion and tourism infrastructure in the coastal zone: problems, consequences and management. *Elsevier Tour Manag* 27. 2006, pp. 517–524. doi:10.1016/j.tourman.2005.10.019 .
- [117] Pianca, C., Holman, R., Siegle, E. Shoreline variability from days to decades: Results of long-term video imaging. *Journal of Geophysical Research: Oceans* 120.3. 2015, pp. 2159-2178.
- [118] Pikelj, K., Ruzić, I., Ilic, S., James, M.R., Kordic, B. Implementing an efficient beach erosion monitoring system for coastal management in Croatia. *Ocean Coast. Manag.* 156. 2018, pp. 223–238.
- [119] Pitman, S.J., Hart, D.E., Katurji, M.H. Application of UAV techniques to expand beach research possibilities: A case study of coarse clastic beach cusps. *Cont. Shelf Res.* 184. 2019, pp. 44–53.

- [120] Pranzini, E., Wetzel, L. Managing Mediterranean beaches: the need for quality and standardised data in beach monitoring at different scales. *Beach Erosion Monitoring*. Nuova Grafica Fiorentina, Firenze. 2008.
- [121] Preti, M. La difesa delle spiagge tra scogliere e ripascimento. *Ecoscienza* 2. 2011, pp. 72–73.
- [122] Preti, M., et al. Integrated beach monitoring at Igea Marina, Italy: Results of ten-years monitoring. *Coast. Eng. Proc.* 1. 2011, pp. 199–226.
- [123] Prezioso, G., Pepe, M., Santamaria, R. Confronto, su territorio campano, tra modello geoidico EGM2008 e modello di ondulazione da grigliati. 2012. doi:10.13140/RG.2.1.4354.8003.
- [124] Pripp, T., Johannessen, J., Eldevik, T. GOCE studies of mean dynamic topography and ocean circulation in the Nordic Seas. *EGU General Assembly Conference Abstracts*. 2013.
- [125] Rapp, R.H., Wang, Y.M.: Geoid undulation differences between geopotential models. *Surv. Geophys.* 14. 1993, pp. 373–380. doi:10.1007/BF00690565.
- [126] Regione Emilia-Romagna. Messa in sicurezza di tratti critici del litorale regionale mediante Ripascimento con sabbie sottomarine-Progettone 3, Progetto esecutivo: relazione generale e illustrativa. 2015.
- [127] Remondino, F., Barazzetti, L., Nex, F., Scaioni, M., Sarazzi, D. UAV photogrammetry for mapping and 3D modelling - Current status and future perspectives. *ISPRS Int. Arch. Photogramm. Remote. Sens. Spat. Inform. Sci.* 38. 2011, pp. 25–31.
- [128] Ritter, A., Munoz-Carpena, R. Performance evaluation of hydrological models: Statistical significance for reducing subjectivity in goodness-of-fit assessments. *Journal of Hydrology* 480. 2013, pp. 33-45.
- [129] Rodella, I., et al. Assessment of the relationship between geomorphological evolution, carrying capacity and users' perception: Case studies in Emilia-Romagna (Italy). *Tourism Management* 59. 2017, pp. 7-22.
- [130] Ružic, I., Marovic, I., Benac, C., Ilic, S. Coastal cliff geometry derived from structure-from-motion photogrammetry at Stara Baska, Krk Island, Croatia. *Geo-Mar. Lett.* 34. 2014, pp. 555–565.
- [131] Scarelli, F.M. et al. Seasonal dune and beach monitoring using photogrammetry from UAV surveys to apply in the ICZM on the Ravenna coast (Emilia-Romagna, Italy). *Remote Sens. Appl. Soc. Environ.* 7. 2017, pp. 27–39.
- [132] Semeoshenkova, V., Newton, A. Overview of erosion and beach quality issues in three Southern European countries: Portugal, Spain and Italy. *Ocean. Coast Manag.* 118. 2015, pp. 12–21.
- [133] Semeoshenkova, V., Newton, A., Contin, A., Greggio, N. Development and application of an Integrated Beach Quality Index (BQI). *Ocean Coast. Manag.* 143. 2017, pp. 74–86.
- [134] Sesli, F.A., Caniberk, M. Estimation of the Coastline Changes Using LIDAR. *Acta Montanistica Slovaca* 20.3. 2015.

- [135] Sistilli, F. Valutazione integrata del sistema spiaggia-duna costiera, in relazione alle dinamiche geomorfologiche, vegetazionali e meteomarine (Ravenna, Italia). PhD Thesis, University of Bologna. 2016.
- [136] Small, C., Nicholls, R.J. A global analysis of human settlement in coastal zones, *Journal of Coastal Research*. 2003, pp. 584-599.
- [137] Song, Y., et al. A DSAS-based study of central shoreline change in Jiangsu over 45 years. *Anthropocene Coasts* 4.1. 2021, pp. 115-128.
- [138] Sorensen, R.M., *Basic coastal engineering*, USA, Springer. 2006, pp. 324.
- [139] Soycan, M., Soycan, A.. Comparison of several techniques for fitting of the EGM08 to GPS/leveling datum. *Arab. J. Sci. Eng.* 39(7). 2014, pp. 5637–5651. doi:10.1007/s13369-014-1136-1.
- [140] Splinter, K.D., Coco, G. Challenges and Opportunities in Coastal Shoreline Prediction. *Frontiers in Marine Science*. 2021.
- [141] Stott, E., Williams, R.D., Hoey, T.B. Ground control point distribution for accurate kilometre-scale topographic mapping using an RTK-GNSS unmanned aerial vehicle and SfM photogrammetry. *Drones* 4.3. 2020.
- [142] Štroner, M. et al. Photogrammetry using UAV-mounted GNSS RTK: Georeferencing strategies without GCPs. *Remote Sensing* 13.7. 2021.
- [143] Taddia, Y., et al. A. Uavs to assess the evolution of embryo dunes. *Proceedings of the International Archives of the Photogrammetry Remote Sensing and Spatial Information Sciences*, Bonn, Germany, 4–7 September 2017, pp. 363–369.
- [144] Taddia, Y., Stecchi, F., Pellegrinelli, A. Coastal Mapping Using DJI Phantom 4 RTK in Post-Processing Kinematic Mode. *Drones*, 4, 9. 2020.
- [145] Tavasci, L. Il monitoraggio dei sistemi di riferimento terrestri mediante tecniche satellitari GNSS: dai sistemi globali ai servizi di posizionamento NRTK. PhD Thesis, University of Bologna. 2016.
- [146] Tavasci, L., Vecchi, E., Gandolfi, S. Definition of the Local Geoid Undulation Using Non-contemporary GNSS-Levelling Data on Subsidence Area: Application on the Adriatic Coastline. *Italian Conference on Geomatics and Geospatial Technologies*. Springer, Cham, 2021.
- [147] Tavasci, L., Vecchi, E., Gandolfi, S. Performance of Atlas GNSS Global Correction Service for High-Accuracy Positioning. *Journal of Surveying Engineering* 147.4. 2021.
- [148] Teatini, P., Ferronato, M., Gambolati, G., Bertoni, W., Gonella, M. A century of land subsidence in Ravenna. Italy. *Environ. Geol.* 47. 2005, pp. 831–846. doi:10.1007/s00 254-004-1215-9.
- [149] Thieler, E.R., et al. The Digital Shoreline Analysis System (DSAS) version 4.0-an ArcGIS extension for calculating shoreline change. 2008-1278. US Geological Survey. 2009.

- [150] Tsai, V.J. Delaunay triangulations in TIN creation: an overview and a linear-time algorithm. *International Journal of Geographical Information Science* 7.6. 1993, pp. 501-524.
- [151] Turner, I.L., Harley, M.D., Drummond, C.D. UAVs for coastal surveying. *Coast. Eng.* 114. 2016, pp. 19–24.
- [152] Unguendoli, S. Propagation of uncertainty across modeling chains to evaluate hydraulic vulnerability in coastal areas. PhD thesis, University of Bologna. 2018.
- [153] United Nations Environment Programme/Mediterranean Action Plan (UNEP/MAP). State of the Mediterranean Marine and Coastal Environment. Greece. 2012. doi:10.13140/RG.2.1.3013.2648.
- [154] Van de Sande, B., Lansen, J., Hoyng, C. Sensitivity of coastal flood risk assessments to digital elevation models. *Water* 4.3. 2012, pp. 568-579.
- [155] Van Groenigen, J.W. The influence of variogram parameters on optimal sampling schemes for mapping by kriging. *Geoderma* 97.3-4. 2000, pp- 223-236.
- [156] Van Rijn, L.C. Coastal erosion and control. *Ocean Coast Manag.* 54. 2011, pp. 867–887.
- [157] Vecchi, E., et al. Third beach nourishment project with submarine sands along Emilia-Romagna coast: geomatic methods and first monitoring results. *Rend. Fis. Acc. Lincei*, 31, 2020, pp. 79–88. doi:10.1007/s12210-020-00879-w.
- [158] Vecchi, E., Tavasci, L., De Nigris, N., Gandolfi, S. GNSS and Photogrammetric UAV Derived Data for Coastal Monitoring: A Case of Study in Emilia-Romagna, Italy. *Journal of Marine Science and Engineering* 9.11. 2021, pp. 1194.
- [159] Vos, K., et al. CoastSat: A Google Earth Engine-enabled Python toolkit to extract shorelines from publicly available satellite imagery. *Environmental Modelling & Software* 122. 2019.
- [160] Walter, T., Blanch, J., Enge, P. Coverage improvement for dual frequency SBAS. *Proc. Int. Technical Meeting of the Institute of Navigation, San Diego: Stanford Univ.* 2010, pp. 344–353.
- [161] Wang, J. Stochastic modeling for real-time kinematic GPS/ GLONASS positioning. *Navigation* 46 (4). 1999, pp. 297–305. doi:10.1002/j.2161-4296.1999.tb02416.x.
- [162] Wang, L., et al. Initial assessment of the LEO based navigation signal augmentation system from Luojia-1A satellite. *Sensors* 18 (11): 3919. 2018. doi:10.3390/s18113919.
- [163] Wheaton, J.M., Brasington, J., Darby, S.E., Sear, D.A. Accounting for uncertainty in DEMs from repeat topographic surveys: Improved sediment budgets. *Earth Surf. Process. Landf. J. Br. Geomorphol. Res. Group.* 2010, 35, pp. 136–156.
- [164] Woolard, J.W., Colby, J.D. Spatial characterization, resolution, and volumetric change of coastal dunes using airborne LIDAR: Cape Hatteras, North Carolina. *Geomorphology* 48. 1-3. 2002, pp. 269-287.

- [165] Zanutta, A., Lambertini, A., Vittuari, L. UAV Photogrammetry and Ground Surveys as a Mapping Tool for Quickly Monitoring Shoreline and Beach Changes. *J. Mar. Sci. Eng.* 2020, 8, 52.
- [166] Zhang, X., Lingkun, L., Fukang, Z. Parameter fitting of variogram based on hybrid algorithm of particle swarm and artificial fish swarm. *Future Generation Computer Systems* 116. 2021, pp. 265-274.

Websites

- [167] <http://dati.isprambiente.it/dataset/ron-rete-ondametrica-nazionale/>
- [168] <http://icgem.gfz-potsdam.de/vis3d/longtime?modelid=971b0a3b49a497910aad23cd85e066d4cd9af0aeafe7ce6301a696bed8570be3>
- [169] <http://www.altimetry.info/radar-altimetry-tutorial/data-flow/data-processing/reference-surfaces/mean-sea-surface/>
- [170] http://www.coastalwiki.org/wiki/Shoreface_profile
- [171] <http://www.euref.eu/symposia/2016SanSebastian/01-05-Alberts.pdf>
- [172] <http://www.fni.it/guida-ecoscandaglio/>
- [173] <http://www.netgeo.it>
- [174] <http://www.pcn.minambiente.it/mattm/>
- [175] <http://www.stoneme.it/risorse/CASO%20RILIEVI.html>
- [176] <https://3dmetrica.it/>
- [177] <https://amslaurea.unibo.it/id/eprint/19783>
- [178] <https://arpae.it/cartografia/>
- [179] <https://bluerobotics.com/learn/ping-sonar-technical-guide/echo-sounder-operating-principle/>
- [180] <https://cultofsea.com/bridge-equipment/echo-sounder/>
- [181] <https://desktop.arcgis.com/en/arcmap/10.3/guide-books/extensions/geostatistical-analyst/choosing-a-lag-size.htm>
- [182] <https://duacs.cls.fr/faq/what-are-the-product-specification/different-sea-surface-heights-used-in-altimetry/>
- [183] <https://earthengine.google.com>
- [184] https://en.wikipedia.org/wiki/Contour_line
- [185] https://en.wikipedia.org/wiki/Delaunay_triangulation
- [186] https://en.wikipedia.org/wiki/Sea_level

- [187] <https://english.defensie.nl/topics/hydrography/coordinate-systems-at-sea/coordinate-reference-systems-for-depth-measurement-at-sea>
- [188] https://geodati.gov.it/geoportale/images/Decreto_10112011_SRGN.pdf
- [189] https://geomatix.net/tides/tidal_levels.html
- [190] <https://geoportale.regione.emilia-romagna.it/download/utility-e-tool/conver-2013-software-per-la-conversione-fra-sistemi-di-coordinate-in-emilia-romagna>
- [191] <https://gisgeography.com/kriging-interpolation-prediction/>
- [192] <https://help.seequent.com/Works/2021.1/en-GB/Content/contaminants/variography.htm>
- [193] <https://hxgnsmartnet.com/it-it>
- [194] <https://iho.int/en/standards-and-specifications>.
- [195] https://lazymodellingcrew.com/post/post_21_nugget_effect_ta/.
- [196] <https://mycollaborativeteam.com/using-monte-carlo-simulations-to-settle-equitable-distribution/>
- [197] <https://ocean-eng.com/en/publics/index/17/>
- [198] https://ozcoasts.org.au/indicators/coastal-issues/beach_erosion/
- [199] <https://pro.arcgis.com/en/pro-app/latest/help/analysis/geostatistical-analyst/understanding-a-semivariogram-the-range-sill-and-nugget.htm>
- [200] <https://pubs.usgs.gov/of/2003/of03-337/figures/fig2.html>
- [201] <https://pubs.usgs.gov/of/2012/1008/html/methods.html>
- [202] https://rstudio-pubs-static.s3.amazonaws.com/666533_4a7c7584d2a64d9e8717c41e99c7a5ed.html)
- [203] <https://scikit-gstat.readthedocs.io/en/latest/userguide/variogram.html>
- [204] <https://sealevel.jpl.nasa.gov/mission/topex/>, <https://www.jpl.nasa.gov/missions/jason-1>.
- [205] <https://servizi-gis.arpae.it/Html5Viewer/index.html?locale=it-IT&viewer&viewer=Geoportal.Geoportal>
- [206] <https://simc.arpae.it/dext3r/>
- [207] <https://statsandr.com/blog/clustering-analysis-k-means-and-hierarchical-clustering-by-hand-and-in-r/#k-means-clustering>
- [208] <https://windy.app/blog/what-are-tidal-datums-lat-and-mllw.html>
- [209] <https://www.3d-archeolab.it/2017/04/tutorial-la-fotogrammetria-automatica-come-funziona-a-cosa-serve/>
- [210] <https://www.aspexit.com/spatial-data-interpolation-tin-idw-kriging-block-kriging-co-kriging-what-are-the-differences/>

- [211] <https://www.ceva-dsp.com/ourblog/what-is-an-imu-sensor/>
- [212] <https://www.deltares.nl/en/projects/global-modelling-of-tides-and-storm-surges/>
- [213] <https://www.eea.europa.eu/soer/2015/countries/mediterranean>
- [214] <https://www.emodnet-bathymetry.eu>
- [215] <https://www.esri.com/content/dam/esrisites/sitecore-archive/Files/Pdfs/library/whitepapers/pdfs/shapefile.pdf>
- [216] https://www.gebco.net/data_and_products/gridded_bathymetry_data/
- [217] https://www.google.com/intl/it_ALL/earth/outreach/learn/introduction-to-google-earth-engine/
- [218] <https://www.hemispheregnss.com/product/atlas-gnss-global-correction-service/>
- [219] https://www.isgeoid.polimi.it/Geoid/Europe/Italy/italgeo05_g.html. Accessed 08 Jan 2021.
- [220] https://www.isgeoid.polimi.it/Geoid/Europe/Italy/ITG2009_g.htm
- [221] <https://www.mareografico.it/?session=0SESSM&syslng=ita&systemen=-1&sysind=-1&syssub=-1&sysfnt=0&code=STAZ&idst=1M>
- [222] https://www.marina.difesa.it/noi-siamo-la-marina/pilastro-logistico/scientifici/idrografico/Documents/disciplinare_tecnico_2021/II%203176%20DISCIPLINARE%20TECNICO%20COMPLETO%20Ed2021.PDF
- [223] <https://www.mathworks.com/help/optim/ug/least-squares-model-fitting-algorithms.html>
- [224] <https://www.ogc.org/standards/wms/introduction>
- [225] <https://www.operandum-project.eu>
- [226] <https://www.psmsl.org/data/obtaining/map.html>
- [227] <https://www.publichealth.columbia.edu/research/population-health-methods/kriging-interpolation>
- [228] <https://www.qgis.org/it/site/>
- [229] <https://www.scratchapixel.com/lessons/mathematics-physics-for-computer-graphics/monte-carlo-methods-mathematical-foundations>
- [230] <https://www.uavnavigation.com/company/blog/what-is-an-IMU>
- [231] <https://www.yellowscan-lidar.com/knowledge/how-lidar-works/>